CONTROLLING FLEXIBLE MANIPULATORS, AN

EXPERIMENTAL INVESTIGATION

A THESIS

Presented to

The Faculty of the Division of Graduate Studies

By

Gordon Greene Hastings

In Partial Fulfillment

of the Requirements for the Degree

Doctor of Philosophy in the

School of Mechanical Engineering

Georgia Institute of Technology

August, 1986

CONTROLLING FLEXIBLE MANIPULATORS, AN

EXPERIMENTAL INVESTIGATION

Approved:

_____
Wayne J. Book, Chairman

_____
John F. Dorsey, E.E.

_____
Jerry H. Ginsberg, M.E.

_____
Benson H. Tongue, M.E.

_____
James I. Craig, A.E.

Date Approved by Chairman___8/8/86_____

DEDICATION

This thesis is dedicated to the memory of John R. Colston, September 27, 1930 - November 27, 1985, friend, mentor, engineer. This thesis is a direct result of his impact on my life.

ACKNOWLEDGEMENTS

I wish to thank my family and parents Robert Francis, and Susan Jane Hastings for their encouragement and support throughout this undertaking. I also wish to acknowledge the efforts made by the members of my committee in preparing me for this work, and for their input to this thesis, most notably Dr. John Dorsey for the material on model order reduction contained in chapter 4. I would additionally like to express special thanks to Dr. Wayne Book, my advisor for his insightful guidance, and friendship over the course of this work.

TABLE OF CONTENTS

LIST OF TABLES

LIST OF FIGURES

ABSTRACT

Lightweight, slender manipulators offer faster response and/or greater workspace range for the same size actuators than traditional manipulators. Lightweight construction of manipulator links results in increased structural flexibility. The increased flexibility must be considered in the design of control systems to properly account for the dynamic flexible vibrations and static deflections. This thesis experimentally investigates real-time control of the flexible manipulator vibrations.

Models intended for real-time control of distributed parameter systems such as flexible manipulators rely on modal approximation schemes. A linear model based on the application of Lagrangian dynamics to a rigid body mode and a series of separable flexible modes is examined with respect to model order requirements, and modal candidate selection.

Balanced realizations is applied to the linear flexible model to obtain an estimate of appropriate order for a selected model.

Describing the flexible deflections as a linear combination of modes results in measurements of beam state, (position, strain etc.), which yield information about several modes. To realize the potential of linear systems theory, in particular to implement full state feedback,

knowledge of each state must be available. Reconstruction of the time varying modal amplitudes form strain measurements is examined. Reduced order observers are utilized to obtain estimates of the modal velocities, from the reconstructed modal amplitudes. State estimation is also accomplished by implemention of a Kalman Filter.

State feedback control laws are implemented based upon linear quadratic regulator design. Specification of the closed loop poles in the regulator design process is obtained by inclusion of aprescribed degree of stability in the manipulator model.

CHAPTER I

INTRODUCTION

This thesis presents the results of an investigation into the control of a flexible manipulator. The investigation focuses on real time control experiments examining dynamic models, and control strategies proposed by past researchers. Analytical work performed was primarily conducted to adapt the models and controllers to the experimental system, and resolve discrepancies between the experimental results, and expected results.

Documentation is provided for the experimental hardware utilized in the experiment, as well as the software generated to implement the controllers. Some tutorial is given in the appendices to bridge the gap between the various topics involved in this work.

1.1 Organization and Readers Guide

The purpose of this section is to present the reasoning behind the layout of the thesis, and provide a short topical description of each section as an aid in finding material of interest to specific readers.

The main body of the work focuses on presenting experimental observations, and comparison of these results to analytical predictions. The appendices contain long

derivations, programs , etc. which may be useful and informative, but are not central to the objectives of the thesis effort.

The first chapter introduces the thesis topic, discusses the organization, and identifies pertinent literature. The chapter concludes by defining the specific problem considered for this investigation.

The second chapter, "Experimental Apparatus", briefly identifies the major components of the experimental system, and provides graphic representation of their interplay. Detail information on the hardware components, and electrical connections are identified in Appendix E.

The third chapter, "Verification of the Linear Dynamic Model", roughly outlines the process for generating the dynamic model used in the controller design algorithms. Experimental observations conducted to evaluate the model are presented and compared to digital simulation. A detail account of the modelling process is contained in Appendix A.

The fourth chapter discusses analytical estimation of required model order. The method of balanced realizations is introduced and applied to the model. This provides quantitative substance to the qualitative results of chapter 3.

The fifth chapter, "Measurement and Reconstruction of Flexible Variables", discusses reconstruction of the flexible variables, and selection of locations for strain

measurement from which the variables are obtained.

The sixth chapter, "Reduced Order Observers", reviews the concept of state observation, and the fundamentals of reduced order observers. Application of reduced order observers to the estimation of modal velocities is discussed including specification of the measurement update gain to obtain robust implementation. Pole placement of the observer poles is evaluated experimentally.

Chapter seven, "Optimal Regulator", addresses the performance of a deterministic optimal regulator design for the flexible manipulator. Various degrees of stability are prescribed in the design process, and the resultant performance recorded. Models with with one and two modes are examined.

Chapter eight, "Kalman Filter", discusses the experimental determination of measurement noise, and presents the closed loop performance based on the Kalman Filter estimates of the states. The amount of plant noise is varied to obtain a robust filter.

Chapter nine discusses several additional results, and observations which had significant impact on the experiment, but do not fit in the other sections.

Chapter ten summarizes the major contributions and results of this work, and identifies future work.

Appendix A gives a detailed account of the dynamic model generation.

Appendix B derives the frequency determinant for a Bernoulli-Euler beam.

Appendix C generates the necessary equations, and solution technique for the Optimal Quadratic Regulator.

Appendix D embraces the Kalman filter origins.

Appendix E gives manufacturers data, results from tests conducted to verify component performance, and electrical connection diagrams.

Appendix F documents the software routines generated for the micro-processor controller.

1.2 Background

A large body of analytical research applicable to the modeling and control of flexible manipulators has accumulated over the last two decades. The following paragraphs briefly chronicle the most pertinent efforts, and highlight major contributions.

All physical systems can be described as continuous in space, and/or time, however, many systems are adequately described using simpler lumped models. To provide responsive, accurate control of flexible manipulators the distributed nature of the mass needs be included in the dynamic model.

The dynamics of distributed systems has been under investigation for many years, and F.T. Brown [I1], 1964, classified the general character of these systems, and at

the same time drew physical analogies between the distributed parameter systems of several fields. Shortly afterwards, this material started appearing in aerospace literature with respect to stabilizing flexible vehicles. For example, work by R.E. Andeen [I2], 1964, applied these ideas to the stabilization of rockets.

Modal control of a distributed parameter systems was discussed as early as 1966 by Lasso [I3], and again by Lasso and Gould [I4], 1966. Lasso and Gould described control law development using classical techniques, and discussed determination of modal quantities from measurements. The modal analysis technique, discussed by Lasso and Gould, is similar in concept to the reconstruction concept used for this study. Wykes, and Mori [I5], 1966, reported on the applicability of this approach to the control of flexible modes in aircraft.

Vaughan [I6], 1968, applied wave propagation concepts to the control of bending vibrations. Vaughan was interested in determining impedance matches for a passive endpoint attachment. Vaughan obtained transfer matrices to describe the dynamic character of a flexible beam. The transfer matrices were similar to those latter developed by Book [I9] to describe the dynamics of flexible manipulators.

Komkov [I7] discussed optimal control of a transverse beam oscillations in 1968. Mirro [I8], 1972, was perhaps the first to discuss the feedback control of a flexible

manipulator. Mirro examined the usefulness of optimal regulators as applied to this problem. This was followed by Book [I9], 1974, who examined the usefulness of transfer matrices in the modeling and control of flexible manipulators. In addition, Book drew conclusions about the response of flexible manipulators to feedback controllers, and discussed design of the flexible member. Neto [I10], 1974, examined the application of modal analysis and Lagrangian formulation of the dynamic system to the analysis and control of flexible manipulators.

Schaechter [I11], 1974, examined the control of flexible vibrations aimed at large scale space structures, and included some experimental investigations. The apparatus was a free hanging truss structure, with actuation suitable for space applications. The paper served to document the apparatus, associated hardware, and modeling difficulties.

Martin [I12], 1978, analytically investigated the control of flexible mechanical systems, and specifically considered the performance of both collocated and non-collocated controllers. This work was aimed at large space structures, and paralleled the work of both Mirro, and Book. Balas [I13], 1978, discussed modal control of large space structures and focused on the impact of controller designs and implementations based on truncated models. The control concepts intended for flexible space structure control usually consider multiple actuators distributed over the

lengths of open truss structures to control the undesired vibrations.

Book, Majette, and Ma [I14], 1979, continued to develop frequency domain techniques for the control and analysis of serial manipulators with multiple flexible links. Hughes [I15], 1979, developed complete, general dynamic relationships for flexible chain systems applicable to flexible manipulators. Balas [I16], 1980, continued to contribute to the field of space structure control with an investigation of modeling based on finite element techniques. The model, although suitable for small amplitude vibrations about an equilibrium configuration, did not properly account for rapid gross motions typical of manipulator applications.

Fujii [I17], 1980, developed functional observers for distributed parameter systems in recognition of the computational requirements of state observers. Truckenbrodt [I18], 1981, concentrated on modelling a fixed base flexible manipulator that was similar to Neto's earlier work. Truckenbrodt, additionally compared the performance of the model to a simple test device and found reasonable agreement for the frequencies of the first four vibratory modes.

Balas [I19], 1982, discussed a need for more practical control concepts satisfying constraints which arise in implementation. Sunada, and Dubowsky [I20], 1982, developed finite elements for flexible manipulators which incorporated

the dynamic effects of gross motions encountered in robotic applications.

Cannon and Schmitz [I21], 1983, discussed characteristics of a very flexible manipulator with open truss construction, and in further work [I22], 1985, investigated end-point position control. The end-point position was measured by an optical sensor external to the manipulator system. Zalucky and Hardt [I23], 1984, examine compensation for static deflections occuring in flexible members using an optical sensor to measure deflections.

Turic and Midha [I24], 1984, obtain generalized equations of motion for elastic systems using finite elements. Turic, Midha, and Bosnik [I25], experimentally examine the ability of the finite element technique of the previous reference to predict the motion of a four bar linkage. Weeks, [I26], presents solution of the boundary value problem describing control of flexible structures by use of integral transforms. Weeks recognized that for real-time implementation the Greens functions could be approximated by expansions of selected eigenfunctions. Bodde n and Junkins [I27], 1984, discussed optimization of the eigenvalues for structural controllers. Junkins [I28], 1985, continued to examine the flexible structure eigenvalue placement problem using optimal linear quadratic regulator design.

Meirovitch and Baruh [I29], 1984, consider the

application of modal filters to reduce model order requirements in control of flexible structures. Sangveraphunsiri [I30], 1984, applied optimal control methods to obtain controller designs for a single link flexible manipulator. Deterministic and stochastic steady-state regulators, as well as time optimal bang-bang controllers were simulated with linear, and nonlinear models. Major and Shain [I31], 1984, consider the control of a flexible truss suitable for space applications, and go on to discuss experiments on a single truss section in 1985 [I32].

Book [I33], 1984, presented the "Bracing Strategy" to achieve higher effective stiffness for flexible manipulators in performance of certain robotic tasks. Lane and Dickerson [I34], 1984, considered the application of visco-elastic damping materials to achieve passive control of flexible vibrations. Alberts et. al., [I35], experimentally evaluated passive damping treatments applied to a single link flexible manipulator. Major and Maples [I36], 1985, considered force control of manipulators with flexible structural elements. Naganathan and Soni [I37], 1986, examine non-linear kinematic formulations of flexible manipulators using finite element techniques.

1.3 Problem Statement

The following section defines the specific physical configuration, and problem addressed in this investigation. A flexible arm limited to motions in the horizontal plane via rotation about a fixed joint is depicted in figure 1-1. The arm is constructed from a single continuous beam. The only control actuation available to the system is a torque delivered at the single rotational joint. The following measurements of the state of the system are available:

1. Joint rotation angle
2. Joint rotational velocity
3. Strain at least two locations

A control torque u, is determined that will rotate the flexible beam from one arbitrary orientation to another specifiable orientation quickly and accurately. This function utilizes the measurements to provide information on the state of the system.

Since the proposed investigation relies heavily on experimental investigation, the performance of physical components add complexity to the problem. Linearity, and responsiveness of the torque source, coulomb and viscous friction of the joint, and measurement noise are but a few of the factors impacting the problem.

1.4 Contribution

The major contributions of this thesis lies in the evaluation of truncated models for use in the control of flexible manipulators. Chapter 3 identifies the importance of mode selection and model order. Chapter 4 proposes a method for apriori estimation of the required model order. Chapter 5 presents a measurement scheme for the time varying modal variables. Chapter 6 develops a reduced order observer for modal velocities. Chapters 7, and 8 evaluate the performance of controllers based on these models. Chapter 9 contains additional information gleaned from the series of experiments. All this information forms the foundation for further work in controlling distributed parameter systems.
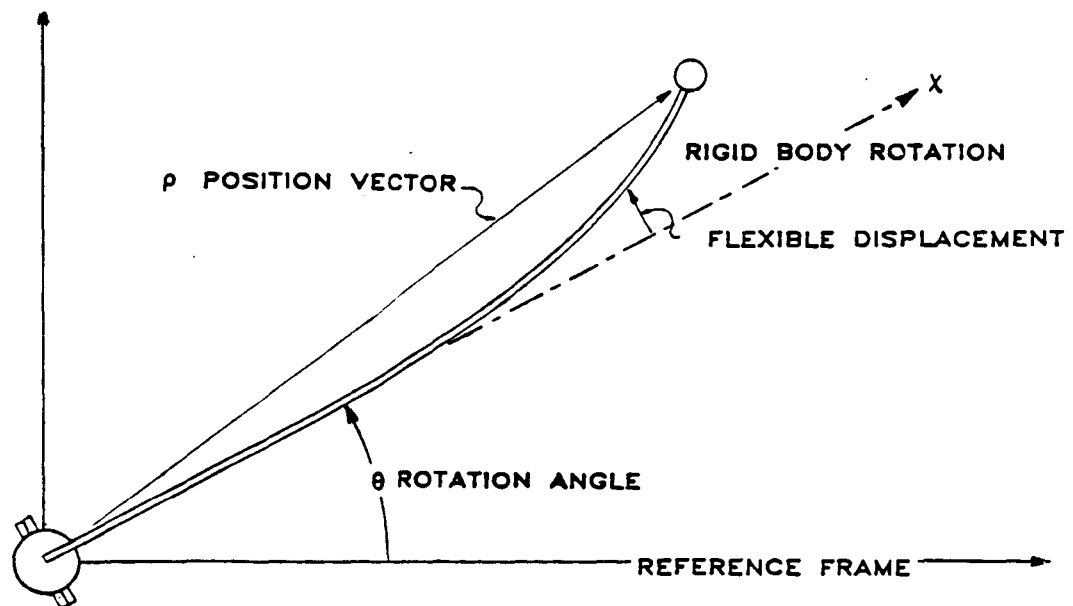
Figure 1-1. Single Link Manipulator

CHAPTER II

EXPERIMENTAL APPARATUS

This section of the thesis introduces the experimental manipulator system. The graphic configuration of the major subsystems and their major functions are identified in this section. This is done to establish a point of reference for the following chapters, and to set the physical scale of the experiment. Manufacturers, specifications, experimental measurements made to assure the performance parameters of key components, and detail diagrams identifying the actual electrical connections are identified in Appendix E.

The experimental hardware is separated into three major subsystems:

- Micro-Processor System
- Manipulator
- Signal Conditioning

Figure 2-1 graphically depicts the system hardware. The micro-processor subsystem consists of a high speed sixteen bit micro-processor with floating point hardware, mass storage, and sensor I/O for data acquisition and control.

The manipulator subsystem consists of the flexible link, torque motor, payload, and sensors. The link sets the scale for the experiment. The arm is a four foot aluminum

beam oriented so that axis of increased flexibility is in the horizontal plane. Four feet is longer than lengths of many "pick and place" industrial robots, yet significantly shorter than proposed scales for flexible manipulators [II1-2]. A commutated DC torque motor provides the motive power for the link.

The payload is provisioned for the addition of weights to allow investigation of the systems sensitivity to payload mass. Several sensors are attached to the flexible manipulator in order to provide information about the state of the link. A potentiometer is mounted to the top of the actuator shaft to measure the rotation of the joint. A
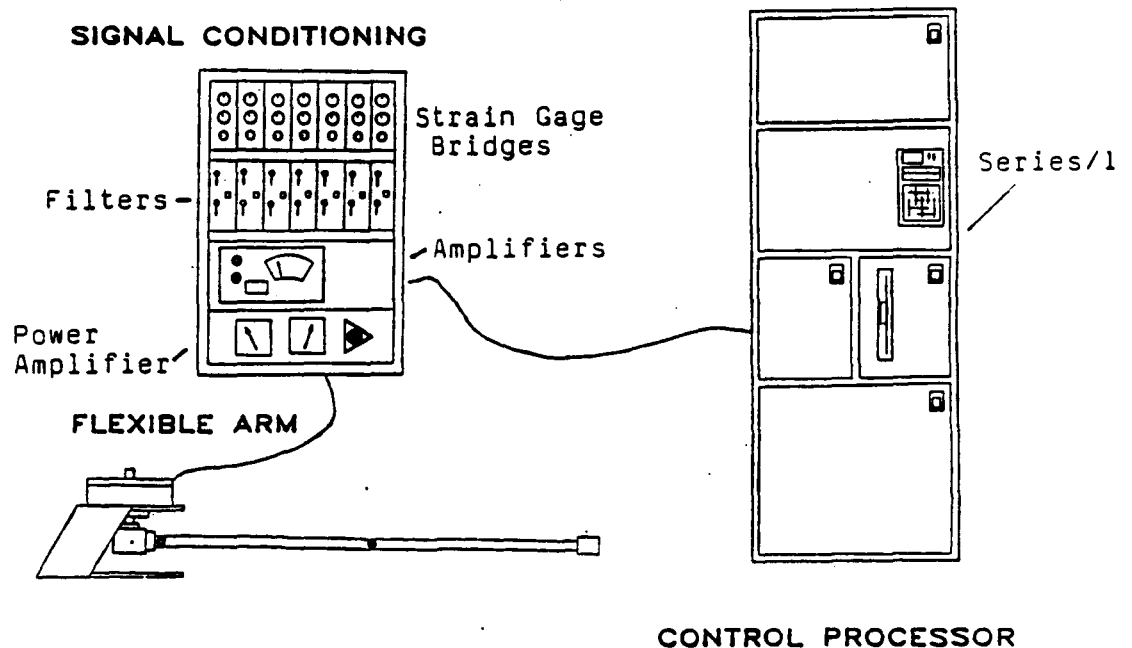
Figure 2-1. Graphic Configuration of
the Experimental Apparatus

tachometer located under the motor housing is used to measure the angular velocity of the joint. Strain gages, mounted at the base and midpoint of the link, provide measurements of the beam deflections.

The signal conditioning subsystem provides interface electronics for the strain gages, angle sensor, tachometer, and torque motor. The strain gages require bridge circuitry and amplification. The angle sensor and tachometer require buffer amplifiers to isolate them from the line loads and provide analog scaling. Four band pass filters are also provided. The torque motor is driven by a large DC servo-amplifier configured to provide currents proportional to the input voltage.

CHAPTER III

VERIFICATION OF THE LINEAR DYNAMIC MODEL

The material in this section of the thesis describes the linear model which formed the basis for most of this investigation into the control of flexible manipulators. The initial sections discuss the modeling process, and steps taken to verify system parameters and algorithm implementation. The latter section compares simulations of the model to experimental measurements.

3.1 Model Generation

This sub-section describes the formation of a linear state space model for the flexible manipulator. The process for forming the model will be outlined in this section; a detailed description is contained in appendix A. The first step of the process is to describe the position of every point along the flexible manipulator. A linear combination of vibratory modes to describe flexible deflections, and a rigid body motion of the center of mass is selected. A manipulator with a rigid body rotation and flexible "clamped-mass" mode is depicted in figure 3-1.

The flexible deflections are described by an infinite series of separable modes. Separability in this instance refers to describing the flexible deflections as a series of

assumed modes [III1] which are products of two functions, each of which is a function of a single variable: one a function of a spatial variable, and the other a function of time. This is noted as:

$$w(x,t)= \int \phi_i(x)q_i(t) \text{ , for } i=1,2...n \tag{3.1}$$

This separability is important in later phases when the model is formed in terms of time varying variables only.

Next the kinetic and potential energies are derived. The distributed character of the flexible manipulator is taken into account via integral expressions over the mass of the entire system in forming the energy expressions. The integral for calculating the kinetic energy, KE, has the
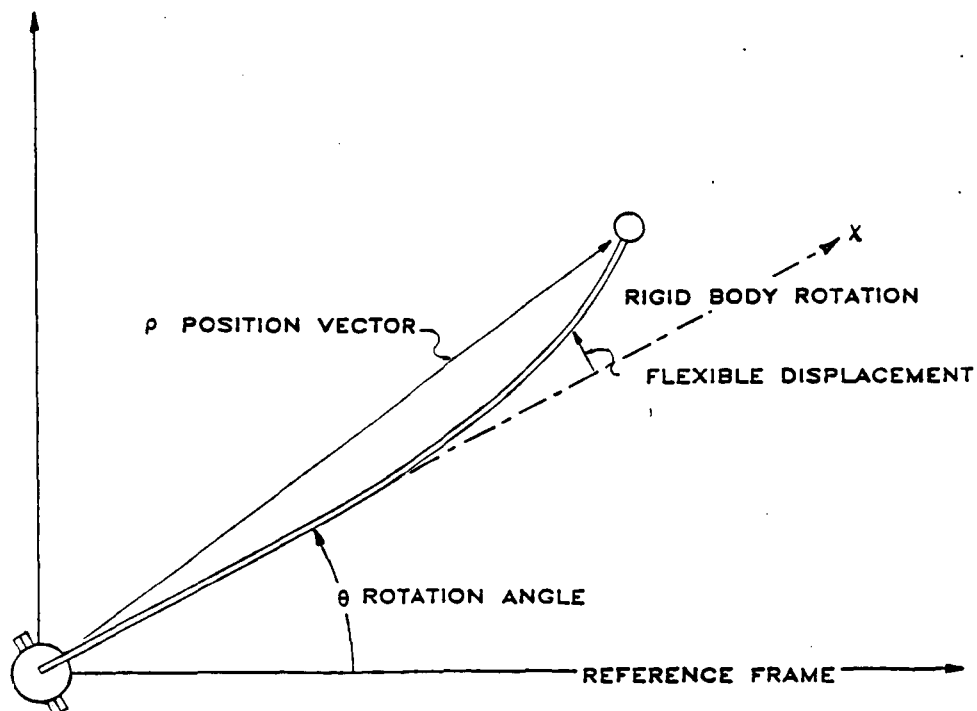
Figure 3-1. Flexible Manipulator

following form;

$$KE = \frac{1}{2} \int \dot{R} \cdot \dot{R} dm \qquad (3.2)$$

where R, the absolute velocity vector, and mass, range over the entire system. The potential energy, PE, of the system is stored in the flexible modes and can be attributed to "modal stiffnesses", K_i, which are evaluated by integrals over the length as shown in equation A.12. Lagrange's equations of motion can be formed from the energies;

$$\frac{d}{dt}\left|\frac{\partial KE}{\partial \dot{\xi}_i}\right| - \frac{\partial PE}{\partial \xi_i} = Q_i \qquad (3.3)$$

where the ξ_i are the coordinates, and Q_i are the generalized work terms associated with each coordinate. Turning the computational crank on the various differentials and integrals as carried out in appendix A results in a coupled set of second order dynamic equations with familiar form;

$$[M]\ddot{z} + [K]z = [Q] \qquad (3.4)$$

$$z = [\theta, q_1(t), q_2(t), \ldots, q_n(t)] \qquad (3.5)$$

M is a mass matrix, K represents stiffness, and Q the input. The dynamic equations are easily organized into a state-space model as shown in equation (3.6). The motor torque at the joint, and the generalized work terms, Q_i, are then related to the rotation of the joint with each variable. Examination of the form of the model reveals the expected result that the coupling between the modes, and the rigid

body motion occurs from inertial terms of the mass matrix.

Equation (3.6) depicts a 2(n+1) order linear model where n is the number of included modes. Non-linear terms arise from the evaluation of equation (3.2) for the kinetic energy, and the specific assumptions employed to obtain a model containing only linear terms is discussed in Appendix A.

$$
\begin{vmatrix} \dot{\theta} \\ \dot{q}_1 \\ \dot{q}_2 \\ \vdots \\ \ddot{\theta} \\ \ddot{q}_1 \\ \ddot{q}_2 \\ \vdots \end{vmatrix} = \begin{vmatrix} 0 & I \\ \hline M^{-1}K & 0 \end{vmatrix} \begin{vmatrix} \theta \\ q_1 \\ q_2 \\ \vdots \\ \dot{\theta} \\ \dot{q}_1 \\ \dot{q}_2 \\ \vdots \end{vmatrix} + \begin{vmatrix} 0 \\ \hline M^{-1}Q \end{vmatrix} |u| \quad (3.6)
$$

3.2 Mode Selection and Frequency Determinant

The remaining task in generating a trial model is the selection of the flexible modes to be used in forming the constant mass and stiffness matrices.

The path chosen in this work is to select admissible functions as candidates which are solutions to closely related problems. These solutions are eigenfunctions for selected "clamped-mass", and "pinned-mass" boundary value

problems. Clamped describes a boundary condition where the joint is fixed against rotation, pinned describes a joint with motor inertia free to rotate, and mass describes the condition of the payload at the other beam boundary. The admissible functions will then satisfy the differential equation, the essential or geometric boundary conditions, and the natural boundary conditions of the free vibration problem.

Appendix B describes the development of the differential equation for a Bernoulli-Euler beam and the solution of selected boundary value problems. The problem is formulated in terms of a frequency determinant for the determination of the eigenfunctions and the associated frequencies.

The experimental apparatus introduced in Chapter 2 was used to examine the model's performance. Table 3-1 identifies the important parameters of the beam which were used as inputs to the modeling process.

Table 3-1. System Parameters

```
Flexible Beam -
Material          - Aluminum 6061-T6
Form              - Rectangular 3/4 x 3/16in
Length            - 48 in
Moment of Inertia - 4.12E-4 in²
EI Product        - 4120 lbf-in⁴
```

3.3 Parameter and Program Verification

This section describes experiments conducted to verify system parameters and program implementation of the model generation process. Initially the frequencies determined via the Bernoulli-Euler beam equations with clamped-mass, and pinned-mass boundary conditions are compared to measured eigenvalues of the beam. This examines beam length, modulus, and density parameters, as well as the suitability of the chosen boundary conditions.

Figure 3-2 shows a measured transfer function from random torques input by the motor to strain at the base of the beam. The peaks correspond to "clamped-mass" modes, as
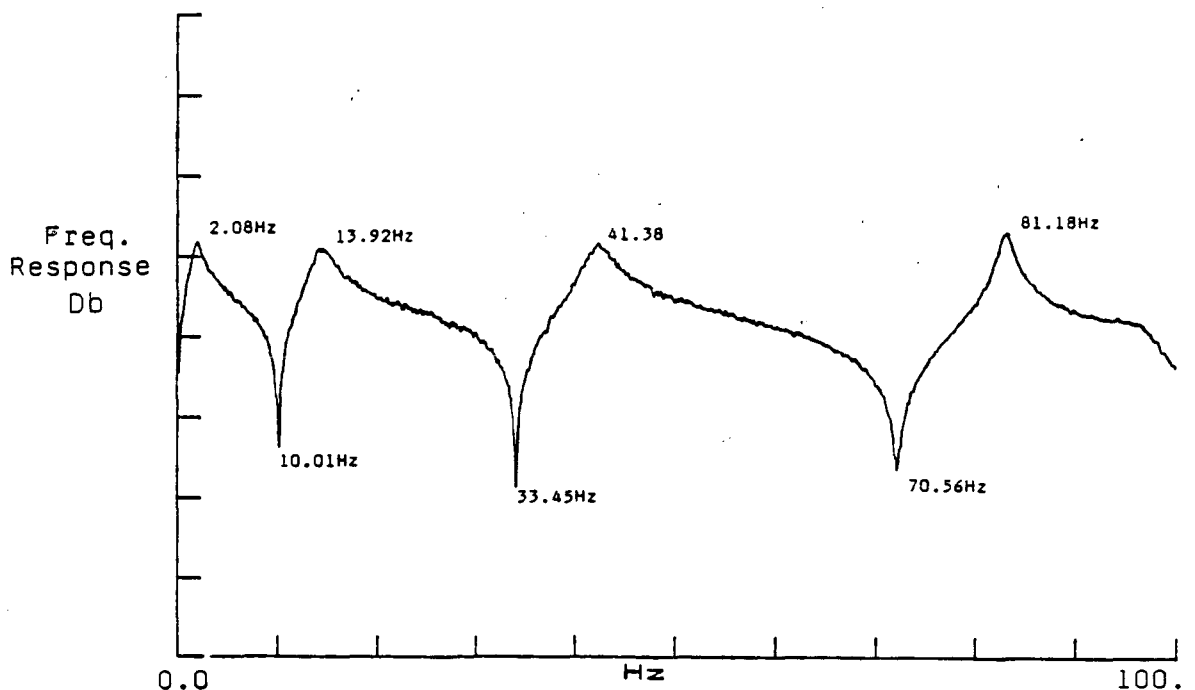
Figure 3-2. Frequency Response

the clamped boundary condition results in modes having maximum moments at the base of the beam. The valleys are associated with "pinned-mass" modes, as this boundary condition results in modes which have small moments which rotate the motor inertia. Martin [III2] discusses measurement zeros which occur in flexible structures.

The vibratory modes were additionally calculated by the frequency determinant described in Appendix B. Table 3-2 compares the measured modal frequencies to those computed using the Bernoulli-Euler Beam. The application of the Bernoulli-Euler formulation to the "clamped mass" case agrees very well with the measured frequencies, however, the "pinned-mass" conditions were not as accurate.

The poorer agreement for the pinned case is attributed to the friction found in the joint hardware; this is a difficult condition to model and may have a significant effect for the small amplitude motions used during the tests.

Table 3-2. Comparison of Modal Frequencies(Hz)

Mode	Clamped-Mass		Pinned-Mass	
	Measured	Calculated	Measured	Calculated
1	2.08	2.096	10.01	9.732
2	13.92	13.989	33.45	31.608
3	41.38	41.524	70.56	62.683
4	81.18	81.225		148.768
5		136.352		216.048

The next step checked the model generation algorithm. Normalization of the modal masses allows the checking of the computations by examining the diagonal components of the stiffness matrix. The stiffnesses should be the square of the modal frequencies input to the process.

The algorithm was checked for both the clamped-mass modes and the pinned-mass modes. Table 3-3 presents a comparison of the modal frequencies input to the modelling process. The results are very good, however it was necessary to use higher precision computations for the higher modes.

Table 3-3. Comparison of Frequencies Determined
by Stiffness Computations

Clamped-mass		Pinned-Mass	
Input	Stiffness$^{1/2}$	Input	Stiffness$^{1/2}$
2.096 Hz	2.096	9.732 Hz	9.732
13.989	13.989	31.608	31.608
40.552	40.524	62.683	62.683
81.225	81.225	148.768	148.768
136.352	136.344	216.048	214.621

3.4 Dynamic Response Comparison

The previous section provides confidence that the beam parameters have been properly identified and modeled by the Bernoulli-Euler beam. The computational procedure has

additionally been checked. The major questions concerning the model can now be investigated:

- Choosing the Modal Candidates
- Required Model Order
- Is a Linear Model of the Coupling Adequate

The following paragraphs describe simulations and experiments conducted to gain insight into the answer to these questions. The simplest and best understood controller for flexible arms is a collocated controller, that is, a control system where the measurement and actuation is located at the same point. A collocated controller was implemented for the experimental system which applied a position gain to joint angle measurements, and a rate gain to angular velocity measurements.

The position gain was selected to provide the rigid body mode with a characteristic time of one second. The rate gain was selected to provide a damping ratio of 0.7. Higher gains could be selected which stress the impact of flexibility on the control strategy, however the chosen gains provide a good starting point well within the operating parameters of the system.

Figure 3-3 displays the measured response of the experimental system to a step change in desired joint angle. Strain measurements presented in the figure, while not used in the controller, provide an indication of the relative modal amplitudes.

The dynamic model was discretized, and simulated for the step angle change. Small amounts of damping, (typically damping ratios ranging from .007-.010, based on transfer function measurements using an impulse hammer as the input and strain at the base as the output [III3]) were introduced into the model for the flexible modes. Additionally, hysteretic joint friction was modeled as coulomb friction [III4] and included in the digital simulation. Inclusion of modal damping and hysteresis in the simulations improved the agreement of the models especially in the time interval after the large initial transients had occurred.

Figure 3-4 shows the results for a model implemented with five clamped-mass modes, while figure 3-5 presents a model using two clamped-mass . modes. The last case simulated used five pinned-mass modes as inputs to the modeling process. This is presented in figure 3-6.

The simulations based upon clamped-mass modes agree the best with measured responses. Surprisingly the model implemented with only two clamped-mass modes agrees almost as well if not better than the higher order model. The poorer agreement of the higher order model is probably due to poor estimation of the damping by use of the impulse hammer measurements. Additional damping in the higher modes from the joint is likely when the joint is in motion. Should the actual manipulator exhibit the higher amplitude
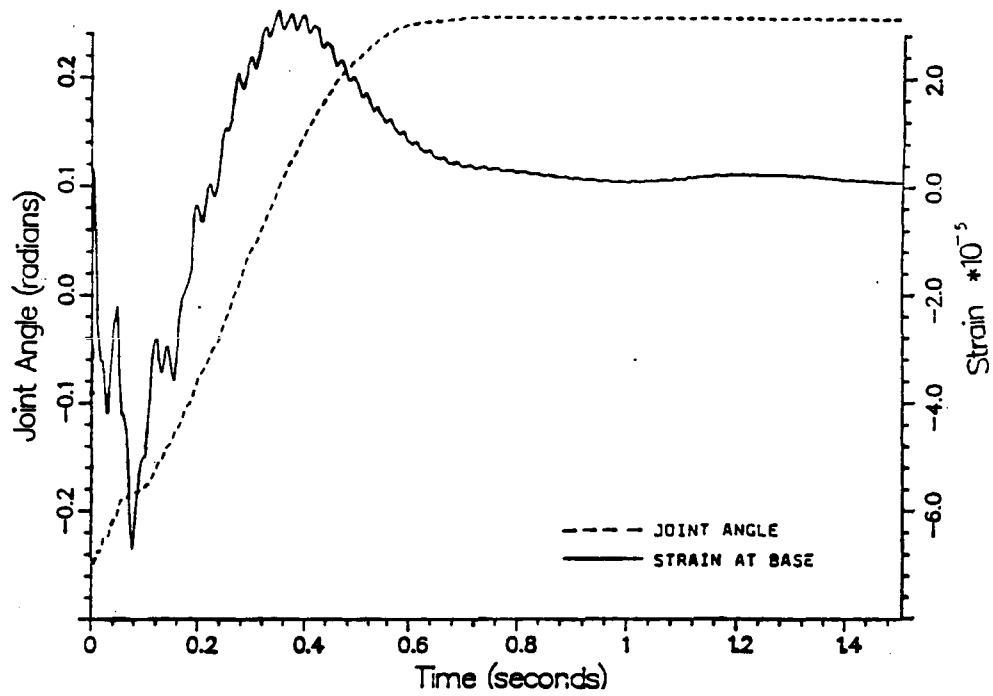
Figure 3-3. Measured Step Response
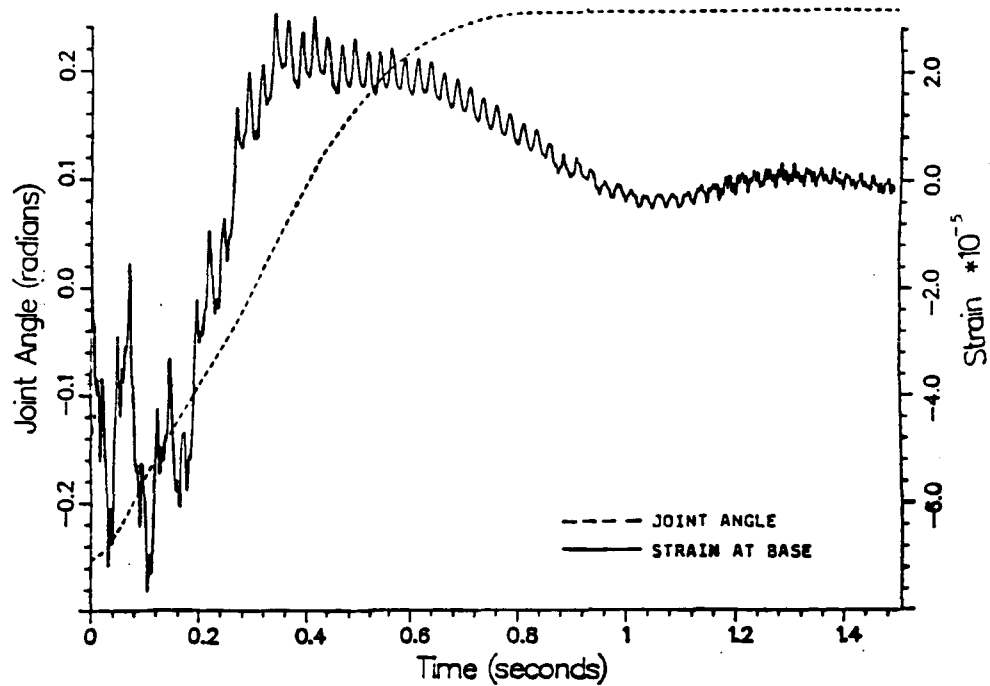
Figure 3-4. Simulation, Five Clamped-Mass Modes.
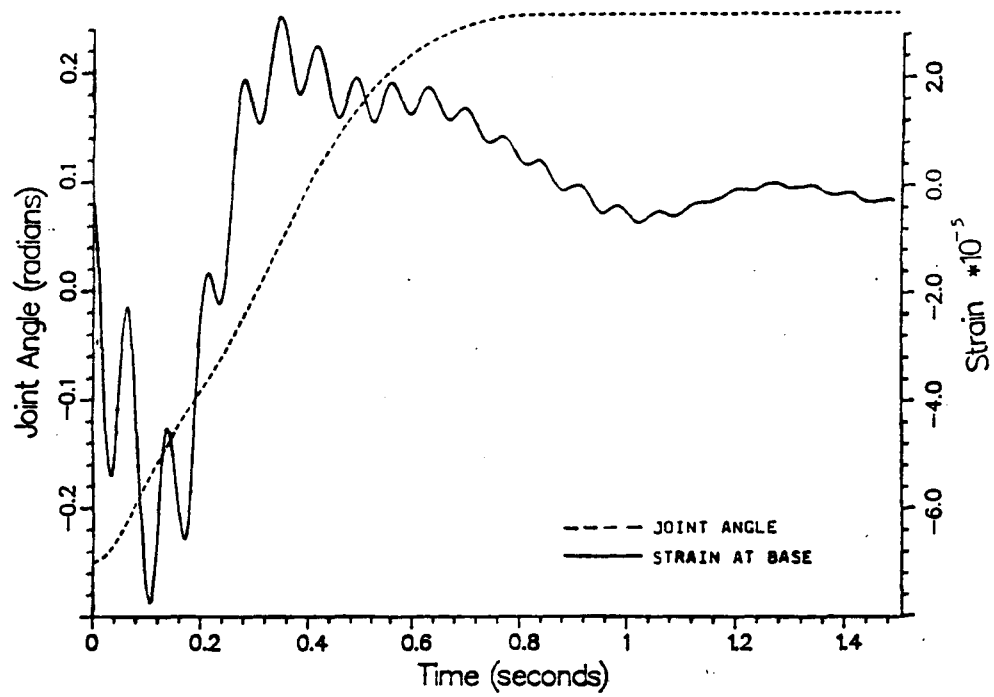
Figure 3-5. Simulated Response, Two Clamped-Mass Modes.
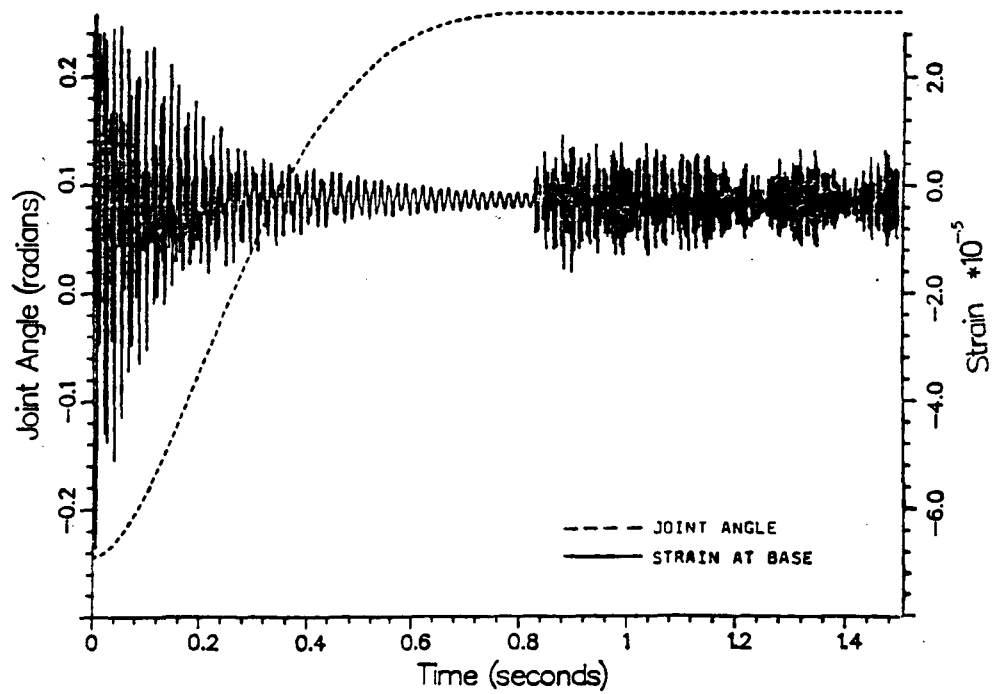
Figure 3-6. Simulated Response, Five Pinned-Mass Modes.

vibrations in the higher frequencies, as shown in figure 3-4, larger models including the higher flexible modes would be required. This presentation maybe somewhat misleading as better determination of damping for the higher modes could provide better results. It is apparent that a dominant portion of the response is adequately characterized by as few as two modes.

3.5 Summary

A modelling process to generate a linear model for use in controlling flexible manipulators was presented, and compared to experimental measurements for a position, and rate feedback controller. The model agreed favorably with the measured response for a selection of clamped-mass assumed modes. The dominant parts of the transient response were characterized by inclusion of as few as two assumed flexible modes.

The selection of appropriate assumed modes must consider the feedback law, as the applied torque dominates the boundary condition at the base of the beam. Clamped-mass modes yielded good results for the simple collocated controller, however this may not prove true for more sophisticated controllers.

CHAPTER IV

MODEL ORDER REDUCTION

Truncation of the modal series is required to achieve a model suitable for implementation in real-time. Based on initial estimates of computational speed a model treating two flexible modes was targeted for this study. While verifying the linearized model, as discussed in the earlier chapter, the two mode model was found to characterize the major portion of the response. This process was completely arbitrary, and satisfactory performance of the controller was in no way guaranteed. It was therefore desirable to seek an analytical means to estimate the required model order, especially when looking forward to research on multi-link systems.

Professor Dorsey, Electrical Engineering Dept./ Georgia Tech., suggested the use of balanced realizations as a method for providing the model order estimate. Balanced realizations is based upon singular value decomposition of linear systems [IV1]. This suggestion was based upon the similarity of the model used in this work to one he was familiar with in power systems research. The linearized version of a power system model is shown in figure 4-1. The states are the $\Delta\delta$ variation in angles, and $\Delta\omega$ variation in speeds for the generators. M represents the inertial matrix

of the generators, γ represents damping. T represents the change in electrical power with respect to the angle variations $\Delta\delta$, and L depicts the change in electrical power with respect to the load power.The linearized model for the manipulator is repeated in figure 4-2. The structural similarities are readily

$$
\begin{vmatrix}
\Delta\dot{\delta}_1 \\
\Delta\dot{\delta}_2 \\
\Delta\dot{\delta}_3 \\
\vdots \\
\Delta\dot{\omega}_1 \\
\Delta\dot{\omega}_2 \\
\Delta\dot{\omega}_3 \\
\vdots
\end{vmatrix}
=
\begin{vmatrix}
0 & I \\
\hline
M^{-1}T & -\gamma I
\end{vmatrix}
\begin{vmatrix}
\Delta\delta_1 \\
\Delta\delta_2 \\
\Delta\delta_3 \\
\vdots \\
\Delta\omega_1 \\
\Delta\omega_2 \\
\Delta\omega_3 \\
\vdots
\end{vmatrix}
+
$$

$$
\begin{vmatrix}
0 & 0 \\
\hline
M^{-1} & M^{-1}L
\end{vmatrix}
|u|
$$

Figure 4-1. Power System Model.

apparent between the two types of systems. Additionally, Dr. Dorsey had robust software machinery evaluating the power system models. Troullinos, and Dorsey [IV2] wrote an introductory paper on model order estimation with this method, and that material is presented next to familiarize readers with the method before discussing its application to the flexible manipulator.

$$
\begin{vmatrix} \dot{\theta} \\ \dot{q}_1 \\ \dot{q}_2 \\ \vdots \\ \ddot{\theta} \\ \ddot{q}_1 \\ \ddot{q}_2 \\ \vdots \end{vmatrix} = \begin{vmatrix} 0 & I \\ \hline & \\ M^{-1}K & 0 \end{vmatrix} \begin{vmatrix} \theta \\ q_1 \\ q_2 \\ \vdots \\ \dot{\theta} \\ \dot{q}_1 \\ \dot{q}_2 \\ \vdots \end{vmatrix} + \begin{vmatrix} 0 \\ \hline \\ M^{-1}Q \end{vmatrix} |u|
$$

Figure 4-2. Manipulator Model.

4.1 Order Reduction of Static Systems

The basic motivation for balancing linear dynamic systems is rooted in linear algebra. Given the system

$$
y = Tx \tag{4.1}
$$

where T is an $n \times m$ matrix, an intuitive, geometric interpretation of the potential redundancy of the system's

variables can be achieved using spaces R(T), R(T') and their respective orthogonal complements Ker(T'), and Ker(T). Ker(T) is the nullspace of T, the subspace spanned by all vectors x such that Tx=0. T' is the transpose of T. Figure 4-3 summarizes the relationships between these four subspaces.

Assume that m<n. Any m-dimensional vector x can be represented as the sum of its projection x_r, on R(T') and x_k, on Ker(T). That is x = x_r + x_k. Similarly any n-dimensional vector y can be represented as y= y_r+y_k, the sum of its projections on R(T) and Ker(T'). Then y_r = Tx = T(x_r + x_k) = Tx_r + 0 = Tx_r. Thus, effectively, T can be thought of as an invertible transformation from R(T') to R(T). The inverse transformation that takes Tx back to x is called the psuedo-inverse [IV3].
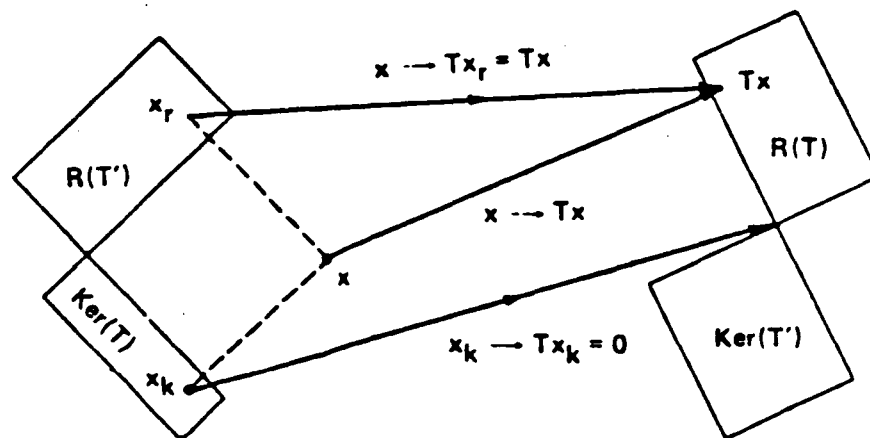
Figure 4-3. Relationship Between Subspaces.

The subspace decomposition described above provides an elegant and intuitive picture of linear transformations. The necessary complement to this theoretical picture is a robust computational method of decomposing the matrix T. Every n x m matrix T can be factored as $T = U\Sigma V'$ with U an n x n orthogonal matrix, V an m x m orthogonal matrix and Σ an n x m matrix that has the special form

$$
\begin{bmatrix}
\sigma_1 & & & \\
& \sigma_2 & \cdot & \\
& & \cdot & \\
& & & \cdot \\
& & & \sigma_m \\
\hline
& & 0 &
\end{bmatrix}
\tag{4.2}
$$

where the σ_i are the nonnegative square roots of the eigenvalue of the matrix T'T. If T is of maximum rank, then all the σ's will be non-zero. If the rank of T is $r<m$, then only the first r diagonal entries will be nonzero, in which case T can be written as

$$
T = [U_r \ U_k]
\begin{bmatrix}
\Sigma_r & 0 \\
0 & 0
\end{bmatrix}
\begin{bmatrix}
V_r' \\
V_k'
\end{bmatrix}
\tag{4.3}
$$

where $\Sigma_r = \text{diag}(\sigma_1, \sigma_2, \cdots, \sigma_r)$ and $U_r, U_k, V_r,$ and V_k are orthogonal matrices which span R(T), Ker(T'), R(T), and Ker(T), respectively.

The singular values have the crucial property that if T is perturbed slightly to $T_\Delta = T + \Delta T$, then the singular values of T_Δ will be "close" to the singular values of T. Thus if T is of $r<m$ then the decomposition of the

transformation T_Δ would yield

$$T_\Delta = [U_{r\Delta} \; U_{k\Delta}] \begin{bmatrix} \Sigma_{r\Delta} & 0 \\ 0 & \Sigma_{k\Delta} \end{bmatrix} \begin{bmatrix} V'_{r\Delta} \\ V'_{k\Delta} \end{bmatrix} \qquad (4.4)$$

where the singular values of $\Sigma_{k\Delta}$ would be small compared to the singular values of $\Sigma_{r\Delta}$. Thus $T = U_{r\Delta}\Sigma_{r\Delta}V'_{r\Delta}$ would be a good approximation of the original transformation $T = U_r\Sigma_r V'_r$. Even in the case where T is known exactly, if the singular values can be segregated into two groups where the members of one group are much smaller than the members of the other, then the matrix $U_{r\Delta}\Sigma_{r\Delta}V'_{r\Delta}$ may still be a useful approximation to the matrix $U_r\Sigma_r V'_r$. It is this latter point of view that is exploited in the next section.

4.2 Singular Value Decomposition Applied to Dynamic Systems

Given the linear time invariant system

$$\dot{x}(t) = Ax(t) + Bu(t) \qquad (4.5)$$

$$y(t) = Cx(t) \qquad (4.6)$$

two transformations are of interest. One is the transformation $T_c(t_1)$ from an initial state, $x(t_0)$, to a subsequent state, $x(t_1)$, under the influence of an input $u(t)$. The other is the transformation $T_0(t_1)$ from an initial state $x(t_0)$ to a subsequent output $y(t_1)$, with no input. The first transformation provides information about the controllability of the system, while the second,

information about the observability of the system. If the system has uncontrollable or unobservable states then the state space can in a sense be interpreted as degenerate, or not of full rank.

The linearized model for the flexible manipulator is assumed to be controllable and observable; this was checked in the computations. What is of interest are states that are nearly uncontrollable or unobservable. As in the static case these estimates can be obtained using singular value analysis for the system [IV4]. With $t_0 = 0$, the transformation from a given initial condition $x(t_0) = x_0$, with input $u(t)$ to $x(t_1)$ is described by [IV5];

$$x(t_1) = e^{At_1} x_0 + \int_0^{t_1} e^{A(t_1-\tau)} Bu(\tau)d\tau \qquad (4.7)$$

For the special case where $x(t_0) = 0$, and $u(t) = \delta(t)\tilde{u}$, where $\tilde{u}$ is a vector of impulse magnitudes,

$$x(t_1) = e^{At_1} B\tilde{u} \qquad (4.8)$$

It can be shown [IV6] that $R[T_c(t_1)] = R[W_c(t_1)]$ where

$$W_c(t_1) = \int_0^{t_1} e^{A\tau} BB' e^{A'\tau} u(\tau)d\tau \qquad (4.9)$$

Similarily for the unforced case

$$y(t_1) = Ce^{At_1} x_0 \qquad (4.10)$$

Thus $Ker[T_0(t_1)] = Ker[W_0(t_1)]$ where

$$W_0(t_1) = \int_0^{t_1} e^{A'\tau}C'Ce^{A\tau}d\tau \qquad (4.11)$$

$W_c(t_1)$ and $W_0(t_1)$ exhibit the same robustness found in the static case [IV7]. Thus if a singular value decomposition of $W_c(t_1)$ yields

$$W_c(t_1) = [U_1 \ U_2] \begin{bmatrix} \Sigma_1 & 0 \\ 0 & \Sigma_2 \end{bmatrix} \begin{bmatrix} V'_1 \\ V'_2 \end{bmatrix} \qquad (4.12)$$

where the singular values of Σ_1 are much larger than the singular values of Σ_2, then the number of nearly uncontrollable states is the dimension of Σ_2. A similar argument holds for $W_0(t_1)$.

One more step, that of balancing the system, is required. The size of the singular values can be interpreted as the "strength" of the individual states. That is, the singular values measure the extent to which a state is influenced by inputs and initial conditions. It can happen that a particular state will appear strong from the controllability perspective and weak from the observability perspective. A given state may, for instance, be strongly amplified by the B matrix and equally attenuated by the C matrix, or vice versa. Balancing the system is a method of equalizing the controllability and observability "ratings" of a state. That is, assuming that the system (eqns 4.5-6)

is minimal, balancing is achieved by finding a transformation, $x(t) = Tz(t)$ such that for the system

$$\dot{z}(t) = \hat{A}z(t) + \hat{B}u(t) \qquad (4.13)$$

$$y(t) = \hat{C}z(t) \qquad (4.14)$$

the controllability grammian $\hat{W}_C(t_1)$ and the observability grammian $\hat{W}_0(t_1)$ are identical. Noting that the controllability and observability grammians of equations (4.5-6) and (4.13-14) are related by

$$\hat{W}_C^2(t_1) = T^{-1}W_C^2(t_1)(T^{-1})' \qquad (4.15)$$

$$\hat{W}_0^2(t_1) = T' W_0^2(t_1) T' \qquad (4.16)$$

the desired transformation T can be obtained as follows. Let

$$W_C^2(t_1) = U_C(t_1)\Sigma_C^2(t_1)U_C'(t_1) \qquad (4.17)$$

$$W_0^2(t_1) = U_0(t_1)\Sigma_0^2(t_1)U_0'(t_1) \qquad (4.18)$$

be singular value decompositions of the two grammians of the unbalanced system. Define

$$H(t_1) = \Sigma_0(t_1)U_0(t_1)U_C(t_1)\Sigma_C(t_1) \qquad (4.19)$$

with singular value decomposition

$$H(t_1) = U_H(t_1)\Sigma_H(t_1)V_H'(t_1) \qquad (4.20)$$

and choose

$$T = U_0(t_1)\Sigma_0^{-1}(t_1)U_H(t_1)\Sigma_H^{\frac{1}{2}}(t_1) = \quad . \qquad (4.21)$$

$$U_C(t_1)\Sigma_C(t_1)V_H(t_1)\Sigma_H^{-\frac{1}{2}}(t_1)$$

It is then a straightforward calculation to show that

$$\hat{W}_C^2(t_1) = [\Sigma_H^{\frac{1}{2}}(t_1)V_H'(t_1)\Sigma_C^{-1}(t_1)U_C'(t_1)] \qquad (4.22)$$

$$[U_C(t_1)\Sigma_C^2(t_1)U_C'(t_1)][U_C(t_1)\Sigma_C^{-1}(t_1)V_H(t_1)\Sigma_H^{-\frac{1}{2}}(t_1)]$$

$$= \Sigma_H(t_1) = \hat{W}_0^2(t_1)$$

By rank ordering the singular values of $H(t_1)$, i.e. the diagonal elements of $\Sigma_H(t_1)$, the balanced model can be divided into two subsystems, one associated with the larger singular values and one associated with smaller singular values as

$$\begin{bmatrix} \dot{z}_1 \\ \dot{z}_2 \end{bmatrix} = \begin{bmatrix} \hat{A}_{11} & \hat{A}_{12} \\ \hat{A}_{21} & \hat{A}_{22} \end{bmatrix} \begin{bmatrix} z_1 \\ z_2 \end{bmatrix} + \begin{bmatrix} \hat{B}_1 \\ \hat{B}_2 \end{bmatrix} u \qquad (4.23)$$

$$y = [\hat{C}_1 \quad \hat{C}_2] \begin{bmatrix} z_1 \\ z_2 \end{bmatrix} \qquad (4.24)$$

The reduced order model is the subsystem associated with the large singular values:

$$\dot{z}_1 = \hat{A}_{11} z + \hat{B}_1 u \qquad (4.25)$$

$$y = \hat{C}_1 \quad z_1 \qquad (4.26)$$

4.3 Application to Flexible Manipulator Model

Using modeling software developed for this thesis a model was generated including one rigid mode, and nine flexible modes. A small joint angle position gain, 50, and velocity gain, -10, was introduced with small amounts of modal damping, (damping ratios of .007-.010), to insure that all eigenvalues had negative real parts before executing the analysis software.

To evaluate the contribution of each mode, and thus infer the required model order, requires some measure of performance. The selected performance index is that proposed by Moore[IV8]. For the manipulator model with N/2 = 10 modes, one rigid and nine flexible, the singular values are rank ordered from the smallest to the largest. Then a performance index of the form:

$$p(i) = \frac{[\sum_{j=1}^{2i} \sigma_j^2]^{\frac{1}{2}}}{[\sum_{k=2i+1}^{2N-2} \sigma_k^2]^{\frac{1}{2}}} \qquad (4.27)$$

is evaluated for i = 1,2,..., N-2 since the singular values occur in complex conjugate pairs. The numerator and denominator of p(i) represent, respectively, the square root of the sum of the squares of the singular values associated with the aggregated and unaggregated modes. Each mode aggregation reduces the number of singular values by two,

and hence at an aggregation level of (N-4)/2, the entire manipulator model has been reduced to one rigid and one flexible mode.

The linear model for the flexible manipulator was evaluated with the above process by Dr. Dorsey with software he had created for analysis of power systems. The result of the computations are presented graphically in figure 4-4, and agree well with the qualitative results presented in chapter3. As can be seen from figure 4-4, the curve makes a sharp change in slope after an aggregation level of six, and the performance level quickly rises. This indicates that most of the model is represented by three modes, one rigid and two flexible, at an aggregation level of (N-6)/2 or 7.
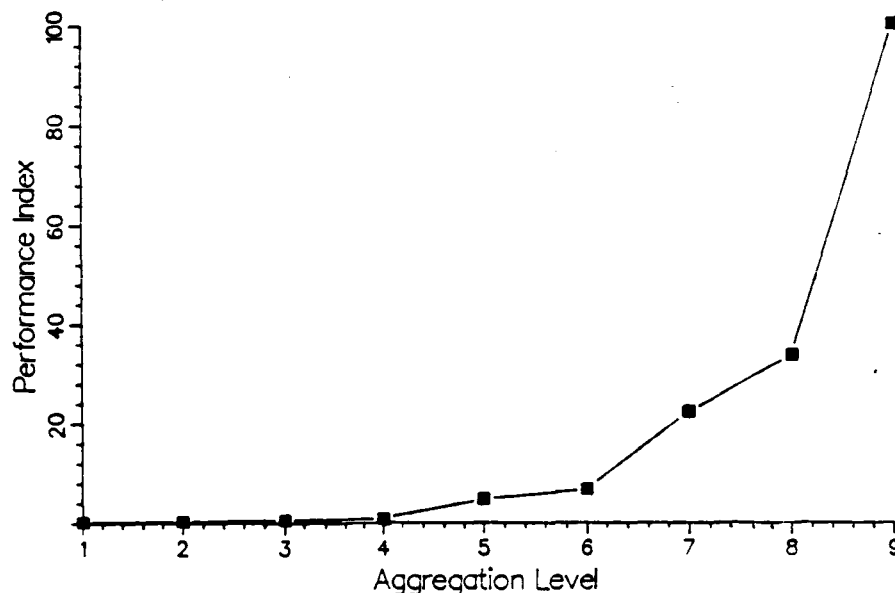
Figure 4-4. Aggregation Level

CHAPTER V

MEASUREMENT AND RECONSTRUCTION OF FLEXIBLE VARIABLES

This section describes the approach used to determine the state variables associated with flexible deflections. The position of any single point along the beam can be described as a combination of the rigid body motion, and flexible deflections. The approach taken in this work is to describe the flexible deflections by a modal series. This means that the flexible deflection is a linear combination of variables, and any single measurement of beam state, position, or strain etc., yields information about several modes.

To realize the potential of linear systems theory, in particular to implement full state feedback, knowledge of each state must be available to the control law. The task then is to gain information about each flexible state variable from the measurements.

5.1 Measurement and Reconstruction

Joint angles, and joint rotational speeds can be measured directly as for rigid manipulators, however for state feedback control of manipulator flexibility it is desirable to make direct measurements of the modal variables. Three types of measurement are currently

receiving attention for experimentally controlling flexibility in manipulators: optical measurement of end point position [V1-2], optical measurement of deflection [V3], and measurement of strain on the link [V4]. The measurement selected for this work is strain. Strain measurement has the following beneficial aspects:

- Isolates beam variables from rigid motions.
- No restrictions on work envelope or positioning.
- High compatibility with harsh industrial environments subjecting the sensors to process sprays of oils, solvents, and dispersed solids.
- Low cost sensor and driving electronics with simple technology base.

Additionally, the concept presented here can be applied almost directly to optical measurements of deflection. Measurement zeroes observed in end-point position measurements [V1] by sensors mounted external to the manipulator may adversely affect application of reconstruction to this means of measurement.

5.2 Strain Relationships

The moment at any location along the beam is related to the curvature of the beam:

$$M = EI\frac{\partial^2 w(x,t)}{\partial x^2} \tag{5.1}$$

The stress of the fibers along the surface of the beam due

to bending can be determined from the moment:

$$\sigma = \frac{Mc}{I} \qquad (5.2)$$

The strain due to bending is then:

$$\varepsilon = \frac{\sigma}{E} \qquad (5.3)$$

The strain can now be given in terms of the beam deflection $w(x,t)$:

$$\varepsilon(x,t) = c\frac{\partial^2 w(x,t)}{\partial x^2} \qquad (5.4)$$

Assumed mode representation of the flexible deflections can be expressed by:

$$w(x,t) = \Sigma\phi_i(x)q_i(t) \qquad (5.5)$$

The strain can then be represented in terms of the assumed modes as:

$$\varepsilon(x,t) = c\Sigma q_i(t)\frac{d^2\phi_i}{dx^2}(x) \qquad (5.6)$$

Equation (5.6) can be expanded to clearly show the contributions of each flexible mode to the measurement of strain at a location $x = a$ on the beam.

$$\varepsilon(a,t) = c[\frac{d^2\phi_1}{dx^2}(a)q_1(t) + \frac{d^2\phi_2}{dx^2}(a)q_2(t) + \qquad (5.7)$$

$$\cdots \frac{d^2\phi_n}{dx^2}(a)q_n(t)]$$

For strain measurements at several locations a, b, ...,m

this relationship can be presented in matrix form:

$$
\begin{vmatrix} \varepsilon(a,t) \\ \varepsilon(b,t) \\ \vdots \\ \varepsilon(m,t) \end{vmatrix} = \begin{vmatrix} c\dfrac{d^2\phi_1}{dx^2}(a) & c\dfrac{d^2\phi_2}{dx^2}(a) & \cdots & c\dfrac{d^2\phi_n}{dx^2}(a) \\ c\dfrac{d^2\phi_1}{dx^2}(b) & c\dfrac{d^2\phi_2}{dx^2}(b) & \cdots & c\dfrac{d^2\phi_n}{dx^2}(b) \\ \vdots & \vdots & & \vdots \\ c\dfrac{d^2\phi_1}{dx^2}(m) & c\dfrac{d^2\phi_2}{dx^2}(m) & \cdots & c\dfrac{d^2\phi_n}{dx^2}(m) \end{vmatrix} \begin{vmatrix} q_1(t) \\ q_2(t) \\ q_3(t) \\ \vdots \\ q_n(t) \end{vmatrix}
$$

(5.8)

The relationship depicted above relates the flexible variables to the strain measurements, and can be expressed as a variable transformation T^{-1}.

$$\varepsilon = T^{-1}q \qquad (5.9)$$

The desired form of the transformation is to "reconstruct" the flexible mode amplitudes from the strain measurements.

$$q = T\varepsilon \qquad (5.10)$$

The number of strain measurements m, is practically a small number, (2, 4 etc.), while the number of modes, n, typically used to characterize vibration is large, (10, 20 etc.). This would result in a rectangular matrix, and direct inversion to obtain the desired reconstruction matrix T would not be possible. In the case of more measurements than modes to be determined, a least squares weighting may be appropriate.

Based upon previous experimental results, discussed in chapter 3, it was decided to investigate a model based upon two assumed modes with reconstruction accomplished from two strain measurements. This case results in a square matrix T^{-1}. Sensor locations for this case can be selected which provide independent measurement of the two modes assuring that T exists.

5.3 Sensor Placement

The next problem to be addressed is the placement of the two strain sensors. The specific type of sensor, and bridge arrangement to reduce sensitivity to temperature, axial, and transverse stresses is discussed in appendix E.
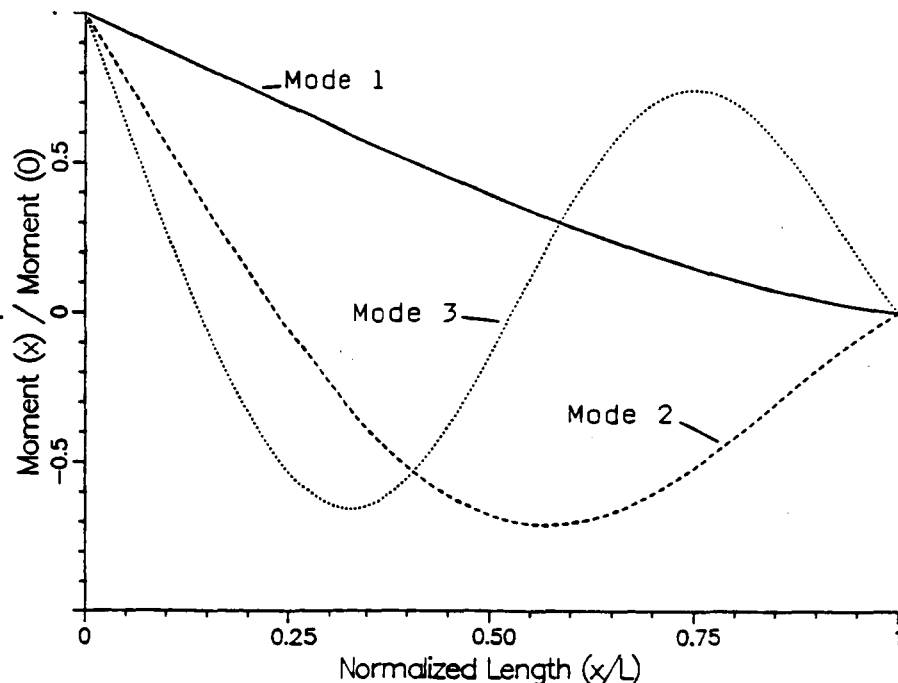
Figure 5-1. Moment Diagram.

The location of the sensors should be selected to provide measurement of significant signal levels, and yet enhance discrimination between the measured modes. Figure 5-1 presents moment diagrams for the first three clamped-mass modes.

All the clamped mode shapes had a peak at the end of the beam attached to the joint. It was decided to place one of the two sensors at the base of the beam to insure measurement of the first mode. Further examination of the moment diagram shows that the second mode moment has a peak just past the midpoint of the beam. Additionally, note that the third mode moment has a zero close to the midpoint of the beam.

It was decided to place the second set of strain gages at the midpoint of the beam. This provides good measurement of the second mode, yet avoids measurement of the third flexible mode. The sign change in the second mode moment, as opposed to the first moment should help the reconstruction algorithm to discriminate between the modal measurements.

CHAPTER VI

REDUCED ORDER OBSERVERS

The main thrust of this section is to describe the application of reduced order observers to the control of a flexible robot arm. Specifically, estimation of the unmeasured modal velocities via the application of a Luenberger [VI1] reduced order observer is presented.

This section begins with a brief section on estimation of state variables with full order observers and the associated error dynamics followed by a discussion of the motivation for using a reduced order observers.

The general relationships for reduced order observers is then developed including expressions for the error. The reduced order observer is then applied to the control of a flexible arm. Design freedom and robustness of the observers concludes this section.

6.1 Observation of the State of a Linear System

Luenberger[VI2] is recognized as pioneering much of the work on the observation of linear systems, however the following derivation is a compilation of the works by Luenberger, Gopinath[VI3], and Fortmann[VI4]. Equations (6.1-3) provide a state space description of a forced linear system with state feedback.

$$\dot{x} = Ax + Bu \qquad (6.1)$$

$$y = Cx, \quad C = I \qquad (6.2)$$

$$u = Ky \qquad (6.3)$$

For such a system knowledge of the initial state x_0, and input history are sufficient for determination of the state at any later time. However, many times the measurement matrix C is not an identity matrix, and alternate schemes must be utilized to realize the desired state controls. Figure 6-1 depicts an open loop observer for estimating the states of a linear system. The subscript m designates
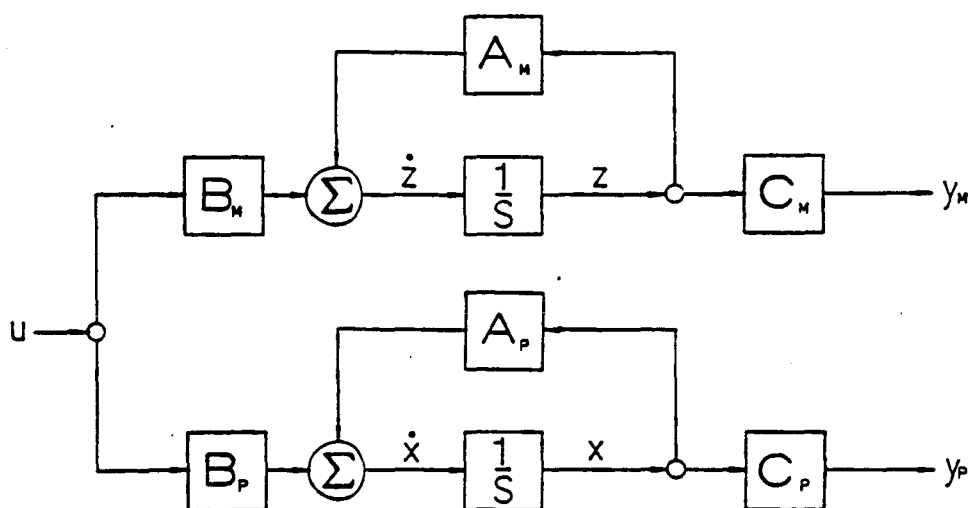
Figure 6-1. Open Loop Observation

modeled elements, while the subscript p refers to elements of the actual physical plant. Unavailability of information regarding initial states and modeling errors make open loop observation of the state variables impractical for most control applications. Figure 6-2 graphically depicts an observer utilizing measurements of the plant to improve the observation and reduce the sensitivity of the estimates of the to modeling errors, and initial states.

For the closed loop observer of figure 6-2 the estimated, or observed state z is described by;

$$\dot{z} = A_m z - LC(x-z) + B_m u \qquad (6.4)$$
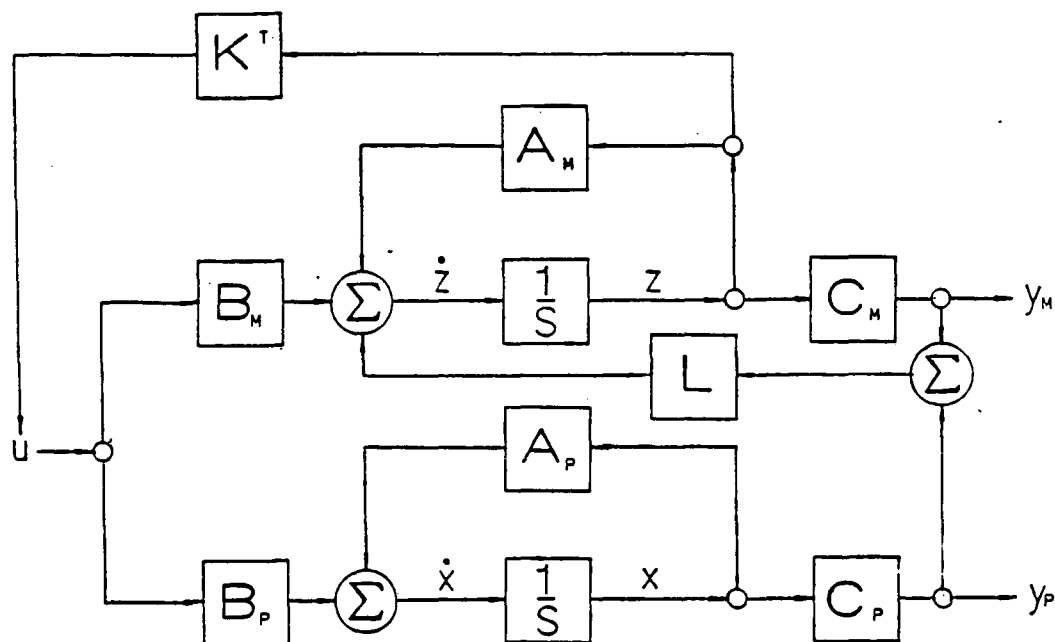
Figure 6-2. Observation with Measurement Update

and the plant state dynamics as;

$$\dot{x} = A_p x - B_p u \qquad (6.5)$$

6.1.1 Error Dynamics

Subtracting equation (6.4) from (6.5) yields and expression for the time rate of change of the error;

$$\dot{x} - \dot{z} = A_p x - A_m z - LC(x-z) + (B_p - B_m)u \qquad (6.6)$$

Accurate modeling of the plant dynamics and input dependence results in a simpler form of the error expression;

$$\dot{e} = (A-LC)e \qquad (6.7)$$

where;

$$e = x - z \qquad (6.8)$$

Examination of this expression for the error dynamics shows that a proper selection of the measurement gain matrix allows an arbitrary specification of the rate at which the error decays. Luenberger [VI1] proved this to be true as long as the system was completely observable, i.e. the pair AC was observable. Additionally, the error dynamics described by equation (6.7) will dominate the behavior even when some modeling errors exist, as long as measurement gain L provides the major contribution to the negative real parts of the eigenvalues.

6.1.2 Separability

The composite system can now be written in the following form;

$$\begin{bmatrix} \dot{x} \\ \dot{z} \end{bmatrix} = \begin{bmatrix} A & 0 \\ LC & A-LC \end{bmatrix} \begin{bmatrix} x \\ z \end{bmatrix} + \begin{bmatrix} B \\ B \end{bmatrix} u \qquad (6.9a)$$

for systems without feedback, and for systems with feedback based upon the estimated states;

$$\begin{bmatrix} \dot{x} \\ \dot{z} \end{bmatrix} = \begin{bmatrix} A & -BK \\ LC & A-LC-BK \end{bmatrix} \begin{bmatrix} x \\ z \end{bmatrix} + \begin{bmatrix} B \\ B \end{bmatrix} u \qquad (6.9b)$$

The eigenvalues of the composite system can be examined more readily after a simple transformation T is applied to the description.

$$T = \begin{bmatrix} I & 0 \\ I & -I \end{bmatrix} \qquad (6.10)$$

Premultiplication by T and postmultiplication by T^{-1} transforms the systems described by equations (6.9a) and (6.9b) into the following forms;

$$\begin{bmatrix} \dot{x}' \\ \dot{z}' \end{bmatrix} = \begin{bmatrix} A & 0 \\ 0 & A-LC \end{bmatrix} \begin{bmatrix} x' \\ z' \end{bmatrix} + \begin{bmatrix} B \\ B \end{bmatrix} u \qquad (6.11)$$

For systems without feedback this system obviously has the eigenvalues of both the plant, and the observer error dynamics. For systems with feedback based upon the estimated states;

$$\begin{bmatrix} \dot{x}' \\ \dot{z}' \end{bmatrix} = \begin{bmatrix} A-BK & -BK \\ 0 & A-LC \end{bmatrix} \begin{bmatrix} x' \\ z' \end{bmatrix} + \begin{bmatrix} B \\ B \end{bmatrix} u \qquad (6.12)$$

This system possess the closed loop poles of the plant in addition to the eigenvalues associated with the error. This separability allows for the design of the observer as a separate task from that of determining the state feedback.

6.2 Luenberger Reduced Order Observers

Direct measurement and reconstruction provides joint angle, joint velocity, and modal amplitude data for the controller. A reduced order observer can be designed to estimate the missing modal velocity amplitudes. The main advantage of a reduced order observer over full state estimation lies in computational savings; this translates into higher sampling frequencies during implementation.

The following paragraphs summarize the work of Luenberger[VI1], and Gopinath[VI3], reviewing the development of the equations which describe the behavior of reduced order observers. The system represented by (6.1-3) can can be partitioned into measured and unmeasured states as follows;

$$\left| \begin{matrix} \dot{x}_1 \\ \dot{x}_2 \end{matrix} \right| = \left| \begin{matrix} A_{11} & A_{12} \\ A_{21} & A_{22} \end{matrix} \right| \left| \begin{matrix} x_1 \\ x_2 \end{matrix} \right| + \left| \begin{matrix} B_1 \\ B_2 \end{matrix} \right| |u| \qquad (6.13)$$

$$C = |I \quad 0| \qquad (6.14)$$

x_1 are the m measure states while x_2 are the unmeasured states to be estimated. Figure 6-3 presents a block diagram

of a reduced order observer which is described by;

$$\dot{z} = A_{22}z - LC(x_2-z) + A_{21}x_1 + B_2u \qquad (6.15)$$

z is the estimate of the states x_2. The error dynamics for this system can be obtained by subtraction of equation (6.18) describing the unmeasured states from the estimation equation (6.15).

$$\dot{e}_2 = (A_{22} - LA_{12})e_2 \qquad (6.16a)$$
$$e_2 = x_2 - z \qquad (6.16b)$$

This estimate depends directly upon the measurement of the states it is desired to determine. The dependence on measurements of x_2 can be eliminated via substitution of (6.20) with the following result;

$$\dot{z} = (A_{22}-LA_{12})z + L\dot{x}_1 - LA_{11}x_1 + (B_2-LB_1)u \qquad (6.17)$$
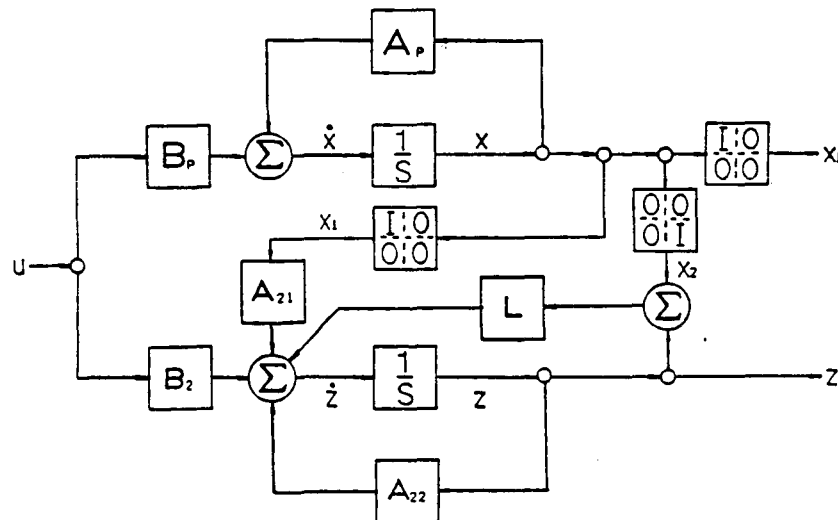
Figure 6-3. Reduced Order Observer

This result, although direct, allows little insight and may cause some confusion. The following derivation follows a more heuristic path, and provides more insight into the derivation process.

To accomplish this, first cull the expressions for the unmeasured states from equation (6.13);

$$\dot{x}_2 = A_{22}x_2 + A_{21}x_1 + B_2u \qquad (6.18)$$

The quantity,

$$A_{21}x_1 + B_2u \qquad (6.19)$$

which appears in equation (6.15) can be considered as a known input as it contains only measure and computed quantities. Next, the expressions for the measured state velocities can be separated and reorganized as;

$$\dot{x}_1 - A_{11}x_1 - B_1u = A_{12}x_2 \qquad (6.20)$$

The terms to the left side of the equal sign;

$$\dot{x}_1 - A_{11}x_1 - B_1u \qquad (6.21)$$

contain only measured quantities, their derivatives, and the computed inputs u. Combining equation (6.18), and (6.20) results in an estimation equation;

$$\dot{z} = (A_{22}-LA_{12})z + A_{21}x_1 + L(\dot{x}_1-A_{11}x_1-B_1u) + B_2u \qquad (6.22)$$

Equation (6.22) provides an observation of the unmeasured states, based on state measurements, the time derivative of the measurements, and the inputs. Additionally, the

measurement gain L appears to have the ability to specify the error dynamics. This equation is represented in block diagram form in figure 6-4.

6.2.1 Adaptation for Implementation

The resultant observation equation (6.22) meets the objective of controlling the rate at which the error converges, and eliminates the sensitivity to initial states as the process proceeds. The equation does, however, require the time derivative of the measured states. The time derivative of the measured states may be the variables it is
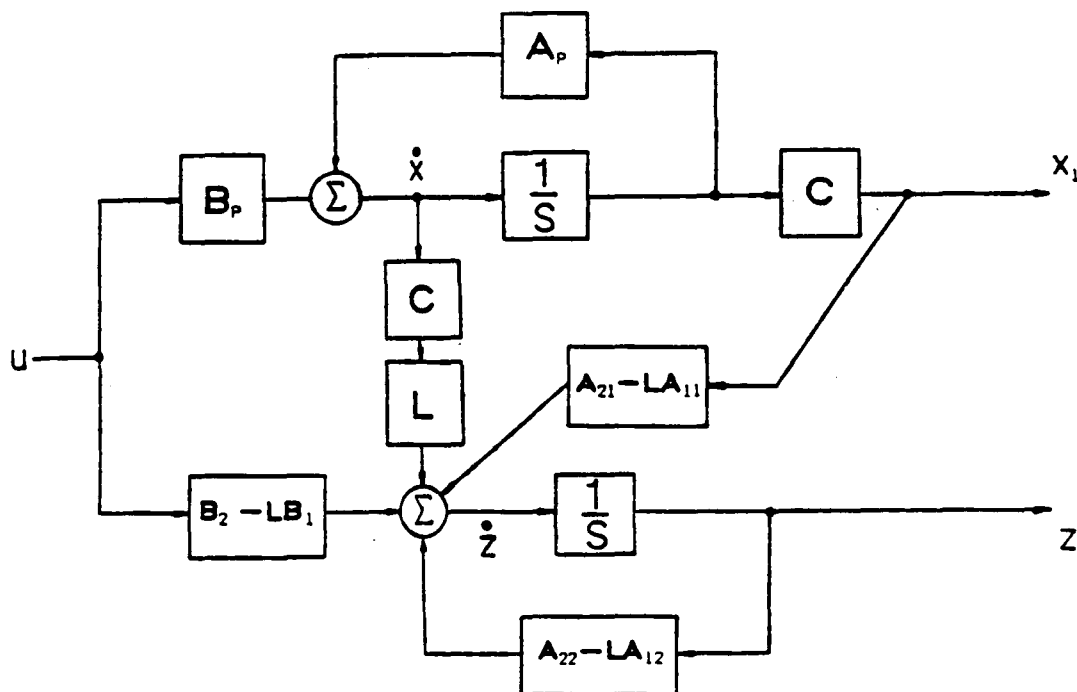
Figure 6-4. Observer with Measurement, and Measurement
Derivatives

desired to estimate. This is indeed the case for the flexible arm.

Figure 6-5 depicts an estimation system which does not require knowledge of the time derivative of the state measurements. This is accomplished by utilizing the following substitution.

$$L\dot{x}_1 = (A_{22} - LA_{12})Lx_1 \qquad (6.23)$$

Insertion of this result into the estimation equation (6.22) yields;

$$\dot{w} = (A_{22} - LA_{12})w + [(A_{21} - LA_{11}) + (A_{22} - LA_{12})L]x \qquad (6.24)$$
$$+ (B_2 - LB_1)u$$

where,

$$z = w + Lx_1 \qquad (6.25)$$

The motivation for this substitution is made more apparent by noting the adjustments made to figure 6-4 in deriving the observer shown in figure 6-5. This adjustment effectively pushes the time derivative of the measurement through the integration block. Gopinath[VI3] showed that the error dynamics remain unchanged.

6.3 Application of Reduced Order Observers to Single Link Flexible Arms

This section describes the application of the general reduced order observer to the single flexible manipulator.

Reconstruction of the modal amplitudes is treated separately, and the following development considers these quantities as inputs for the estimation of the modal velocities.

Following the earlier partitioning scheme for measured, x_1, and unmeasured, x_2, states the state vectors for the flexible manipulator can then be organized as;

$$x_1^T = [\theta, q_1, q_2, \ldots, q_n, \dot{\theta}] \qquad (6.26)$$

$$x_2^T = [\dot{q}_1, \dot{q}_2, \ldots, \dot{q}_n] \qquad (6.27)$$

where the requirement is to form an estimate z of the modal velocities contained in the x_2 state vector. This form is directly compatible with the state space formulation derived
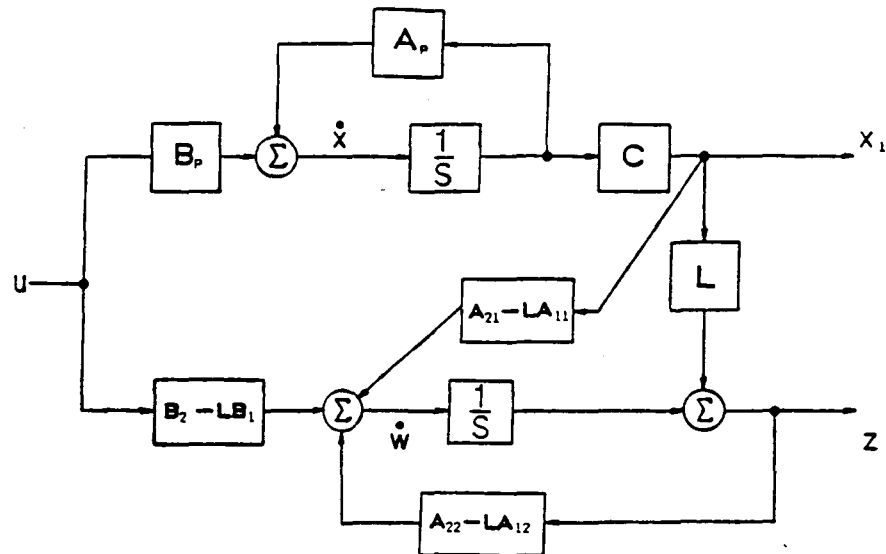
Figure 6-5. Adaptation for Implementation

in the dynamic modeling section. A conversion of the continuous estimation equations developed above to digital form appropriate for implementation in a micro-processor is accomplished by zero order hold equivalence.

6.3.1 Specification of the Measurement Gain L

The actual selection of the measurement gain matrix L for the flexible arm system is not as direct as that implied by a casual glance at the error dynamic equation (6.16). The estimation equation for the modal velocities of an n mode series is depicted in equation (6.28).

$$\dot{w} = [F]w + [L']x_1 + [B']u \qquad (6.28a)$$

$$F = A_{22} - LA_{12} \qquad (6.28b)$$

$$L' = (A_{21} - LA_{11}) + (A_{22} - LA_{12})L \qquad (6.28c)$$

$$B' = B_2 - LB_1 \qquad (6.28d)$$

$$z = w + Lx_1 \qquad (6.28e)$$

Where F the estimator dynamic matrix is nxn. Specification of estimator dynamic matrix F in equation 28a above results in n^2 equations. The measurement gain matrix L', however, is nx(n+2) and will have n^2+2n terms. Thus, a specification of the error dynamics does not completely determine the elements of L. This will occur whenever more state measurements are made than there are states to be estimated. This allows significant freedom to the designer, and use of this freedom to improve system

robustness will be discussed next.

6.4 Pole Placement and Robust Observers

The design freedom mentioned earlier can be used to
increase the robustness of the observer system. By examining
figure 6-6, a block diagram of the control implementation,
it is apparent that the observer utilizes commanded torque
as opposed to the actual torque. If the depicted system is
broken at node A, which would correspond to the servo-amp
for the motor turned off, the earlier discussion of poles
for the combined observer/plant system does not apply. The
poles are no longer separable, and the observer displays
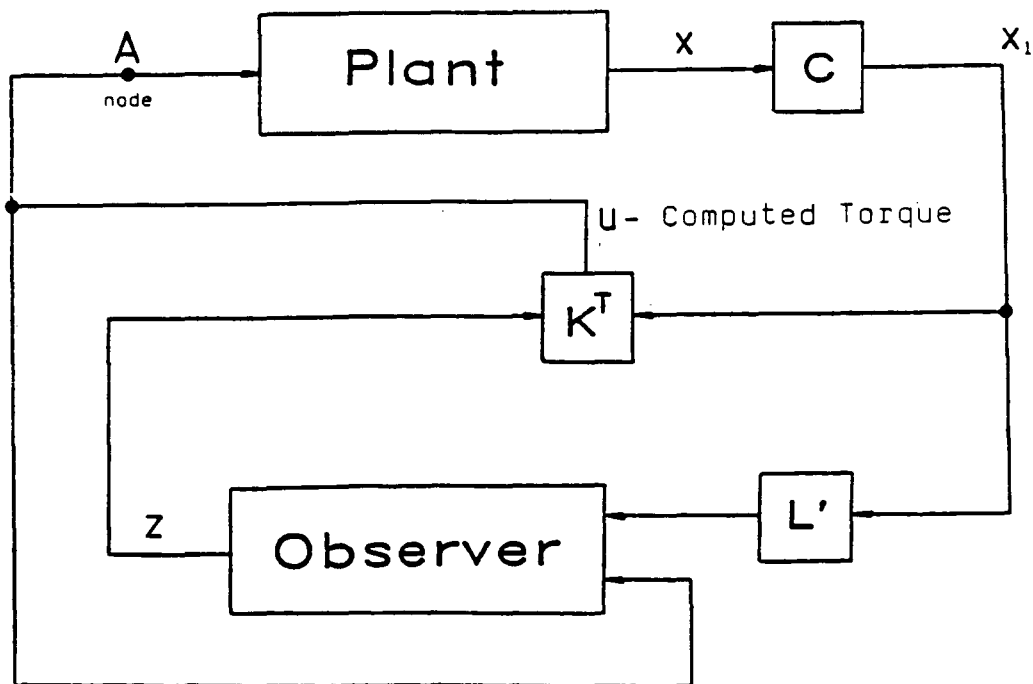
Figure 6-6. Implementation Block Diagram

"closed loop" poles described by;

$$A_{22}- LA_{12}-(LB_1-B_2)K_2 \qquad\qquad (6.29)$$

K_2 is a gain vector associated with modal velocities. These poles are not identified in the earlier discussion for observer design. Initial disturbances are readily available to this system via state measurement, and unstable poles quickly result in estimates which saturate the system. This results in an experimental system with a "hard start" behavior.

Problems of a similar nature were discussed by Doyle [VI5], and the reduction of sensitivity to this problem was termed an increase in robustness. The equations for the closed loop observer poles are combined with the equations for the observer dynamic matrix for determining the elements of the measurement gain matrix L.

6.5 Experimental Investigation

Real-time experiments were conducted to investigate modeling assumptions, and observer design performance. The major issues arising during implementation result from the truncation of the modal series made to achieve a low order model, and hardware performance. Balas [VI6] considered the possibility of control "spill-over" into the higher neglected modes having deleterious effects. Also, the proximity of the flexible poles to the imaginary axis makes the system intolerant of unmodeled phase terms introduced by

hardware[VI7].

6.5.1 Control Algorithm

A linear quadratic steady state regulator with a prescribed degree of stability was designed and implemented for a two mode model. The controller design was executed for a sample and hold system. An optimal regulator design was selected with gains large enough to contrast the step response performances of the different observer dynamic specifications. At low gains stability is hardly a problem, and at very large gains, component performance begins to cloud the observations.

6.5.2 Measured Performance

The first issue investigated was the impact of the cycle time of the controller. The reconstruction, observation, and control algorithm executed at roughly 178 Hz, more than ten times the flexible frequency to be controlled, yet only twice the fourth modal frequency and four times the third. The first four clamped modes of the system are presented in table 6-1.

Table 6-1. Natural Frequencies(Hz)

Mode	Measured	Calculated
1	2.08	2.096
2	13.92	13.989
3	41.38	41.524
4	81.18	81.225

The effect of the controller cycle time was examined by considering the step responses of a collocated controller (sensor and actuator at the same location) using joint angle, and joint velocity executing at 500Hz, as shown in figure 6-7, and at the speed of observer/controller, 178Hz, shown in figure 6-8. The joint angle, and strain at the base of the beam were used to characterize the time response. The gains utilized were the same as for the joint angle and joint velocity of the optimal regulator. The longer cycle time associated with the 178Hz controller resulted in a noticeable increase in the excitation of the third flexible mode. The amplitude of the flexible vibration is not as dramatic as the strain response.

Next, a zero order hold equivalent observer was designed with the discrete poles equivalent to negative real poles two and a half times the frequencies of the flexible poles being examined. The relationship between the flexible modes and the observer poles is shown in table 6-2. The result for this observer is shown in figure 6-9. The controller was most sensitive to the modal velocity
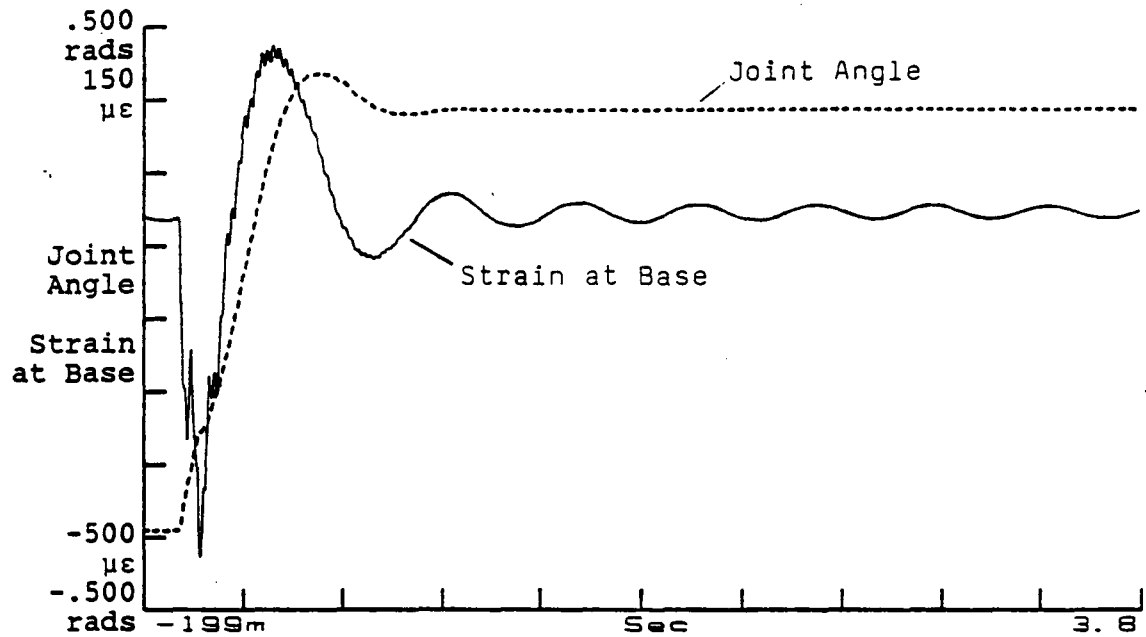
Figure 6-7. 500Hz Collocated Controller.
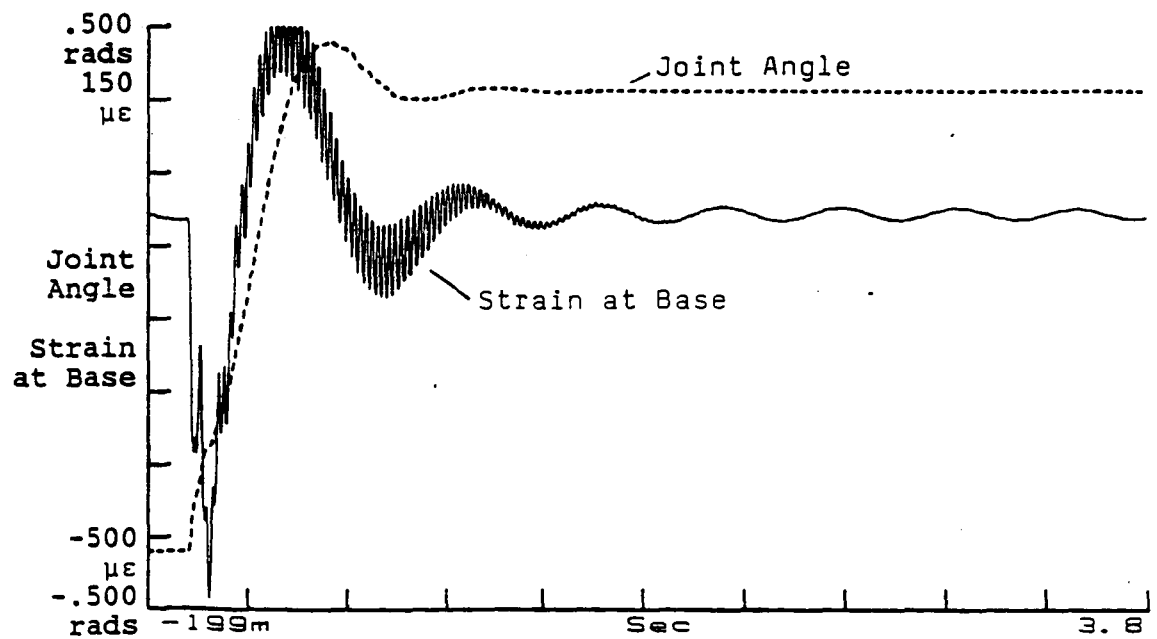
Figure 6-8. 178Hz Collocated Contoller

Table 6-2. Relationship between Flexible Modes
and Observer Poles

Modal Frequency	Equivalent Continuous Pole	
	Case 1(2.5x)	Case 2(5.0X)
2.08Hz	-5.2	-10.40
13.92Hz	-34.8	-69.60

gains produced by the observer. The instabilities did not occur in the modes which were being treated by the truncated model, but in the modes truncated for the model. The fourth mode at 81Hz also had an increased response although this is not apparent in the response. This is due to measurements and control torques aimed at the first two frequencies "spilling" over into the higher modes.
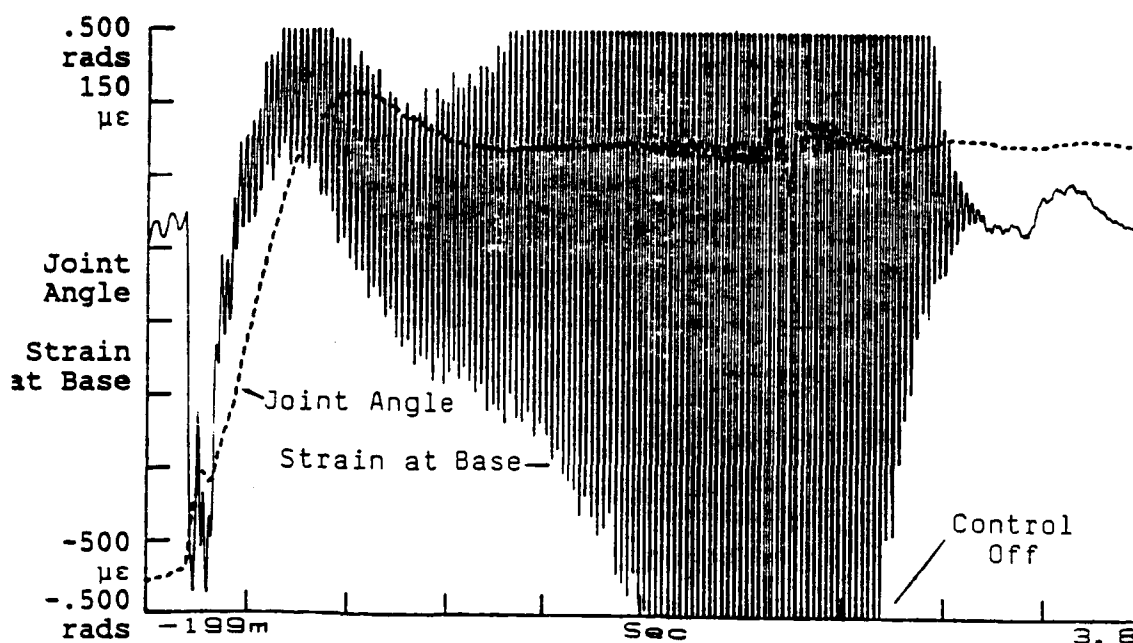
Figure 6-9. Step Response Case 1.

The measurement was repeated for an observer with poles at five times the flexible mode being treated. The relationship between the poles and the flexible modes is presented in table 2. The response for this observer/controller combination is shown in figure 6-10. This controller does a very good job of controlling the first two flexible modes, reducing the amplitude of the strain and quickly damping the vibration. The untreated third mode however is still noticeably excited, and the power spectrum indicated an increased excitation of the fourth mode.
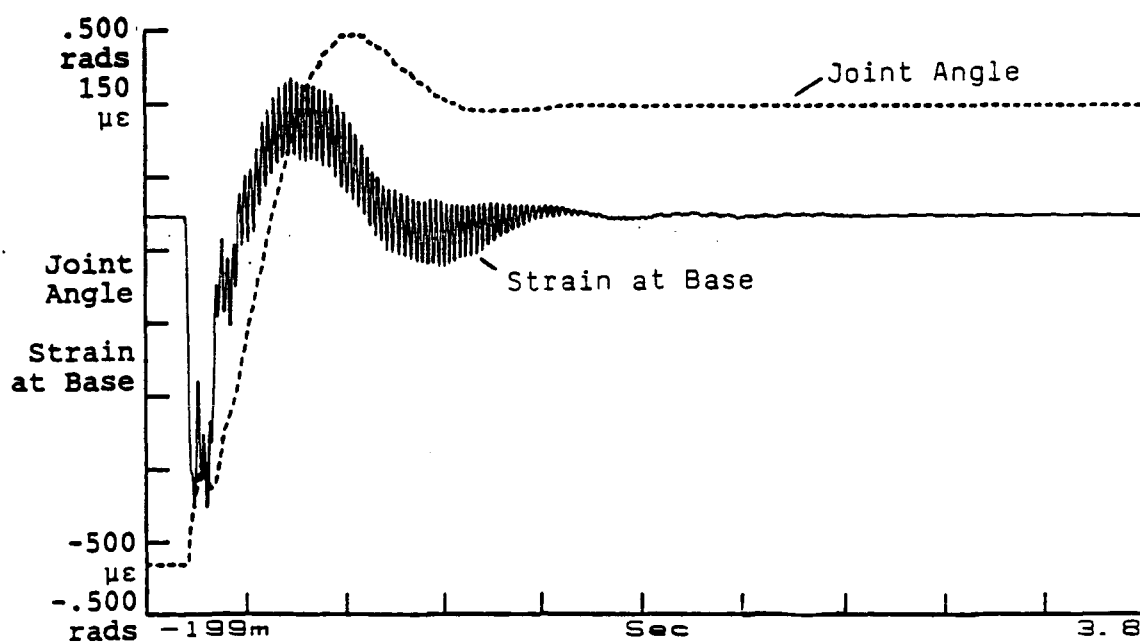
Figure 6-10. Step Response Case 2.

At higher gains, especially modal velocity gains even this observer yielded unstable results in the higher modes, though the controlled modes were consistently well damped. The indicated trend is to push the observer poles farther and farther to the left. Placing the faster observer pole equivalent to ten times the second flexible mode's pole results in characteristic times for the observer approaching the cycle time of the controller. The response for this observer/controller combination is depicted in figure 6-11. This combination resulted in significant excitation of the third mode, and for the first time a dramatic response in the fourth mode. This is counter to the trend, and most
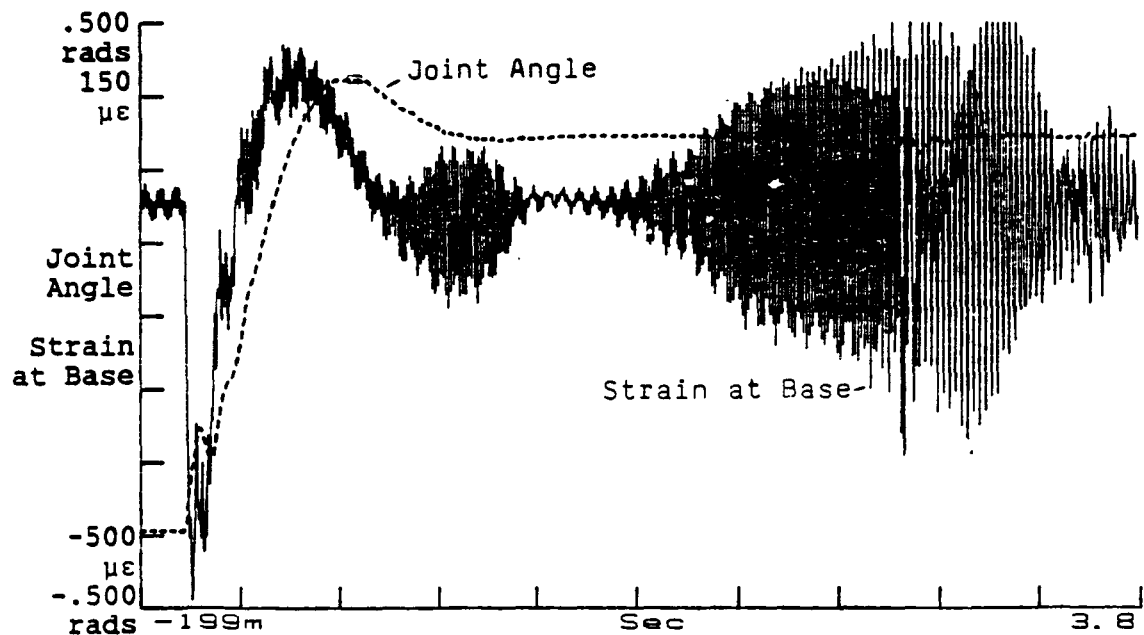
Figure 6-11. Step Response, Poles 10 x Mode

likely represents a fatal combination of increased noise sensitivity as the observer poles are pushed father to the left, and aliasing resulting from the controller cycle rate.

6.6 Summary

Reconstruction and observation of flexible variables for use in controlling a single link flexible arm has been successfully demonstrated. The results indicate that the negative real parts of the observer poles must be placed at least five times the magnitude of the flexible mode's frequency being estimated, and possibly faster for higher gains. Control spill-over was observed in several of the cases investigated, and was aggravated by slow observers to the point of unstable responses for some designs. A dominant factor in the design of high performance observers/ controllers for flexible systems appears to be the response of the higher modes. The application of passive damping [VI7], treating the neglected higher modes, may reduce the performance requirements of the observer/control system.

CHAPTER VII

OPTIMAL REGULATOR

7.1 Introduction

This section discusses the results of implementing an optimal linear state feedback controller based on quadratic criteria for the experimental arm. A steady state, or regulator, design with prescribed degree of stability was investigated experimentally. The control law K for the linear system described by,

$$\dot{x} = Ax + Bu \qquad (7.1)$$

$$u = K^T x \qquad (7.2)$$

is selected so as to minimized the quadratic performance index of equation (7.3)

$$PI = \frac{1}{2} \int [x^T Q x + u^T R u] dt \qquad (7.3)$$

over the process. The steady state gain solution is sought. The formulation and solution to this problem with a prescribed degree of stability, α, is discussed in detail in Appendix C, including modification for the discrete sampled and hold implementation.

The regulator is implemented for two models which include a single flexible mode, and two flexible modes in addition to the rigid mode. Inclusion of more flexible modes

hopefully increases the model accuracy and controller performance. Increasing the model order has a significant cost in cycle speed of the digital controller. The regulator which treats two flexible modes is discussed first.

7.2 Two Flexible Mode System

Based on initial estimates of computational capabilities, and initial experimental results examining model performance discussed in chapter 3, a base design treating the rigid motion, and two flexible modes associated with clamped-free vibration modes was selected. This selection of model order was supported by work which is recorded in chapters 3 and 4. The performance of a regulator based on this model is discussed in this section.

7.2.1 Controller Design

The parameters available to the designer affecting the performance of the LQR controller are the elements of the weighting matrices and the prescribed degree of stability. The initial weighting matrices utilized were taken from Sangveraphusiri's[VII1] earlier design and simulation work. Varying the elements of the weighting matrices as a tool for achieving performance improvements of the controller was extremely difficult. There is not a direct or intuitive approach to modification of the elements of the matrices which relates to performance goals, except in a broad sense. Gains are easily increased by reducing penalties on

actuation, but selectively altering velocity, or position state penalties had strange impacts on performance.

The most useful method for altering the performance was found to be obtained by varying the prescribed degree of stability. This proved to result in consistent trends, compatible with design intuition.

7.2.2 Implementation

The controller was implemented in software described in appendix F. A cycle time of 5.9 milliseconds was achieved for the two flexible mode controller. The controller results are inexorably linked to the performance of the modal velocity observer. The implemented observer was that presented in chapter 6 with error dynamics five times faster than the open loop poles being estimated. Good results, predicted from controller designs based on the truncated model, were often not realized in experiment. The experimental system was extremely sensitive to the second flexible mode damping gain as discussed in chapter six.

This limitation on damping in the second mode, apparently due to available computational speed, prevents a rigorous examination of this controller. Controller design by the use of a prescribed degree of stability can be extended to act as a pole placement algorithm. Specification of the diagonal elements of the stability matrix associated with the each of the states of a specific mode, the minimum degree of stability for each mode can be affected

independently. The stability matrix, resultant gains, and closed loop system eigenvalues for the first case to be discussed are presented in table 7-1.

Use of the prescribed degree of stability as a pole placement algorithm allowed for evaluation of the "best" combination for the two mode controller. The second flexible mode was made to have as great a degree of stability as possible without introducing instabilities into the higher modes as noticed in the observer evaluation. The performance of the system was then evaluated as the degree of stability for the rigid, and first flexible mode was increased independently of the second flexible mode.

7-1. Design Results, Stability Gain Vectors, Closed Loop Eigenvalues for Figures 7-1 and 7-2

Stability Matrix
α = diag[2.50 2.50 .2 2.50 2.50 .2]

Continuous Gains
F(collocated) = 111.2E+4   0.   0. 474.1 0.   0.
F(modal) =   111.2E+4 -406.7 -291.6 474.1 15.7 -6.40

Continuous Eigenvalues

Collocated Controller		Modal Controller	
-3.239	3.053E-16	-4.95	-4.78E-12
-11.98	-3.026E-15	-5.04	4.86E-13
-4.246	+/-15.11	-4.99	+/- 18.97
-.3071	+/-88.99	-.401	+/- 89.06

Discrete Gains
F(collocated) = 871.9   0.   0. 373.1 0.   0.
F(modal) =   871.9 -297.8 177.4 373.1 11.7 -5.3

Discrete Eigenvalues

Collocated Controller		Modal Controller	
.962	9.497E-18	.969	-.112
.975	-5.002E-15	.969	.112
.969	+/-9.539E-2	.976	+/-.0112
.863	+/-5.009E-1	.863	+/-.5008

7.2.3 Experimental Results

The first experiment conducted in this stage of the work was to compare a collocated controller to a modal controller by implementing the same joint variable gains in each case. A step response in joint angle was commanded, and the response measured. The response figures all contain two parts, part a depicts joint angle time response and motor current, part b presents strain measurements from the base and midpoints of the beam. The current represents torque applied at the joint, and the strain is a measure of the bending due to the flexible modes.

The degree of stability was the parameter varied for this test. The prescribed degree of stability was increased by increments of .25 until the stability of the collocated controller started to degrade, as shown in figure 7-1 (degraded response being an increase in the flexible mode response). The closed loop eigenvalues for the collocated case and modal controller are shown in table 7-1. Further increases of the prescribed degree of stability resulted in instabilities of the third flexible mode, for the collocated controller.

A modal controller with the same prescribed degree of stability in the rigid and first flexible mode, with limited stability in the second flexible is shown in figure 7-2. The increased stability of the higher mode is readily apparent in the strain response. After the large initial

transient, the torque response tries to actively control the flexible vibration. Note however that the flexibility is not fully controlled; this is thought to be due in part to hysteretic friction of the joint.

The degree of stability was increased for the rigid and first flexible mode, resulting in higher gains which would hopefully overcome the joint friction. The step response is repeated as shown in figure 7-3. The addition of the modal controller allows higher gains on the joint variables than was allowed for the collocated controller alone with this cycle time. The gains, and eigenvalues from the design process are shown in table 7-2. Note the increased damping of the
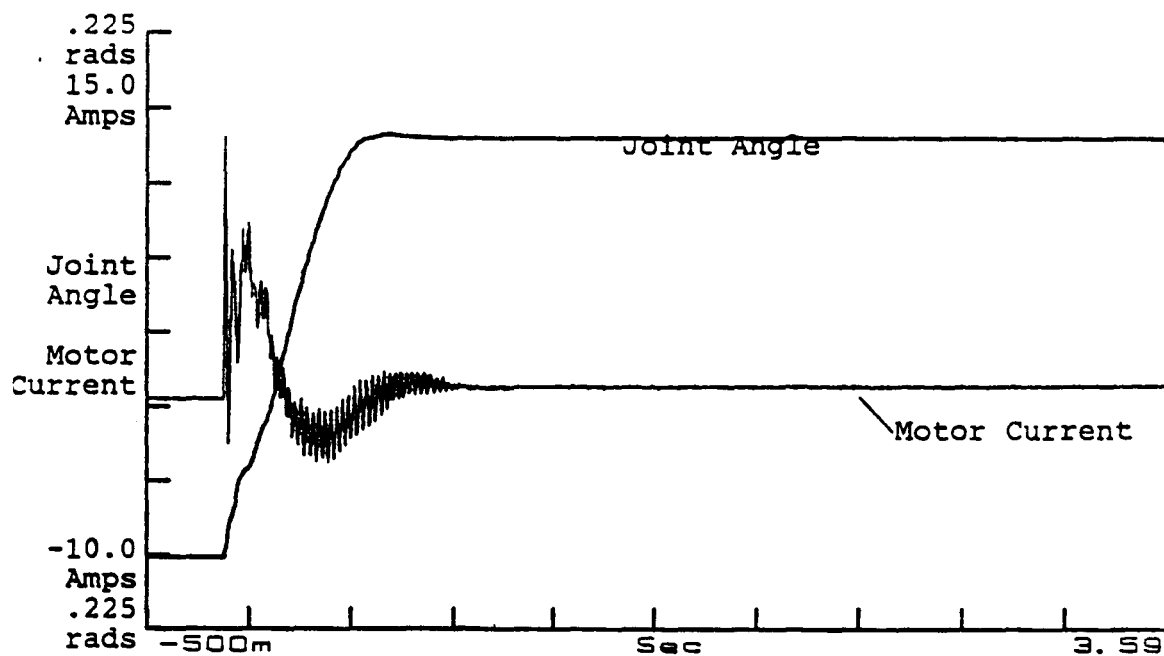
Figure 7-1a. Collocated Controller,
α = diag[2.50 2.50 .2 2.50 2.50 .2],
Joint Angle/Motor Current Step Response
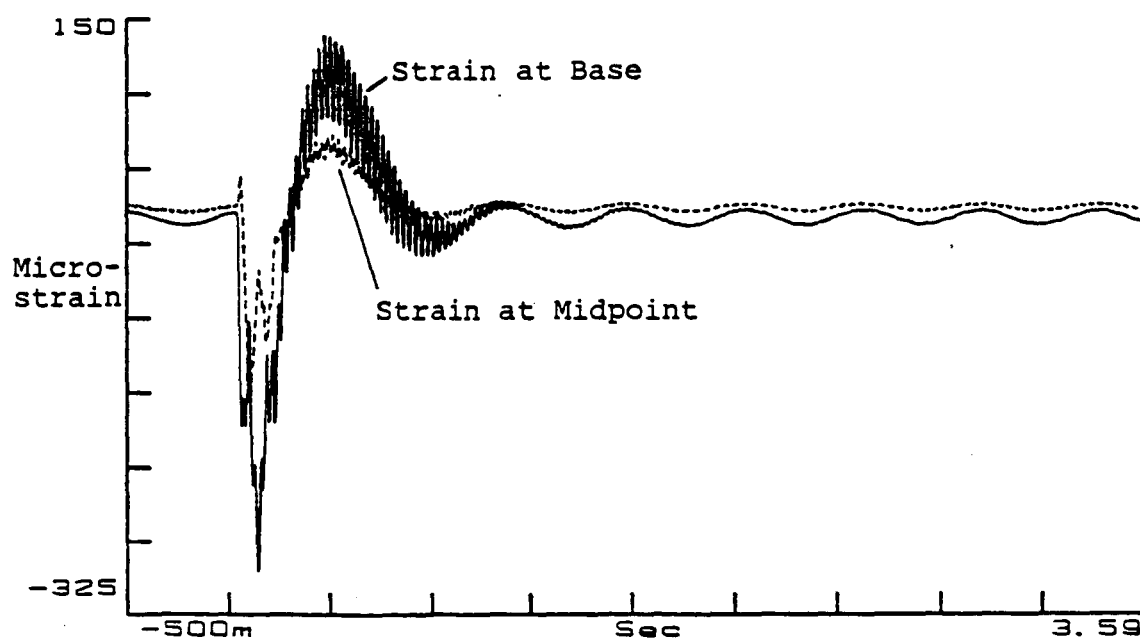
Figure 7-1b. Collocated Controller,
Strain at Base/Midpoint Step Response
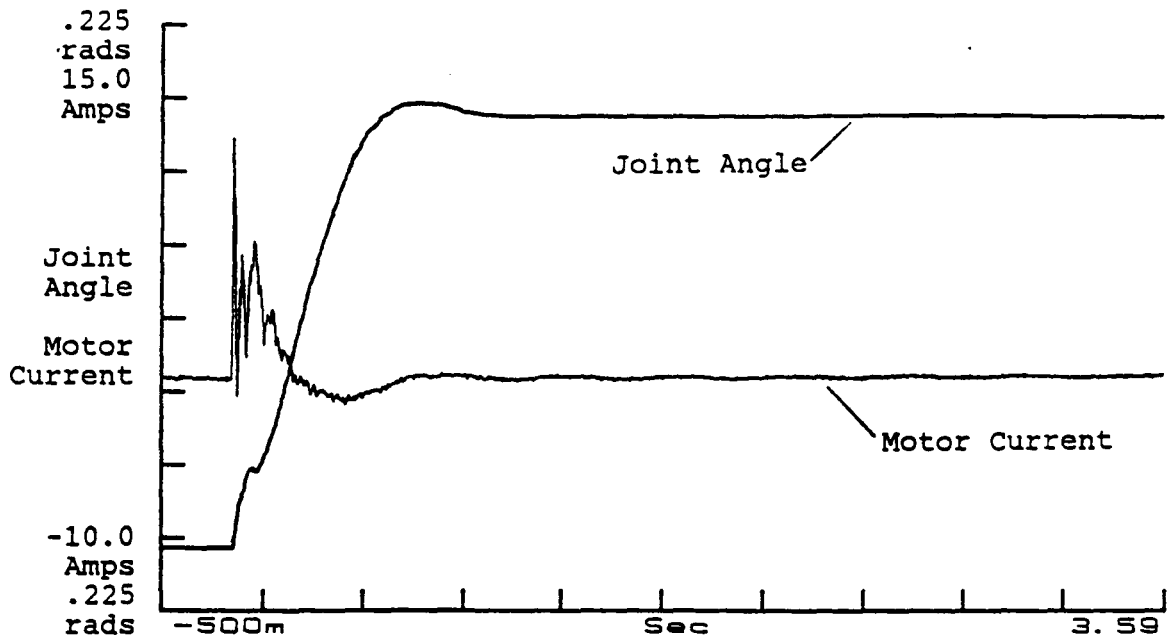
Figure 7-2a. Modal Controller,
α =diag[2.50 2.50 .2 2.50 2.50 .2],
Joint Angle/Motor Current Step Response
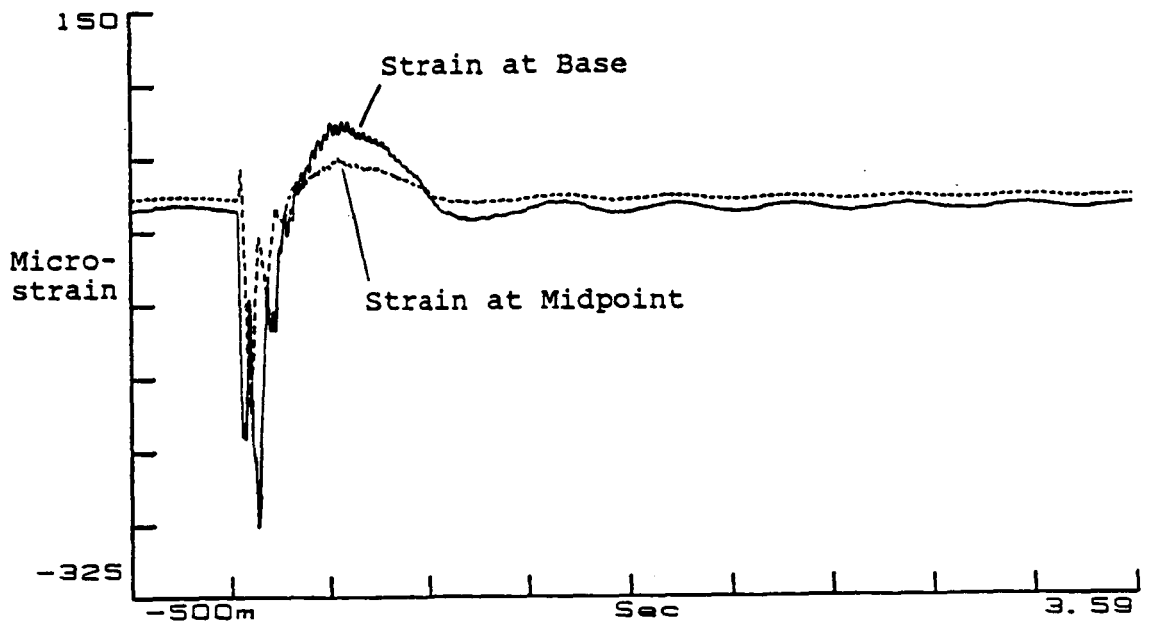
Figure 7-2b. Modal Controller,
Strain at Base/Midpoint Step Response
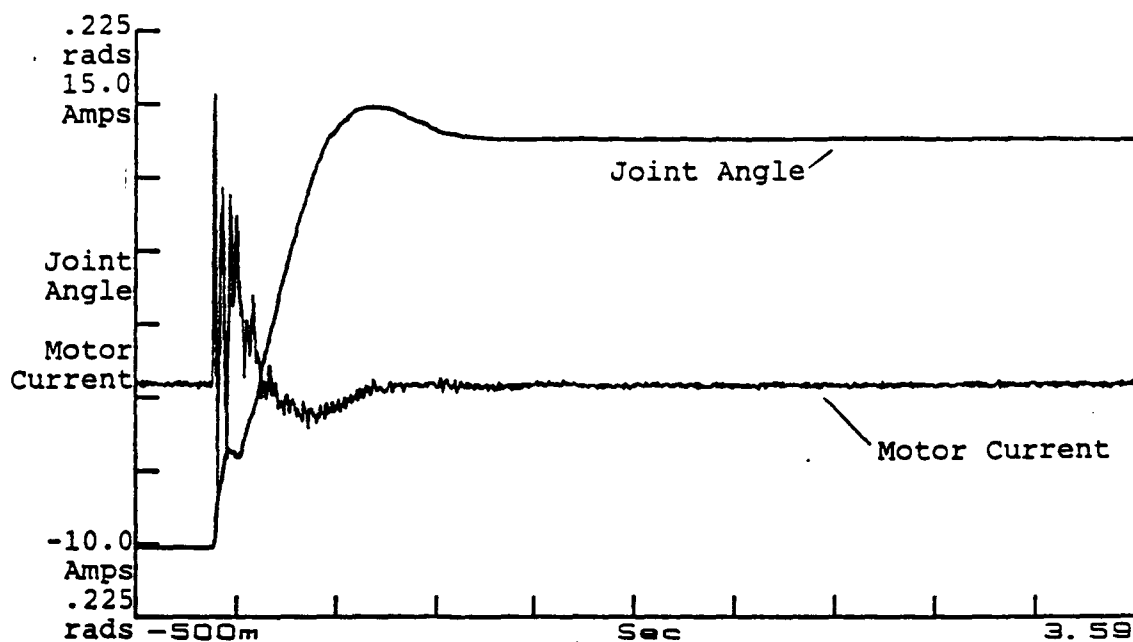
Figure 7-3a. Modal Controller,
α = diag[3.25 3.25 .2 3.25 3.25 .2],
Joint Angle/Motor Current Step Response
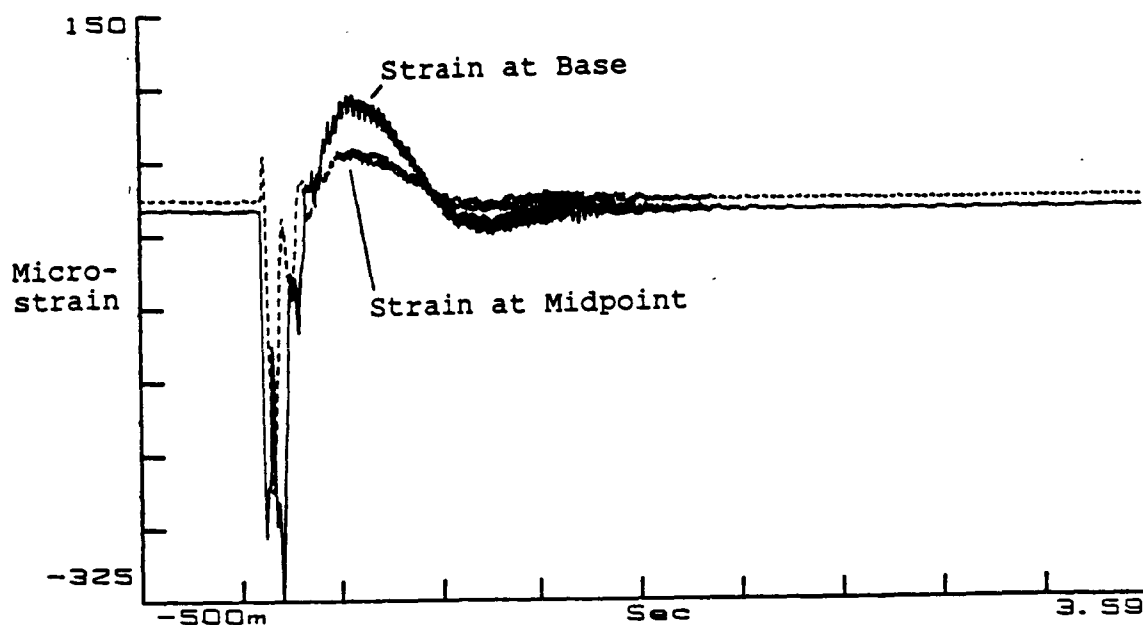
Figure 7-3b. Modal Controller,
Strain at Base/Midpoint Step Response

Table 7-2. Design Results, Stability Gain Vectors,
Closed Loop Eigenvalues for Figure 7.3

Stability Matrix
α = diag[3.25 3.25 .2 3.25 3.25 .2]

Continuous Gains
F(modal) = 1964.9 -699.1 -318.4 668.1 31.6 -1.83

Discrete Gains
F(modal) = 1523.2 -494.8 -34.5 520.8 23.6 -1.68

Continuous Eigenvalues Modal Controller		Discrete Eigenvalues Modal Controller	
-6.44	-7.49E-12	.961	-.113
-6.55	7.31E-12	.961	.113
-6.50	+/- 18.99	.969	+/-.0144
-.399	+/- 89.06	.863	+/-.5008

flexible mode in the response. This controller implemented with this prescribed degree of stability, however, appeared to be sensitive to noise and would often go into a steady vibration of limited amplitude. A second step command or touch of the hand would often stop the vibration, but marginal stability had been achieved in the fourth flexible mode at roughly 83hz. Once the beam vibration was stopped by use of the hand, it would remain motionless until perturbed. This change is most likely caused by a change in the joint damping from viscous friction, (when it is in motion), to coulomb friction as it stops. The step response is captured again for a case where this steady vibration is sustained over the interval in figure 7-4.

Further increases in the prescribed degree of stability yielded similar instabilities in the higher
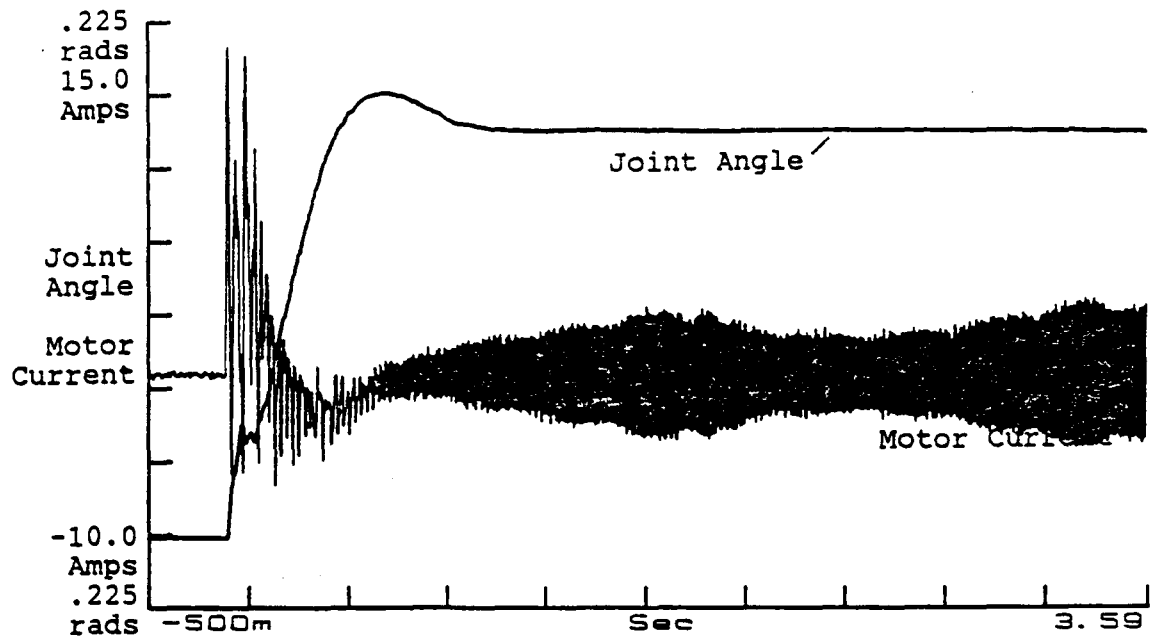
Figure 7.4a. Modal Controller, Large α,
α = diag[3.25 3.25 .2 3.25 3.25 .2],
Joint Angle/Motor Current Unstable Step Response
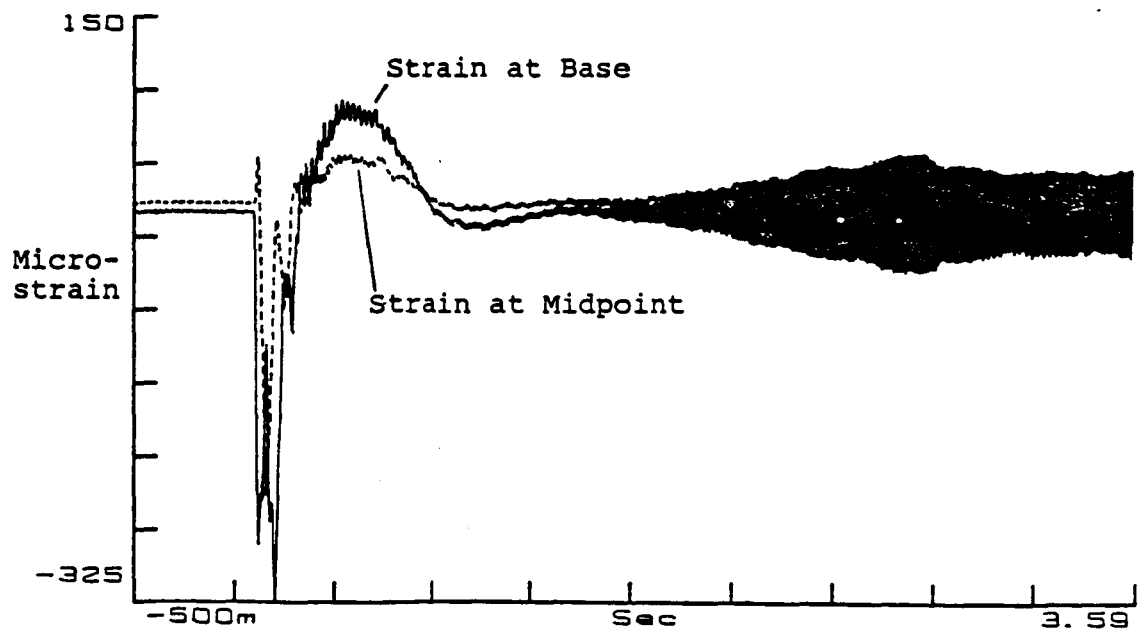
Figure 7.4b. Modal Controller, Large α,
Strain at Base/Midpoint Unstable Step Response

C-2
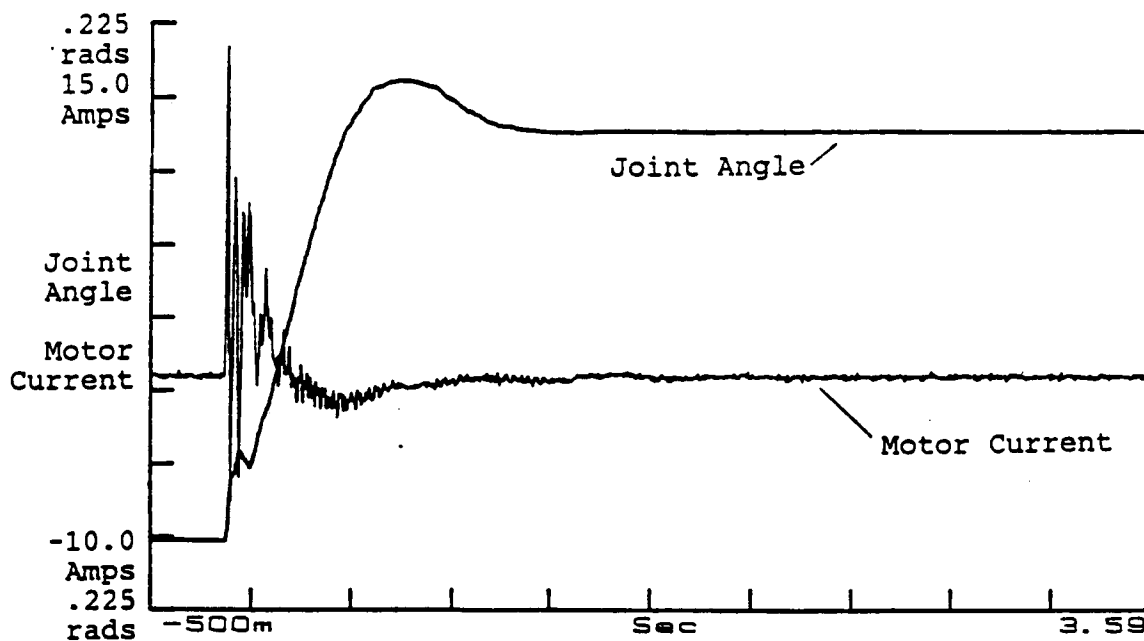
Figure 7.5a."Best" Modal Controller,
α = diag[3.25 ? .2 3.25 ? .25], Increased Modal Amplitude
Gain, Joint Angle/Motor Current Step Response
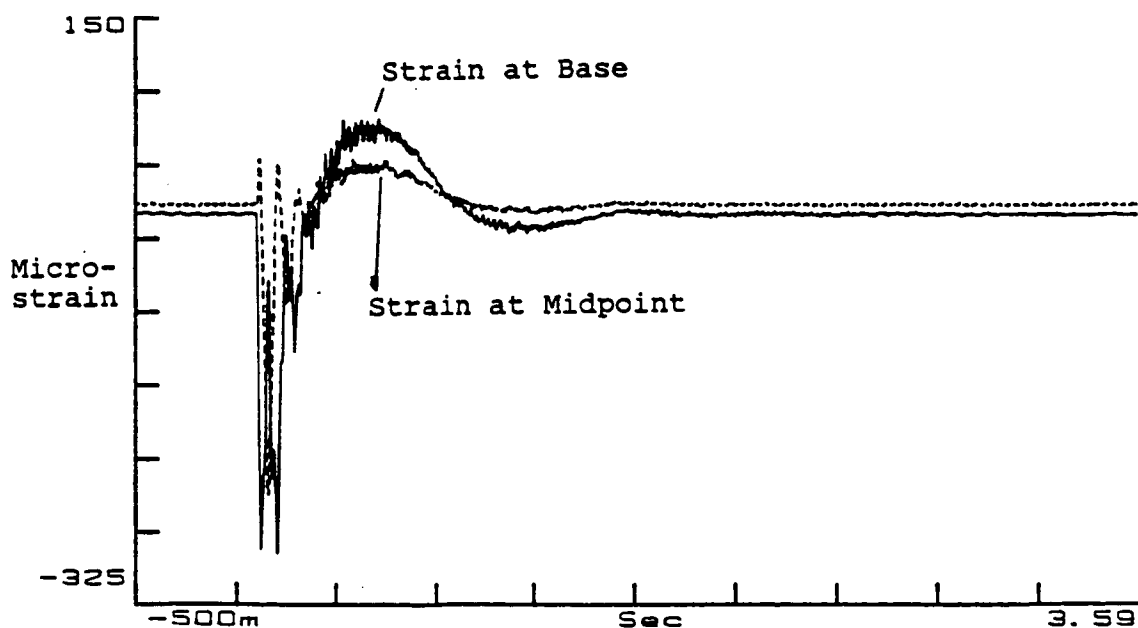
Figure 7.5b. "Best" Modal Controller, Increased Modal
Amplitude Gain, Strain at Base/Midpoint Step Response

flexible modes. The parameter observed to cause this affect was the damping gain on the first flexible mode. Trial and error indicated that higher modal amplitude gains resulted in a more stable response for the same modal damping gain. This trend of modal stiffness gain increasing system damping is supported by work done in the single mode section.

The modal amplitude gain was increased until a "best" (most stable with respect to disturbances) response was obtained for the same first flexible mode damping gain. This response is shown in figure 7-5, and the design parameters presented in 7-3. Further increases in modal amplitude gain resulted in higher levels of excitation in the untreated modes.

The modal controllers did improve the response of the flexible mode, and in the latter cases did yield satisfactory control over the first flexible mode. Additionally, with the modal controller larger gains could

Table 7-3. Design Results, Stability Gain Vectors,
Closed Loop Eigenvalues for Figure 7-5

Stability Matrix
α = diag[3.25 ? .2 3.25 ? .2]

Discrete Gains
F(modal) = 1523.7 -900.0 34.5 520.8 23.5 -1.68

        Discrete Eigenvalues
         Modal Controller
         .970   -.303E-17
         .976   .175E-17
         .969   +/-.0884
         .908   +/-.4137

be applied to the joint variables than was possible with the collocated controller. The next question to be addressed is the robustness of these control laws. The next section investigates the noise sensitivity, and payload sensitivity.

7.2.4 Disturbance Rejection and Robustness

In the preceding section control laws were selected which yielded faster settling times in the design process by effectively moving the continuous closed loop poles farther and farther into the left half plane using the prescribed degree of stability. This results in larger and larger gain values. This section will investigate the disturbance rejection and robustness of the control laws, examining what, if any, penalties are incurred with the higher gain values. First disturbance impulses will be applied to the experimental system, and then changes in payload mass from the design value will be examined.

7.2.4.1 Disturbance Impulse Response

An impulse hammer was used to apply a disturbance to the beam at the payload. This would correspond to the arm making contact with a work piece or bracing surface. The amplitude of the impulse was selected to cause a peak disturbance of roughly five to six inches at the payload. The time domain response of the beam was found to be the most revealing measurment, though frequency domain results could be obtained from the hammer impulse signal. Though the

signal from the hammer was not utilized in these measurements, the design of the hammer still enhanced the operators control of the impulse delivered to the beam. The response of the collocated control law of 7-1 above is shown in figure 7-6

The beam was additionally struck at random locations along its length with similar responses. The response of the modal control law with the same prescribed degree of stability on the joint and first mode state variables is shown in figure 7-7.

The response of modal control law which achieved the highest prescribed degree of stability, (design data in table 7-2), is shown in figure 7-8.

The modal control law with a high degree of prescribed stability, and the "best" control law, while able to control the flexible vibration had large peaks and a good deal of activity in the impulse response. This indicates that the tighter control laws with large gain values are more susceptible to disturbances.
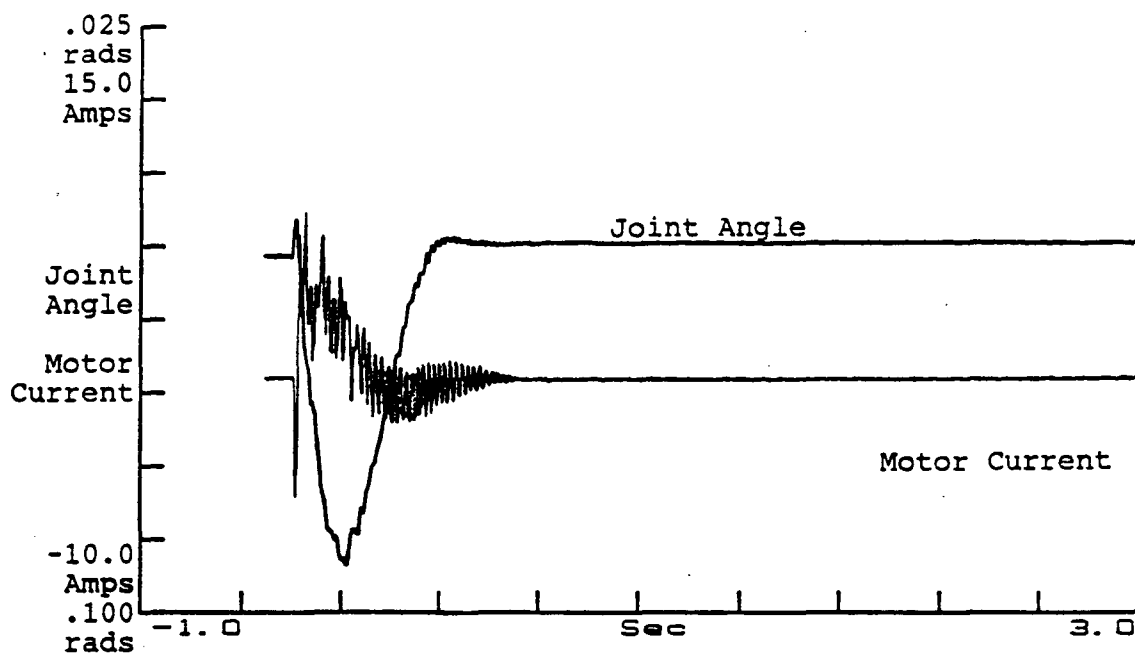
Figure 7-6a. Collocated Controller, Disturbance Impulse,
Joint Angle/Motor Current Response
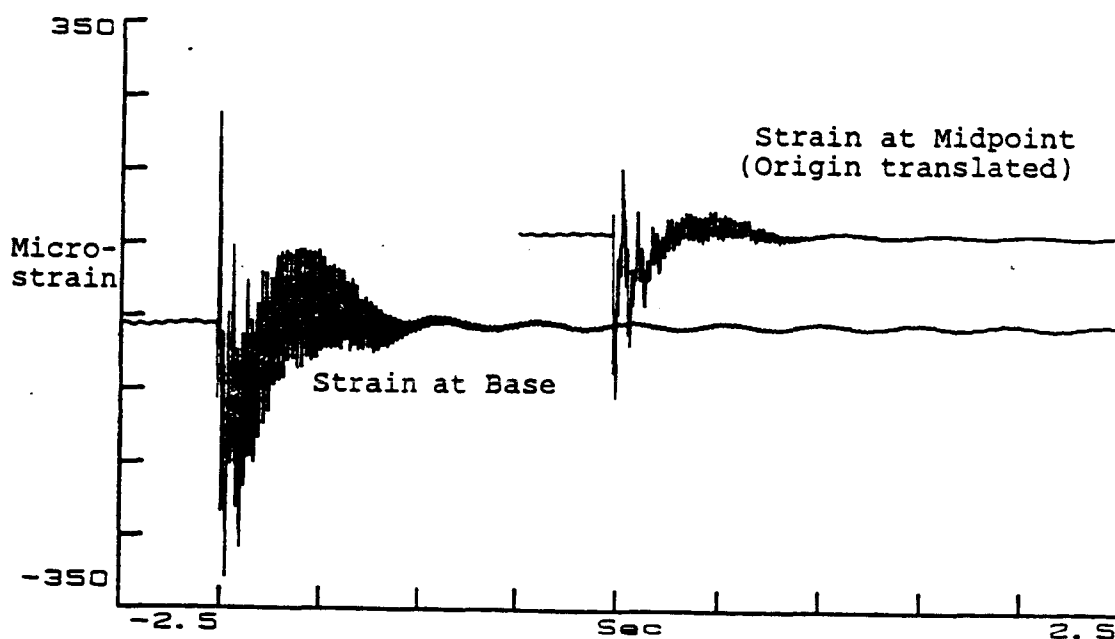
Figure 7-6b. Collocated Controller, Disturbance Impulse,
Strain at Base/Midpoint Response
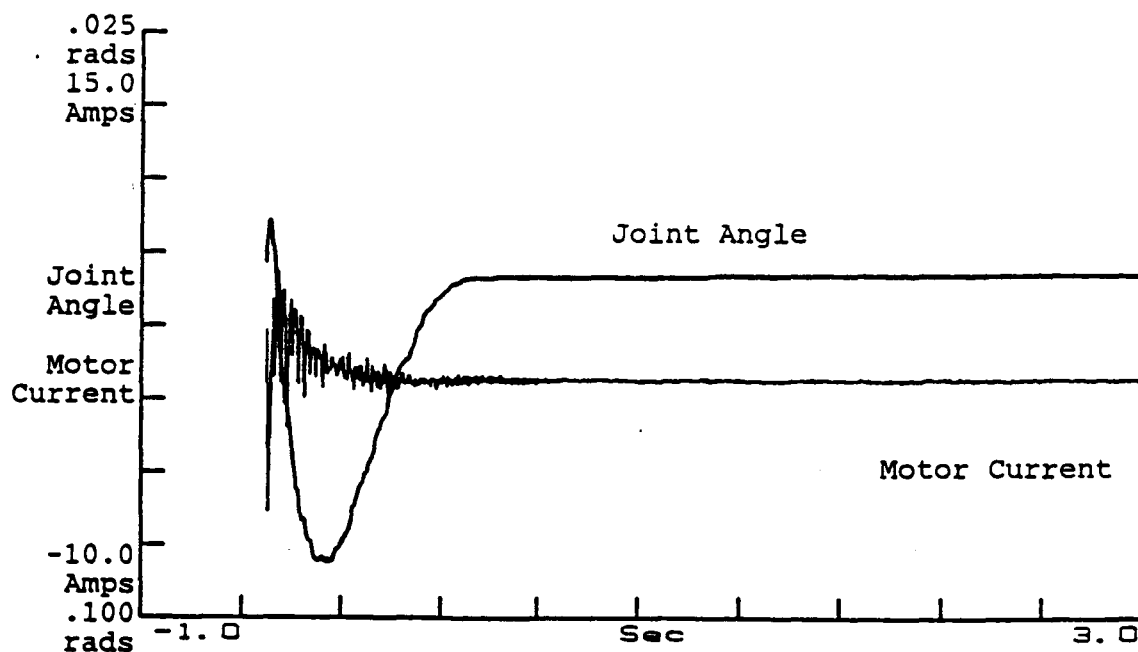
Figure 7-7a. Modal Controller, Disturbance Impulse,
Joint Angle/Motor Current Response
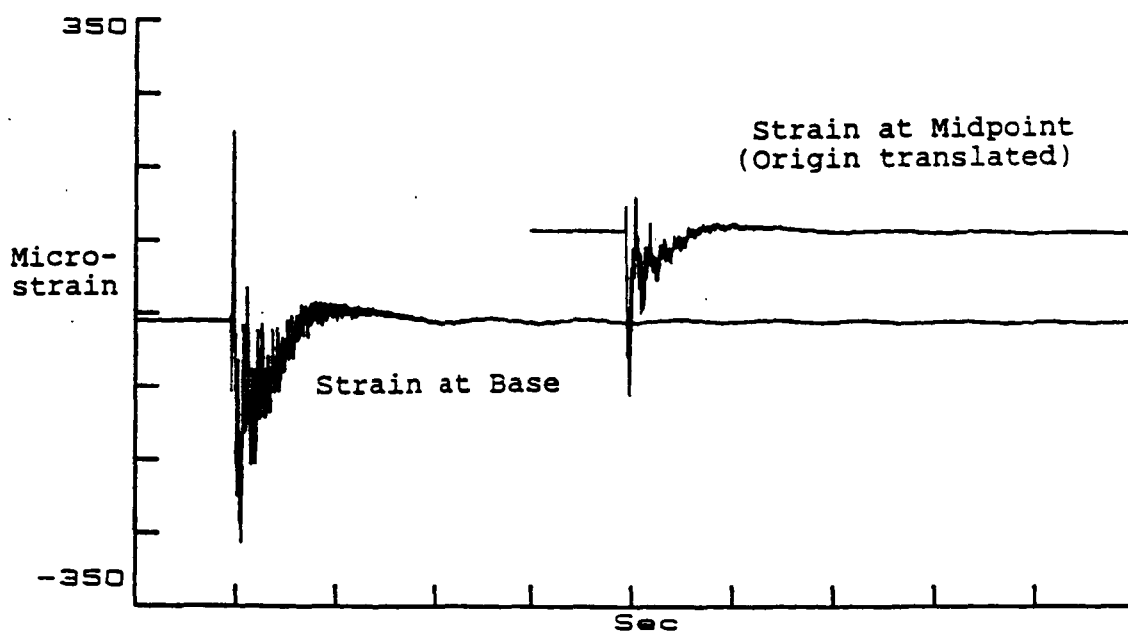
Figure 7-7b. Modal Controller, Disturbance Impulse,
Strain at Base/Midpoint Response
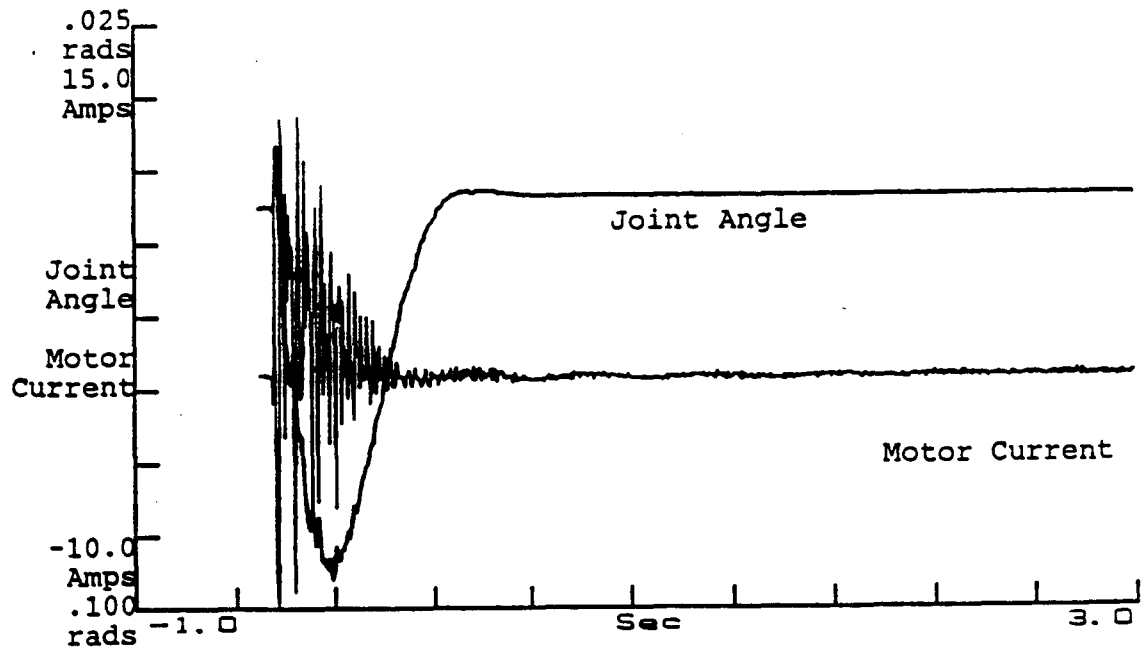
Figure 7-8a. Large α Modal Controller, Disturbance Impulse, Joint Angle/Motor Current Response
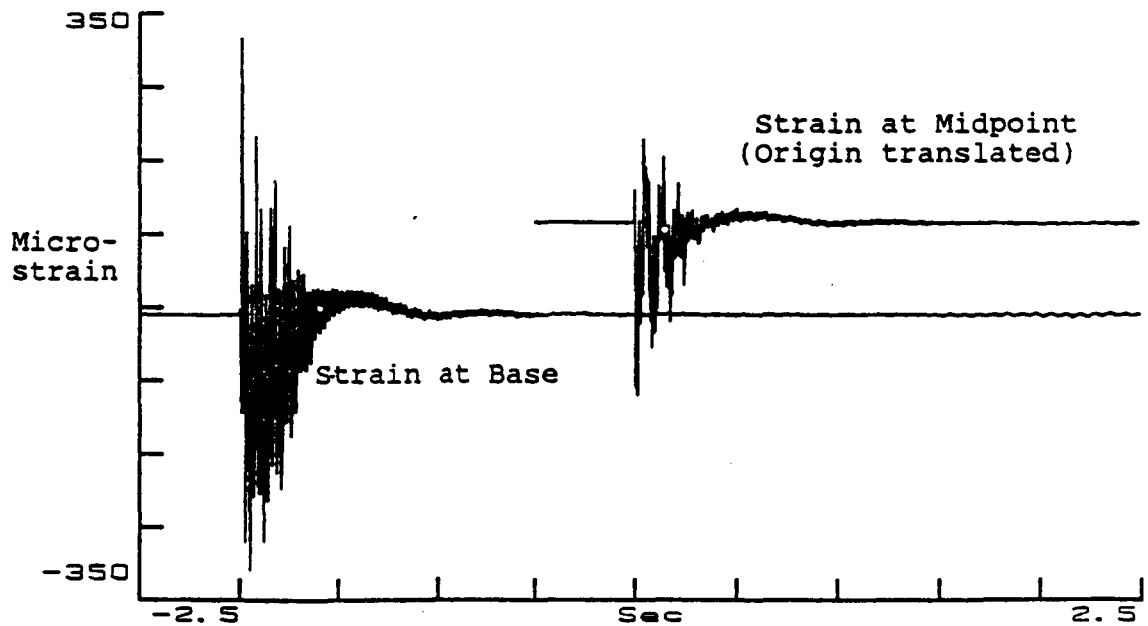
Figure 7-8b. Large α Modal Controller, Disturbance Impulse, Strain at Base/Midpoint Response
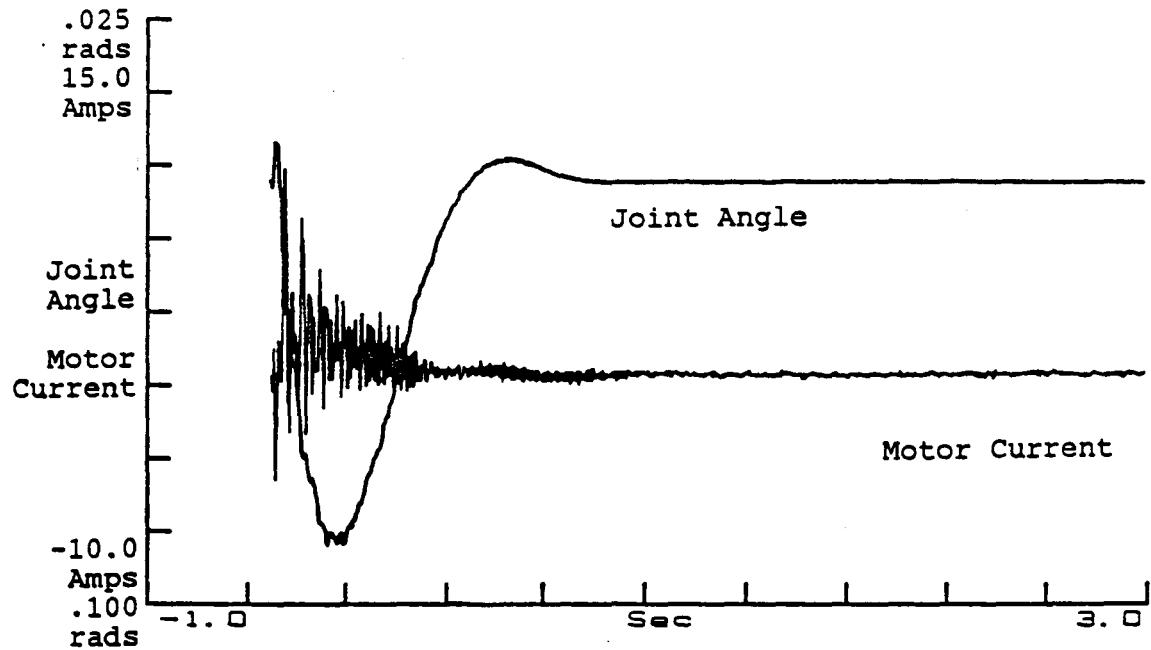
Figure 7-9a."Best" Modal Controller, Disturbance Impulse,
Joint Angle/Motor Current Response
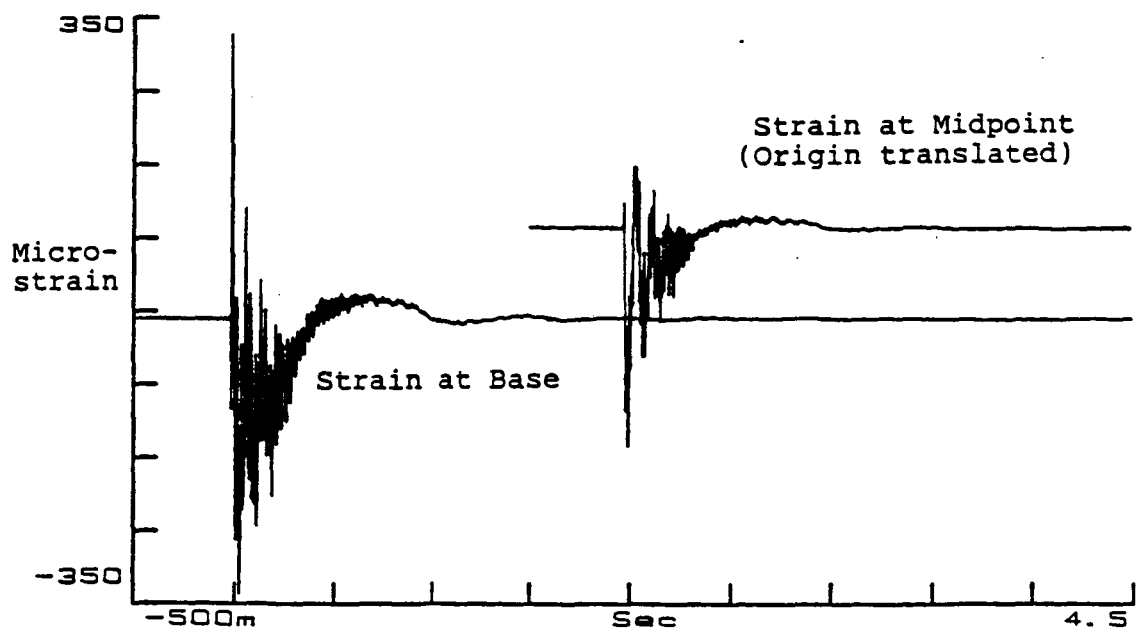
Figure 7-9b."Best" Modal Controller, Disturbance Impulse,
Strain at Base/Midpoint Response

7.2.4.2 Payload Sensitivity

The ability of the controller to tolerate variations in payload mass is of interest in real applications where a variety of objects must be handled. The payload was increased to a total of four times the design payload, and the step response observed again. Responses for the control laws are shown in figures 7-10, through 7-14.

The additional payload mass resulted in increased overshoot of the joint angle, and modal variables typical of the expected reduction in damping ratio. Additionally, the response of the higher untreated flexible modes was greatly reduced in all cases, even the case of the modal controller with a large prescribed degree of stability. This is due to increased separation of the higher frequencies due to the variation in boundary condition at the payload end of the beam.
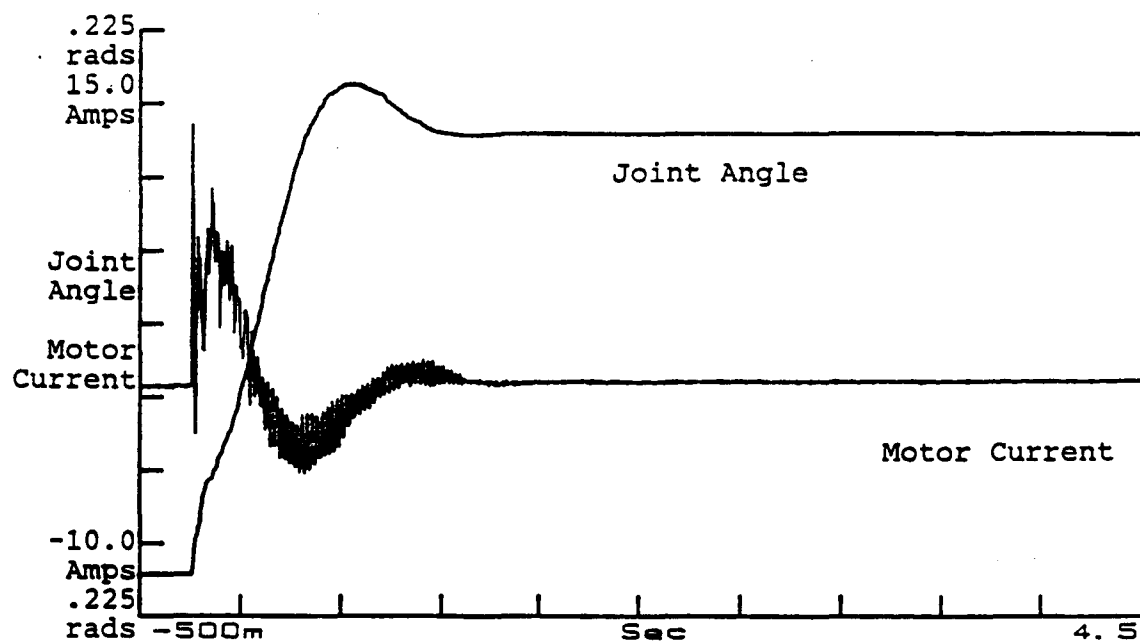
Figure 7-10a. Collocated Controller, 4 Times Payload,
Joint Angle/Motor Current Response
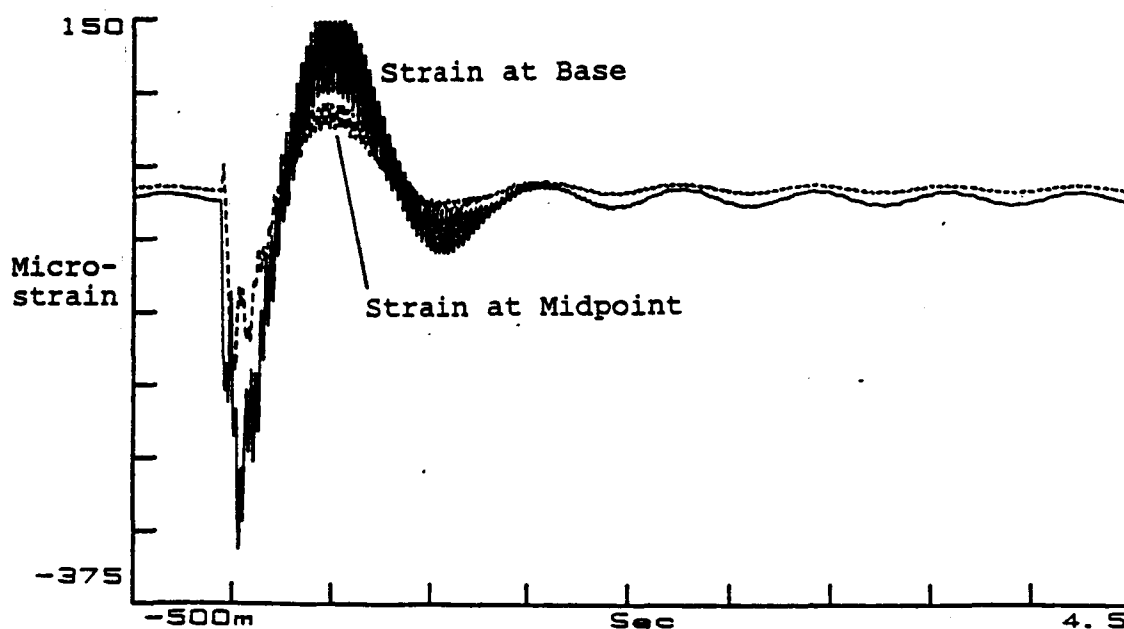
Figure 7-10b.Collocated Controller, 4 Times Payload,
Strain at Base/Midpoint Response
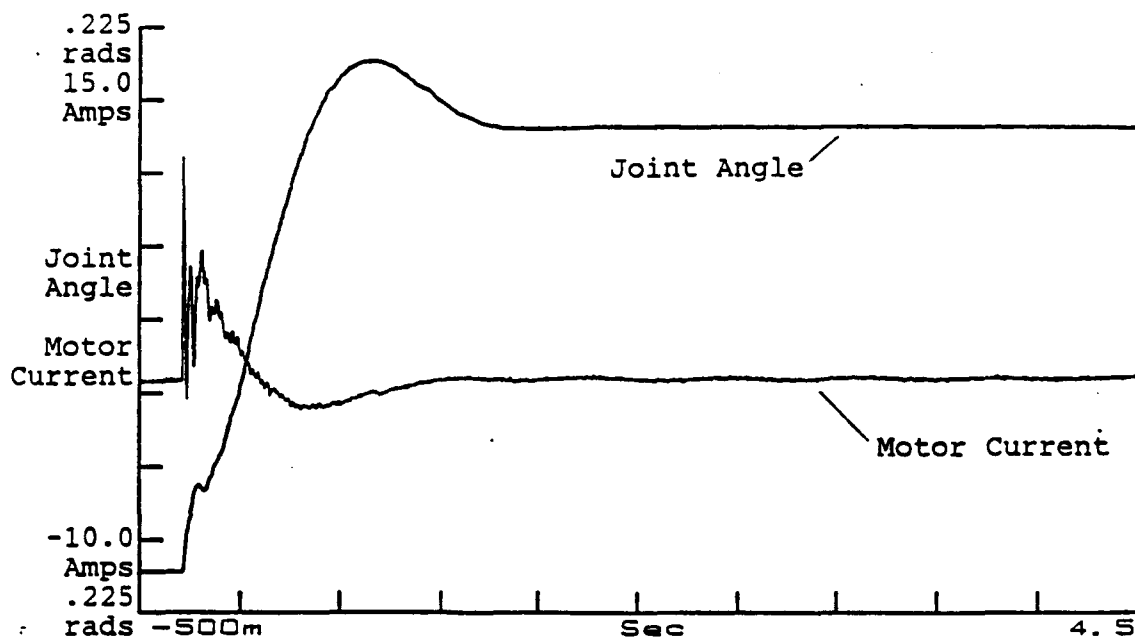
Figure 7-11a. Modal Controller, 4 Times Payload,
Joint Angle/Motor Current Response
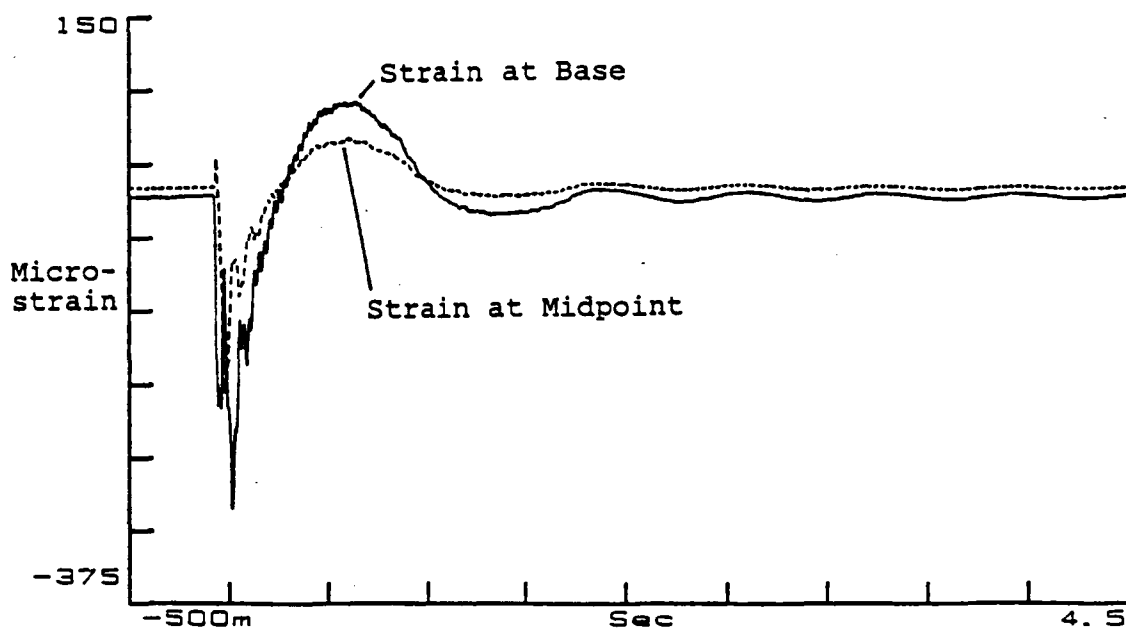
Figure 7-11b. Modal Controller, 4 Times Payload,
Strain at Base/Midpoint Response
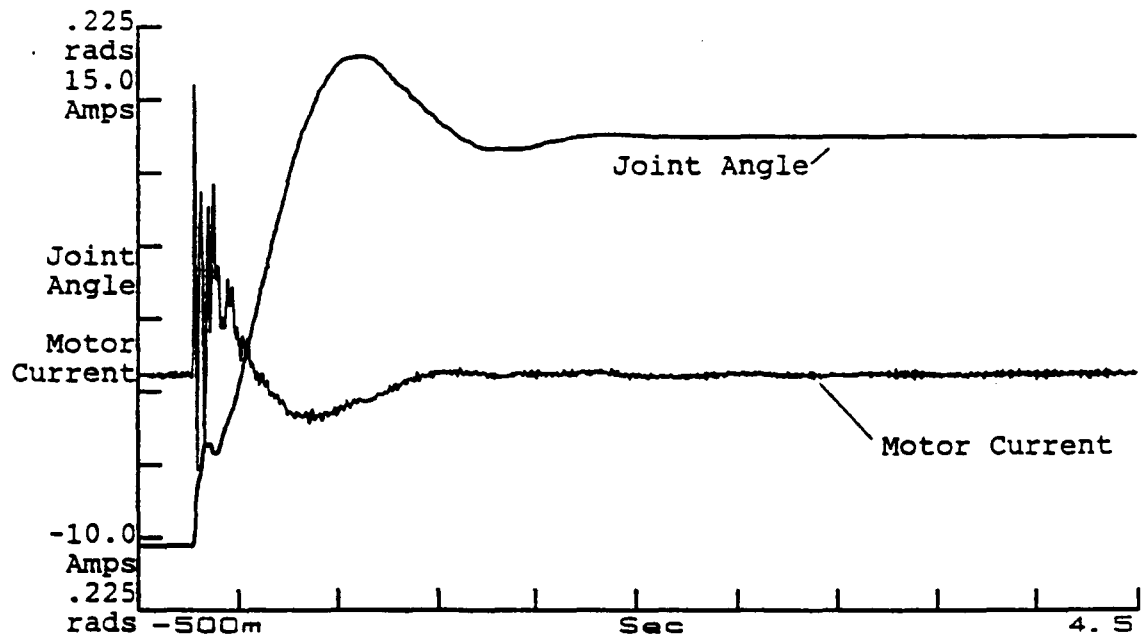
Figure 7-12a. Large α Modal Controller, 4 Times Payload, Joint Angle/Motor Current Response
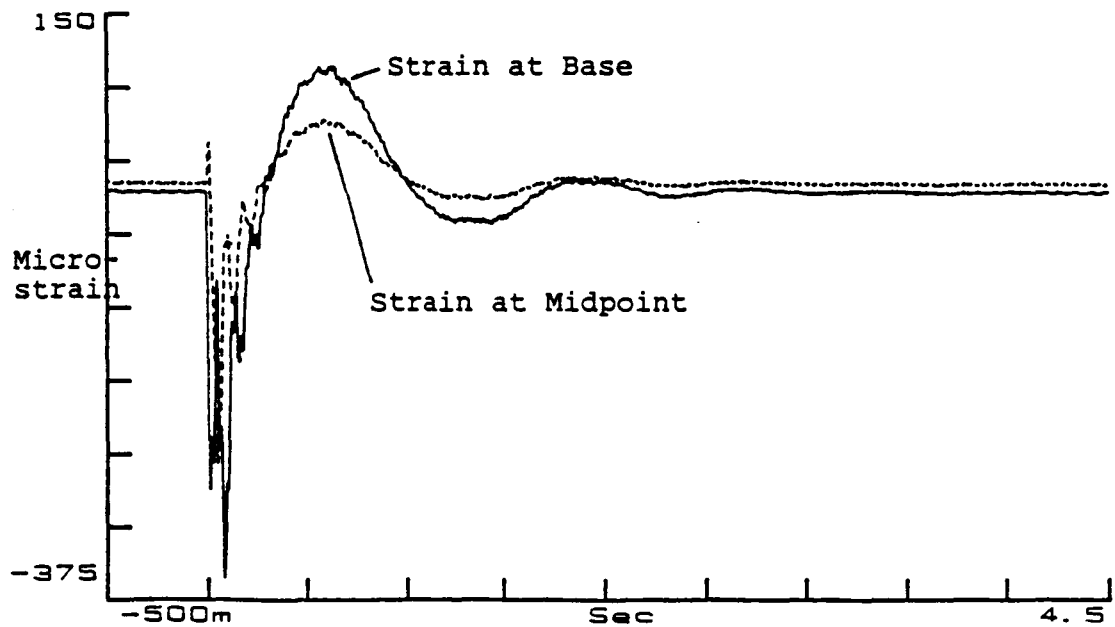
Figure 7-12b. Large α Modal Controller, 4 Times Payload, Strain at Base/Midpoint Response
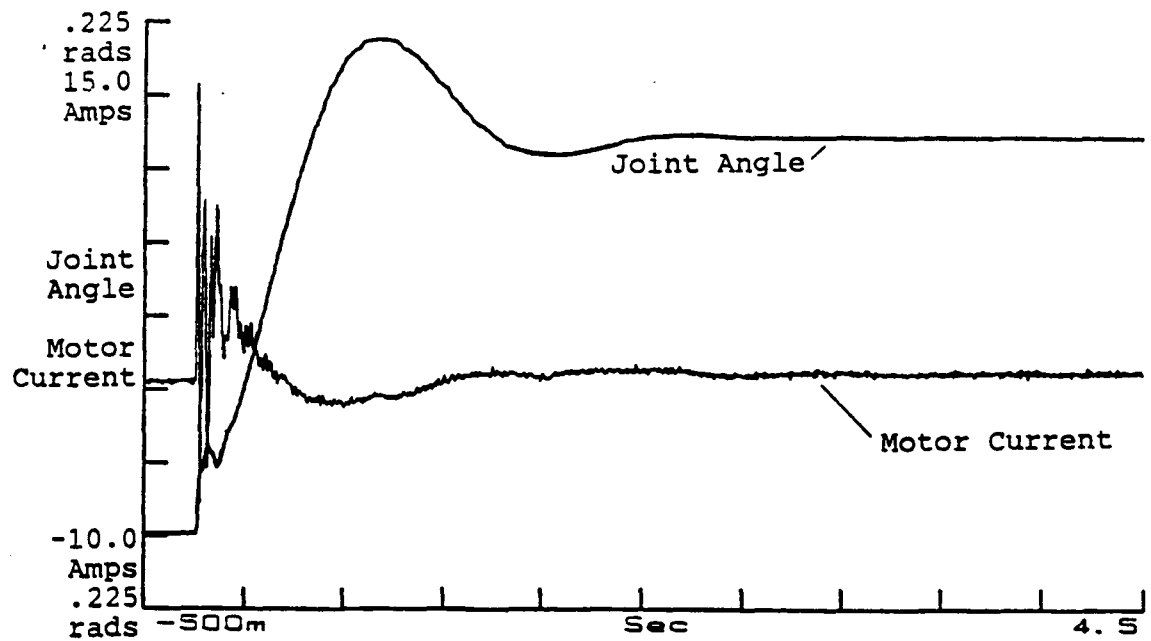
Figure 7-13a. "Best" Modal Controller, 4 Times Payload,
Joint Angle/Motor Current Response
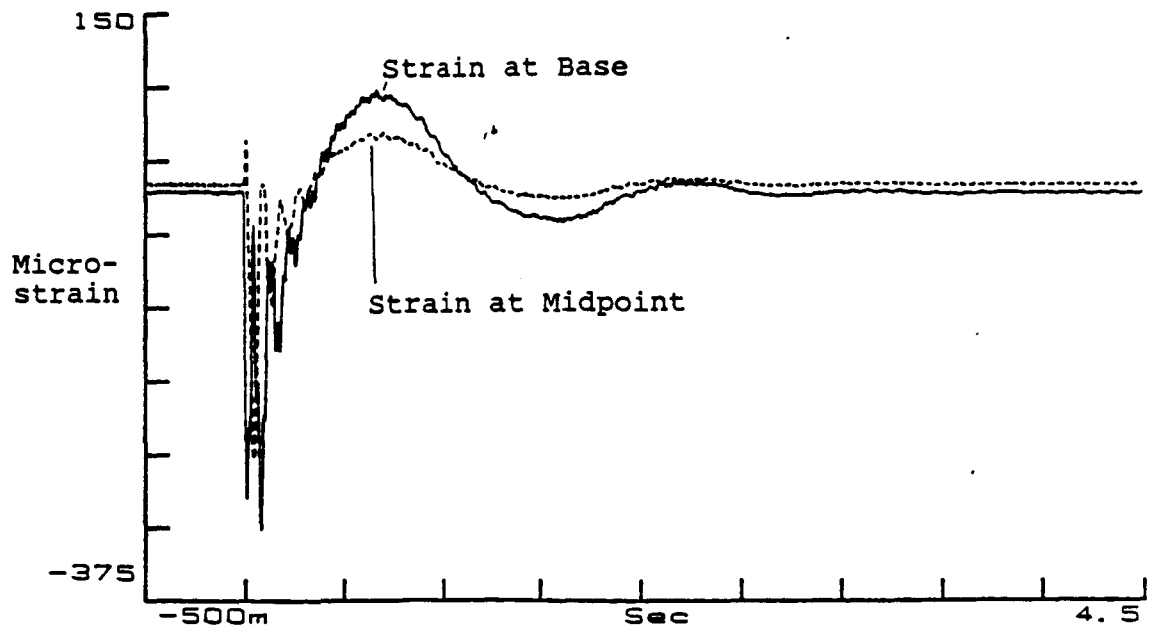
Figure 7-13b. "Best" Modal Controller, 4 Times Payload,
Strain at Base/Midpoint Response

7.3 Single Flexible Mode System

Computational speed, and not model order, appeared to be the limiting factor in many of the experiments conducted. Therefore the design and implementation were repeated for a system model comprised of the rigid mode, and one flexible mode. The first clamped-mass mode shape was selected for inclusion in the model.

7.3.1 Design and Implementation

Once again the prescribed degree of stability proved to be the fastest and most flexible method for placing the system poles. However the low frequency of the first flexible mode and increased computing speed allowed for a placement of the single observer pole equivalent to ten times the frequency of the modal velocity being estimated.

The modal reconstruction/observer/control law combination for the single mode case operated at a cycle time of 4.8 milliseconds.

7.3.2 Experimental Results, Prescribed Degree of Stability

The first experiment conducted in this stage of the work was to compare the performance of the collocated controller operating at the frequency of the faster one mode controller to the earlier collocated response. The same collocated gains as those used for the controller with two flexible modes was applied to the single flexible mode system. The step response is shown in figure 7-14.

There is a marked reduction in the excitement of the third flexible mode when compared to the collocated controller operating at the slower cycle time of the two mode system. A single flexible mode controller with the same prescribed degree of stability as the collocated case was implemented, and the step response is shown in figure 7-15. The single mode controller achieves a smoother more damped response over the two mode controller primarily because of the increased speed of the observer and sampling frequency.

The prescribed degree of stability for the collocated controller operating at the speed of the faster single mode controller could be increased significantly over that of the slower two mode system before the same amount of excitement was observed in the third flexible mode. Additionally at the higher gains more damping was observed after the initial step transient in the first flexible mode. This is thought to result from the higher control actions overcoming the hysteretic friction of the joint. The response for this collocated controller is shown in figure 7-16.
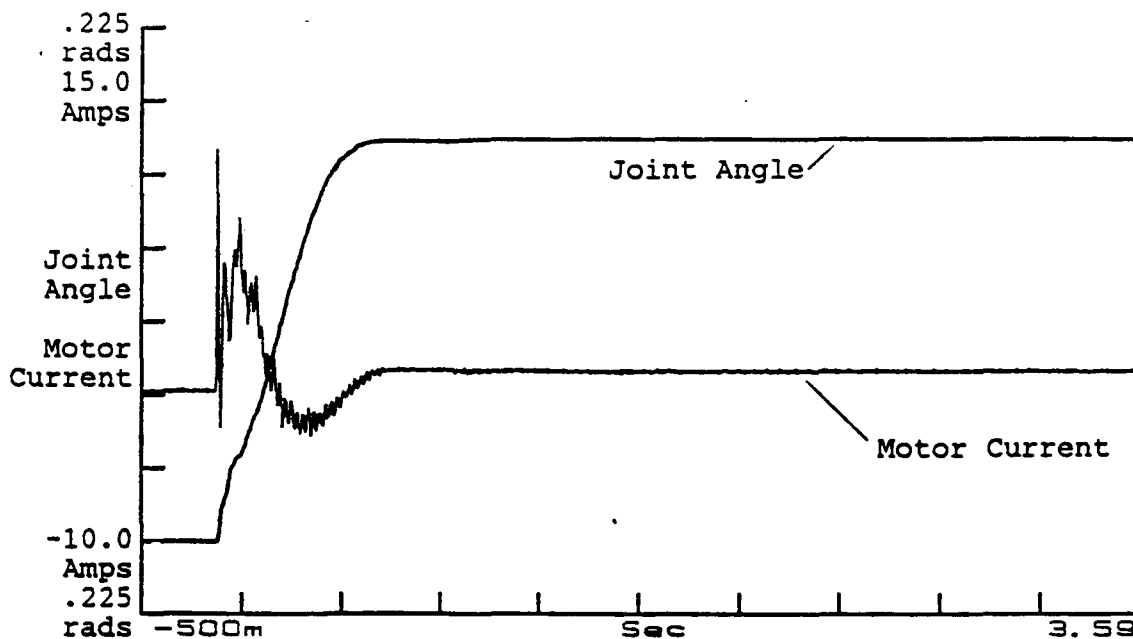
Figure 7-14a. Collocated Controller,
$\alpha = \text{diag}[2.5\ 2.5\ 2.5\ 2.5]$,
Joint Angle/Motor Current Step Response
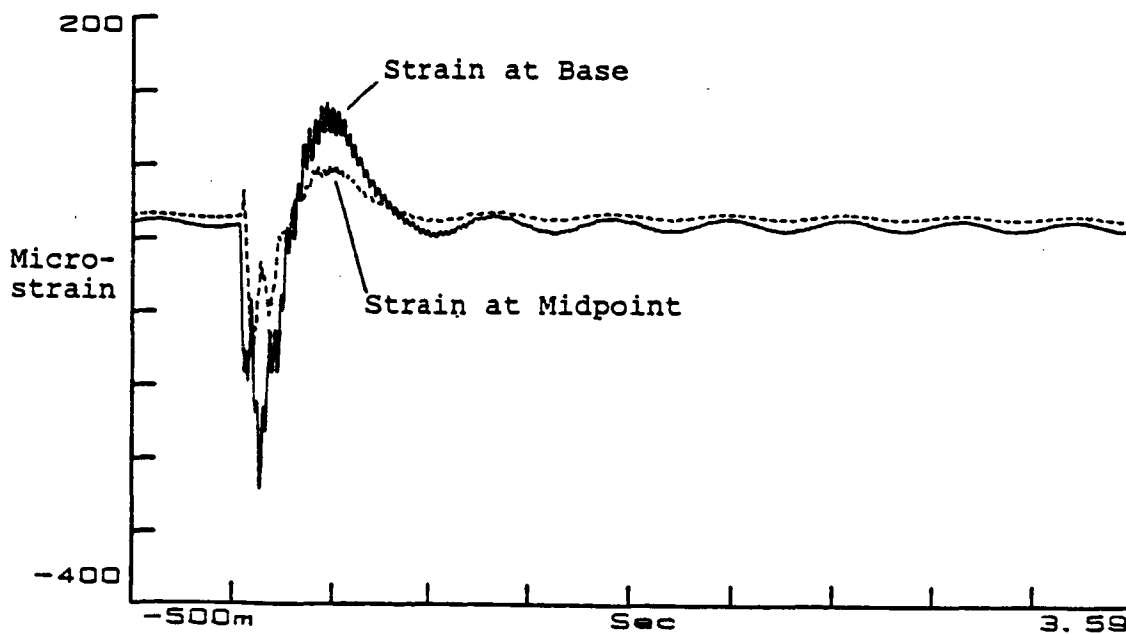
Figure 7-14b. Collocated Controller,
Strain at Base/Midpoint Step Response
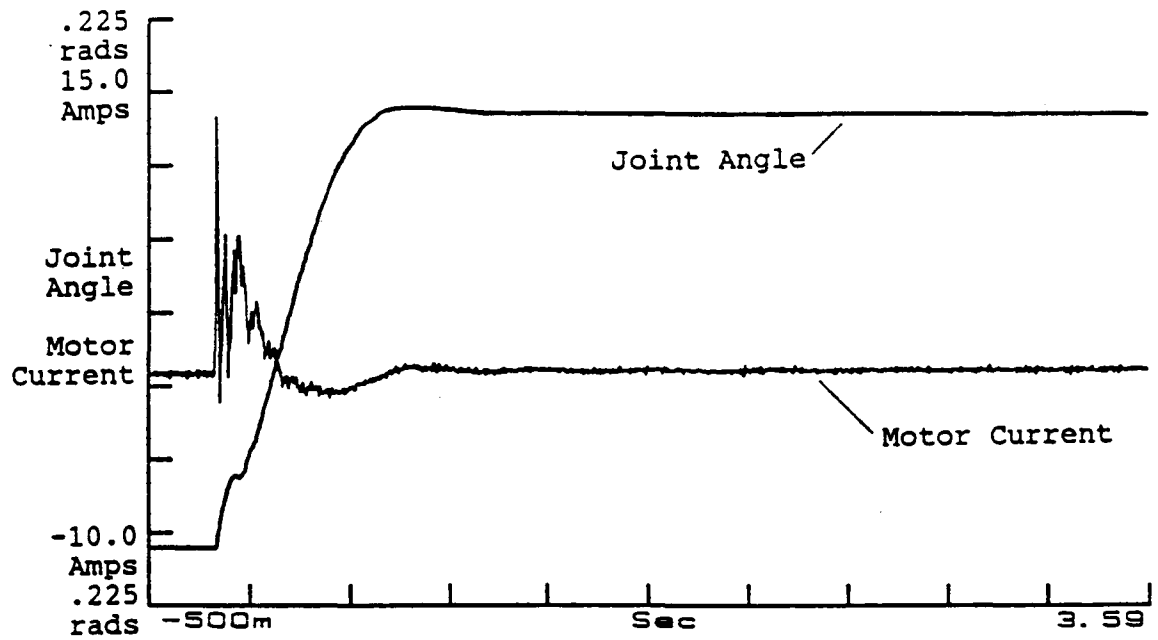
Figure 7-15a. Modal Controller,
α = diag[2.50 2.50 2.50 2.50],
Joint Angle/Motor Current Step Response
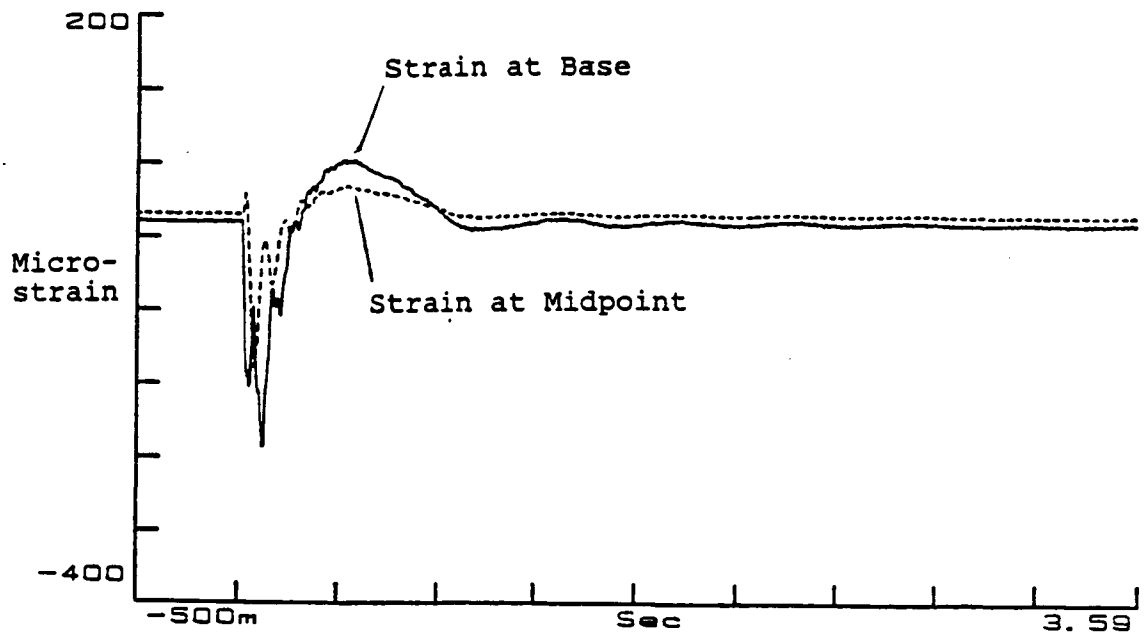
Figure 7-15b. Modal Controller,
Strain at Base/Midpoint Step Response
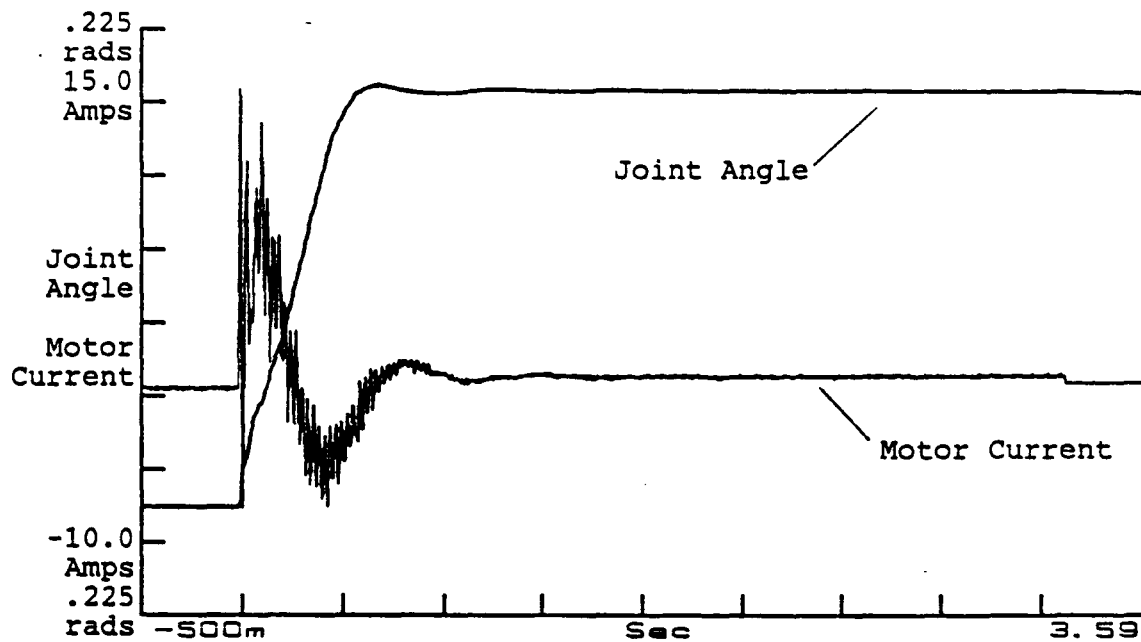
Figure 7-16a. Tighter Collocated Controller,
α = diag[3.0 3.0 3.0 3.0],
Joint Angle/Motor Current Step Response
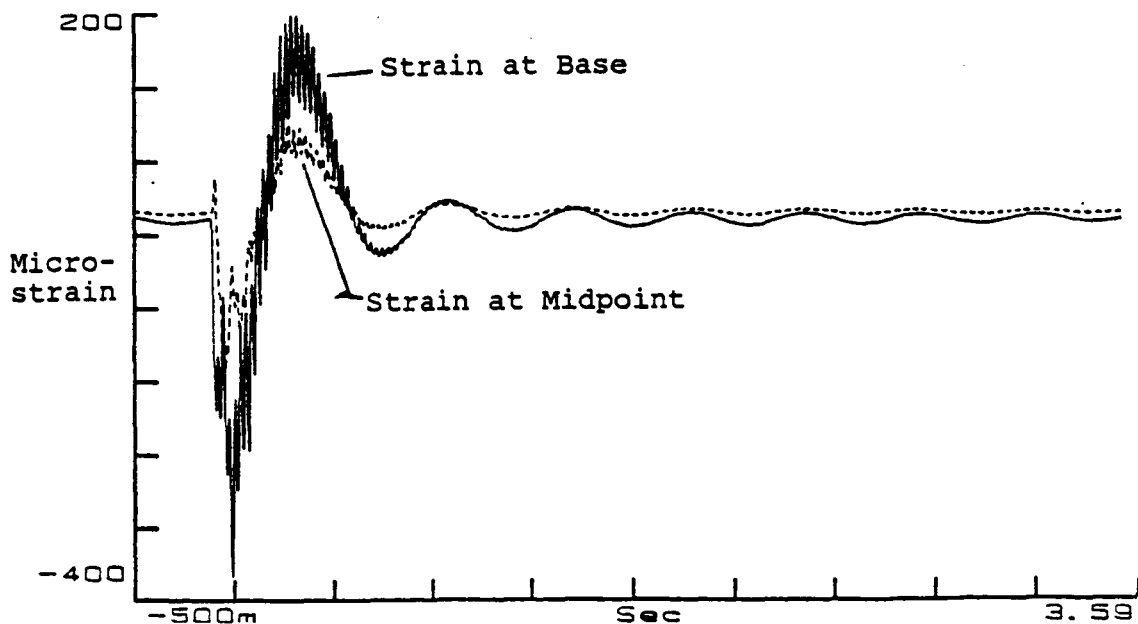
Figure 7-16b. Tighter Collocated Controller,
Strain at Base/Midpoint Step Response

A modal controller for the first flexible mode was implemented with the same prescribed degree of stability in both the rigid and flexible mode as that for the collocated controller. This response is shown in figure 7-17. Note again the success of the modal controller at reducing the excitation of the first flexible mode, and the higher flexible modes, not treated by the model until the amplitude gets very small. The design data for the controllers of figures 7-14,15,16,17 is presented in tables 7.4-5

Table 7-4. Design Results, Stability Gain Vectors, Closed Loop Eigenvalues for Figures 7-14 and 7-15

Stability Matrix
α = diag[2.50 2.50 2.50 2.50]

Continuous Gains
F(collocated) = 1112.   0.   474.1 0.
F(modal) =   1112. -406.7 474.1 15.7

Continuous Eigenvalues

	Collocated Controller		Modal Controller	
	-3.215	-3.306E-16	-4.434	2.305E-15
	-12.45	1.669E-16	-5.744	-3.199E-15
	-4.333	+/-15.11	-5.203	+/-19.01

Discrete Gains
F(collocated) = 871.9   0.   373.1 0.
F(modal) =   871.9 -297.8 373.1 11.7

Discrete Eigenvalues

	Collocated Controller		Modal Controller	
	.967	1.536E-18	.959	+/-.152
	.981	-1.570E-28	.992	+/-.106
	.975	.0778		
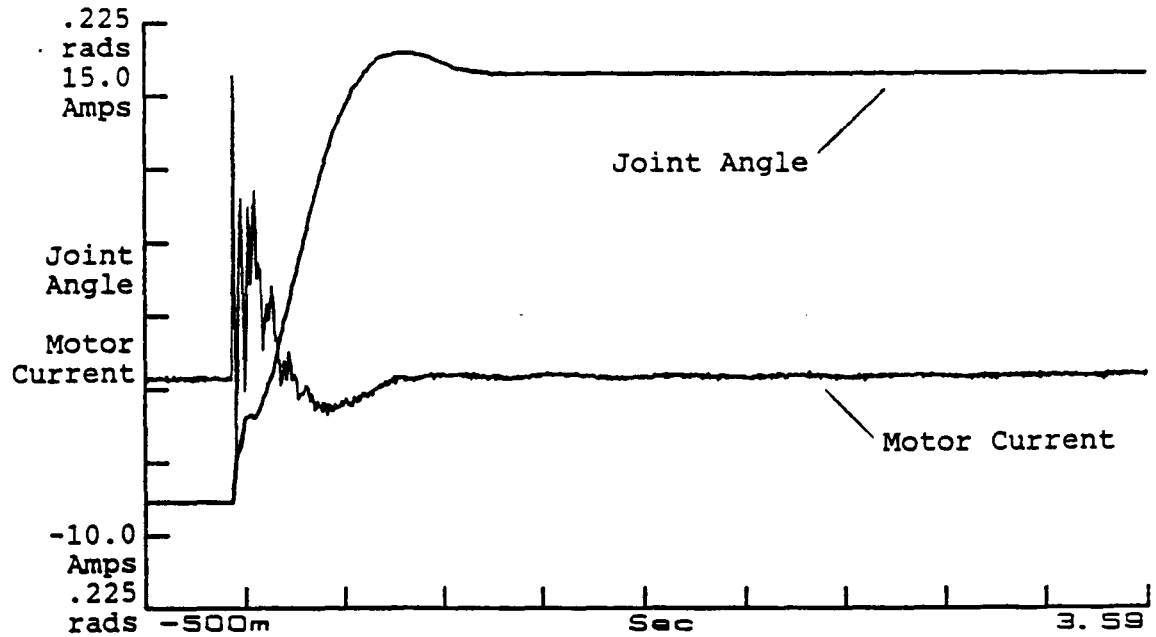
Figure 7-17a. Tighter Modal Controller,
α = diag[3.0 3.0 3.0 3.0],
Joint Angle/Motor Current Step Response
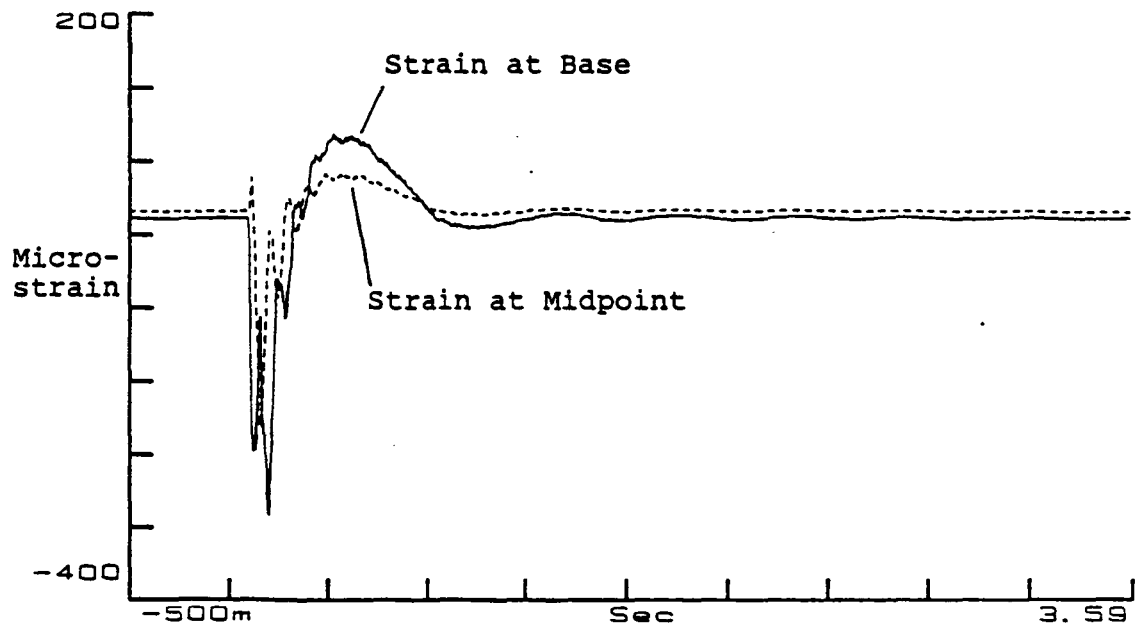
Figure 7-17b.Tighter Modal Controller,
Strain at Base/Midpoint Step Response

Table 7-5. Design Results, Stability Gain Vectors,
Closed Loop Eigenvalues for Figures 7-16 and 7-17

Stability Matrix
α = diag[2.75 2.75 2.75 2.75]

Continuous Gains
F(collocated) = 1346.4   0.   527.0 0.
F(modal) =   1346.4 -470.9 527.0 21.1

Continuous Eigenvalues
        Collocated Controller   Modal Controller
        -3.327   -3.341E-16   -5.50   +/-.0065
        -16.11   2.435E-15   -5.50   +/-19.13
        -4.065 +/-14.388

Discrete Gains
F(collocated) = 1294.3   0.   509.7 0.
F(modal) =   1294.3 -419.2 509.7 19.2

Discrete Eigenvalues
        Collocated Controller   Modal Controller
        .928   9.380E-18   .970   +/-.320E-16
        .983   -7.735E-19   .969   +/-.089
        .976   +/-.0684

The prescribed degree of stability was increased by increments of .25 until until the largest degree resulting in a stable response was achieved. The response for the resulting control law is presented in figure 7-18. This controller results in large applied torques during the initial transient and an increased level of noise throughout the response in the torque and strain traces. The stability and damping of the first flexible mode is definitely increased, however the settling time for the system has not been significantly increased. The large torques applied to slew the joint variables at high gains causes large flexible deflections which, although highly damped, require time to
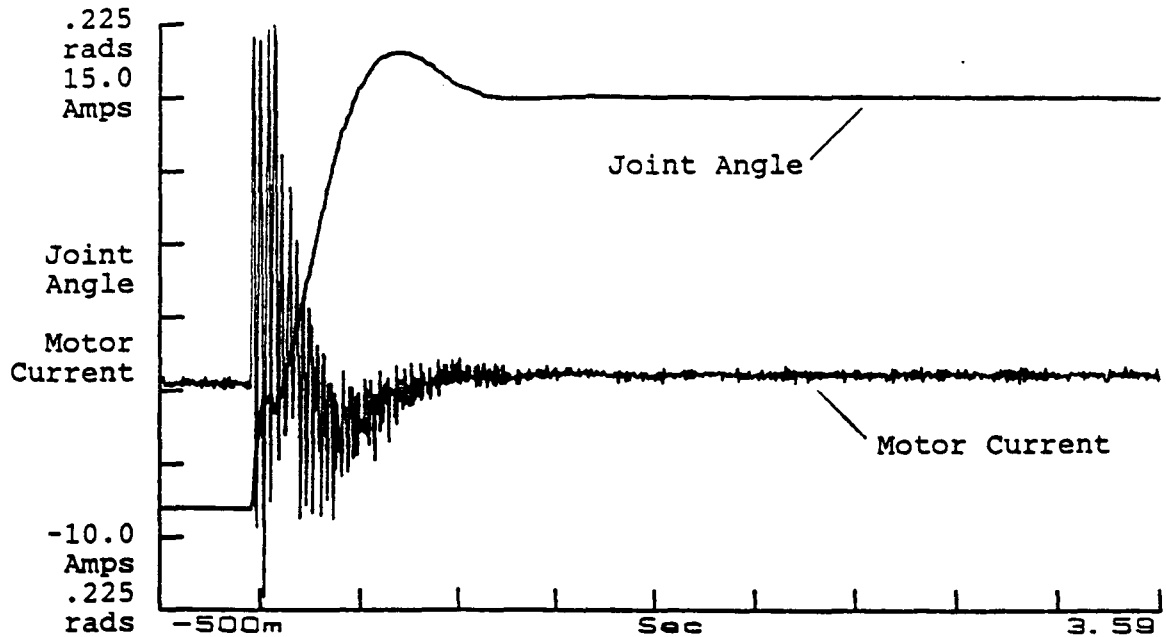
Figure 7-18a. Large α Modal Controller,
α = [3.75 3.75 3.75 3.75],
Joint Angle/Motor Current Step Response
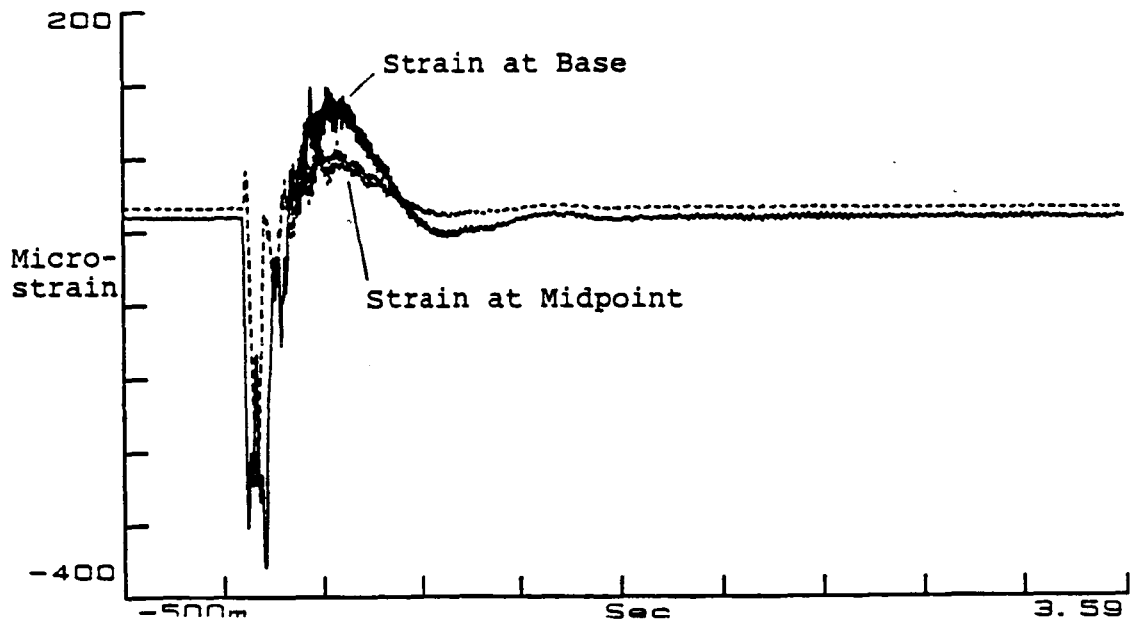
Figure 7-18b. Large α Modal Controller,
Strain at Base/Midpoint Step Response

settle out. The design results for this case are shown in table 7-6.

Table 7-6. Design Results, Stability Gain Vectors,
Closed Loop Eigenvalues for Figure 7-18

Stability Matrix
α = diag[3.75 3.75 3.75 3.75]

Continuous Gains
F(modal) = 2668.0 -840.3 806.2 47.7

Discrete Gains
F(modal) = 2528.3 -758.4 770.2 43.3

Continuous Eigenvalues Modal Controller		Discrete Eigenvalues Modal Controller	
-7.50	+/- .0049	.958	+/-.149E-17
-7.50	+/- 19.13	.960	+/-.0877

7.3.3 Experimental Results, Pole Placement

Increasing the prescribed degree of stability by equal amounts for both the rigid and flexible modes did not achieve the desired result of improving the settling time for the system. Although large amounts of damping was successfully introduced into the flexible mode the overall settling time did not consistently improve. Large overshoots of joint angle were necessary to reduce the excitement of the flexible mode, and the large gains associated with high degree of stability introduced noise into the system.

This indicated that better results might be obtained if more stability was prescribed for the flexible mode than the rigid mode. A prescribed degree of stability for the joint angle was selected which achieved a rapid slew rate in

the earlier experiments, yet which did not tend excite the flexible mode as much as the largest degrees of stability prescribed for the joint variables. The stability for the flexible mode was then moved as far left as would allow for a stable response. This result is shown in figure 7-19, and the design data in table 7-7.

Table 7-7. Design Results, Stability Gain Vectors,
Closed Loop Eigenvalues for Figure 7-19

Stability Matrix
α = diag[2.75 3.50 2.75 3.50]

Continuous Gains
F(modal) = 1372.0 -736.4 553.1 14.2

Discrete Gains
F(modal) = 1306.8 -664.1 529.1 11.6

Continuous Eigenvalues Modal Controller		Discrete Eigenvalues Modal Controller	
-5.22	+/- 1.00	.961	+/-.089
-7.27	+/- 19.46	.974	+/-.0042
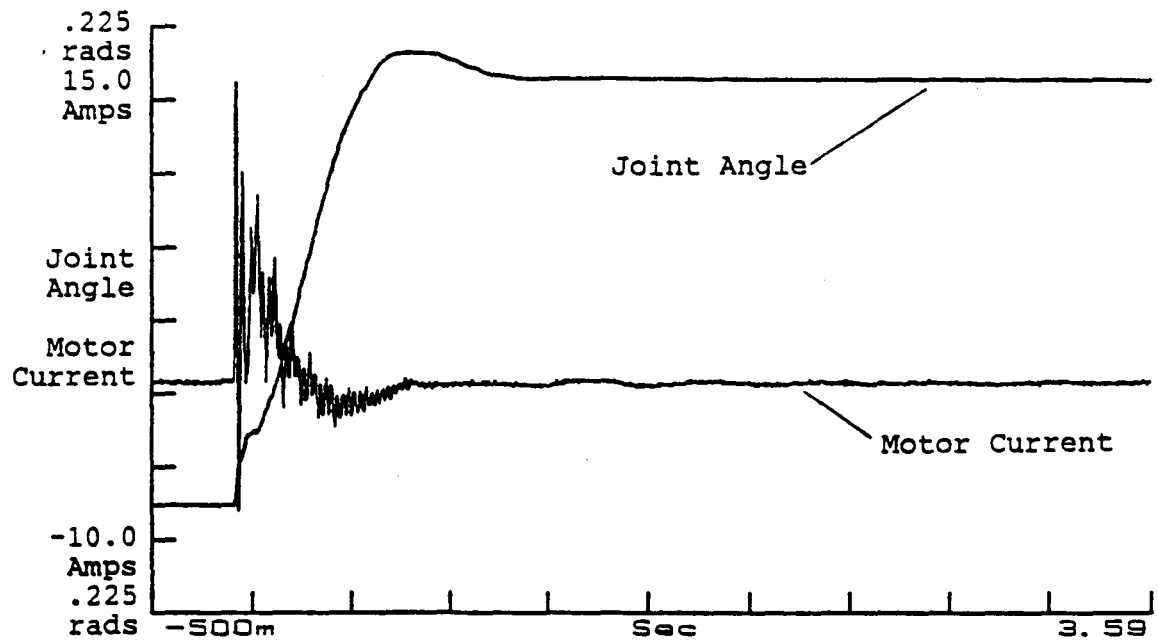
Figure 7-19a. Modal Controller,
α = diag[2.75 3.5 2.75 3.25],
Joint Angle/Motor Current Step Response
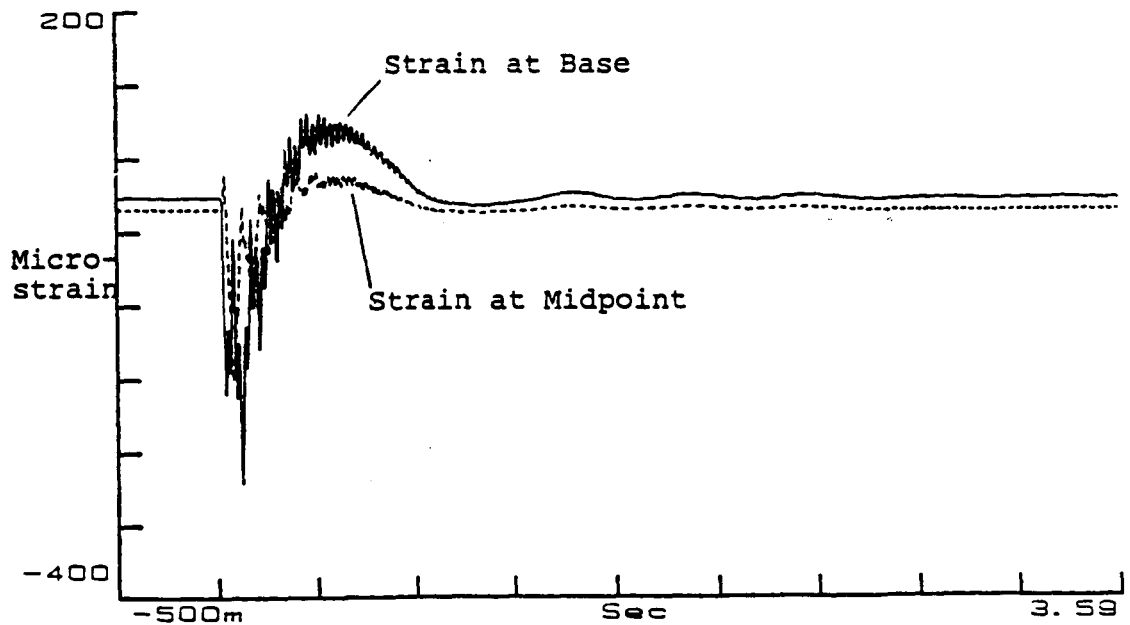
Figure 7-19b. Modal Controller,
Strain at Base/Midpoint Step Response

An interesting result of this design procedure is that samller amounts of modal damping are required to move the flexible pole to the left than when both the rigid and flexible are moved to the left in equal amounts. However, the resultant trace shown in figure 7-19 does not show the predicted damping. The modal damping was increased to observe its effect, and this result is shown in figure 7-20.

Table 7-8. Design Results, Gain Vectors,
Closed Loop Eigenvalues for Figure 7-20

Discrete Gains
F(modal) = 1306.7 -664.0 529.9 43.2

Continuous Eigenvalues Modal Controller		Discrete Eigenvalues Modal Controller	
-4.56	+/-1.61	.978	+/-7.40E-3
-3.88	+/- 21.96	.976	+/-.104

The additional damping resulted in a very nice response, with the shortest settling time and least overshoot of all the designs. The resultant design parameters are contained in table 7-8. Two additional conditions are thought to be of interest in the identifying the behavior of this combination. One case is the largest possible stable combination of amplitude and rate gain on the flexible mode. The second case is the application of modal velocity gain alone to the flexible mode. The case where large modal gains are coupled with moderate joint
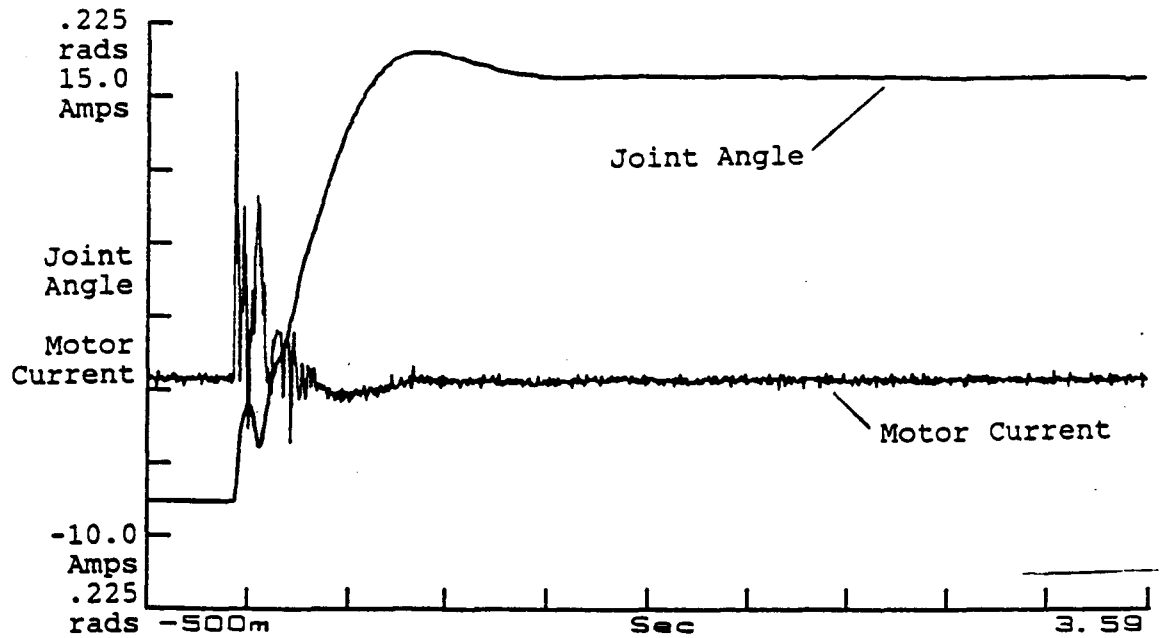
Figure 7-20a. Increased Modal Damping, Modal Controller,
Joint Angle/Motor Current Step Response
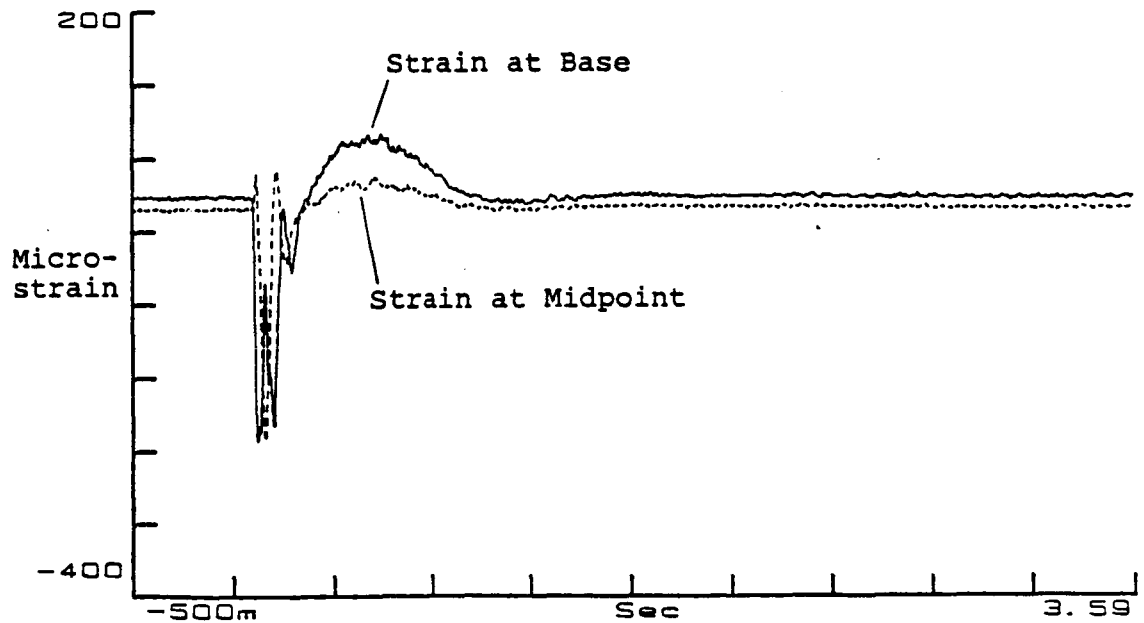
Figure 7-20b. Increased Modal Damping, Modal Controller,
Strain at Base/Midpoint Step Response

variable gains is depicted in figure 7-21. This is seen to result in excitement of the second flexible mode.

Table 7-9. Design Results, Stability Gain Vectors,
Closed Loop Eigenvalues for Figure 7-21

Discrete Gains
F(modal) = 1306.7 -2000.0 529.9 50.0

Continuous Eigenvalues Modal Controller		Discrete Eigenvalues Modal Controller	
-2.71	+/-2.53	.969	+/.1364
-4.91	+/-28.62	.976	+/-.012

Two cases of modal velocity gain only on the flexible mode coupled with reasonable joint variable gains were selected. Figure 7-22 depicts the response for a large amount of damping gain which achieved a stable response. Note that the first flexible mode while damped, is not damped as well as when coupled with some amplitude gain.

Table 7-10. Design Results, Gain Vectors,
Closed Loop Eigenvalues for Figure 7-22

Discrete Gains
F(modal) = 1306.7 -0.0 529.9 40.0

Continuous Eigenvalues Modal Controller		Discrete Eigenvalues Modal Controller	
-3.41	3.6E-16	.951	1.33E-18
-9.95	1.70E-17	.984	-1.76E-19
-2.13	+/- 18.36	.985	+/-.087
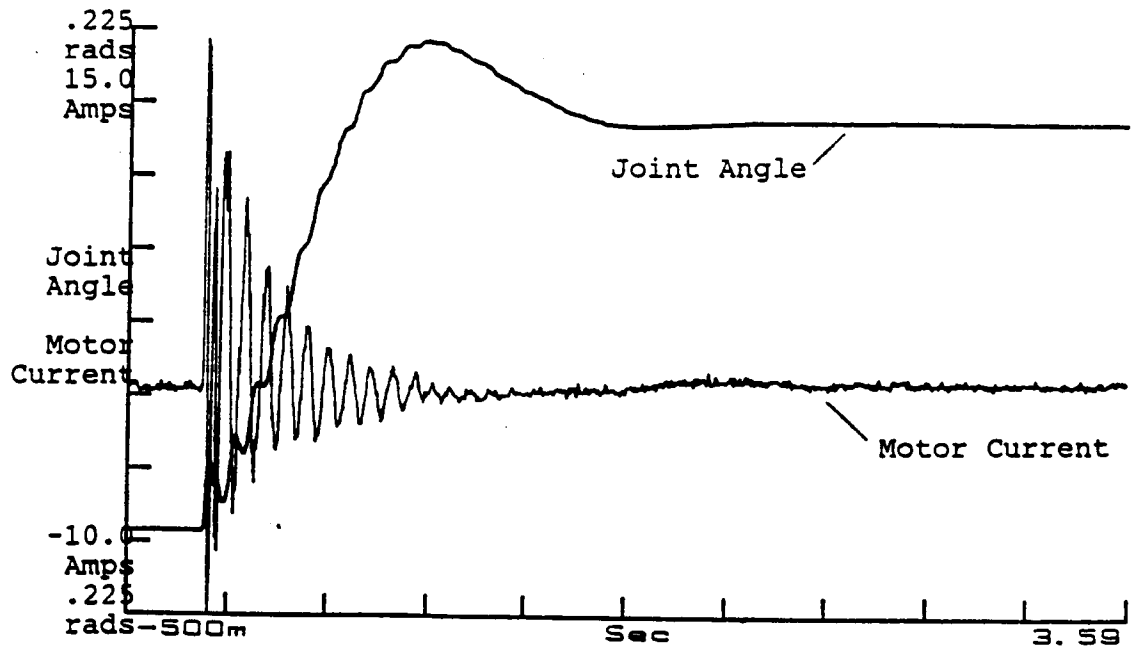
Figure 7-21a. High Stiffness,Modal Controller,
Joint Angle/Motor Current Step Response
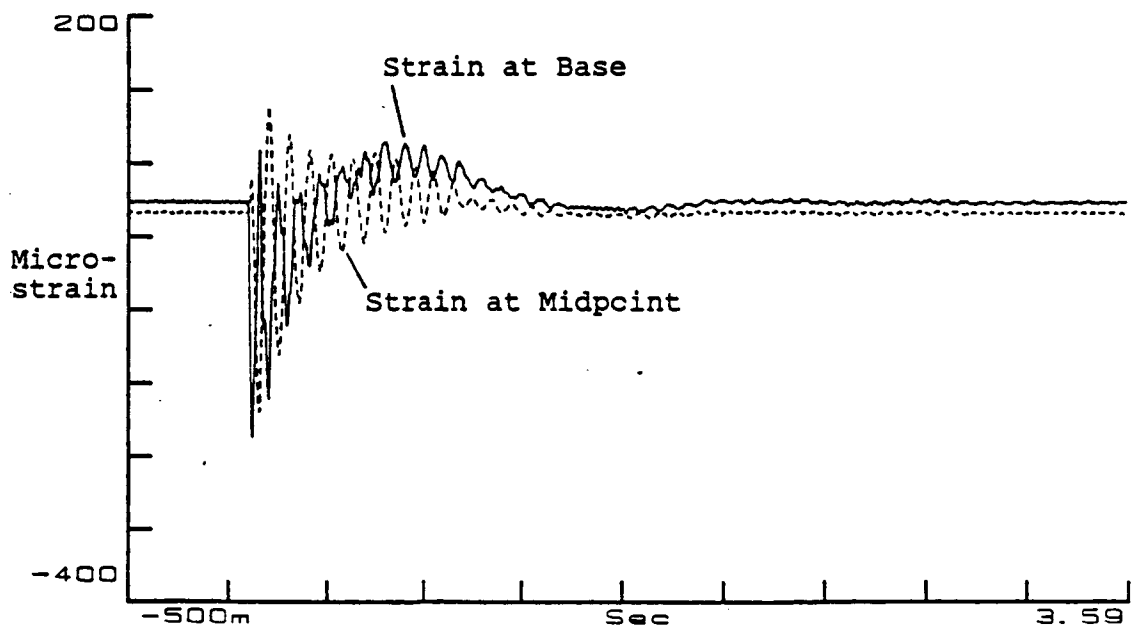
Figure 7-21b. High Stiffness, Modal Controller,
Strain at Base/Midpoint Step Response
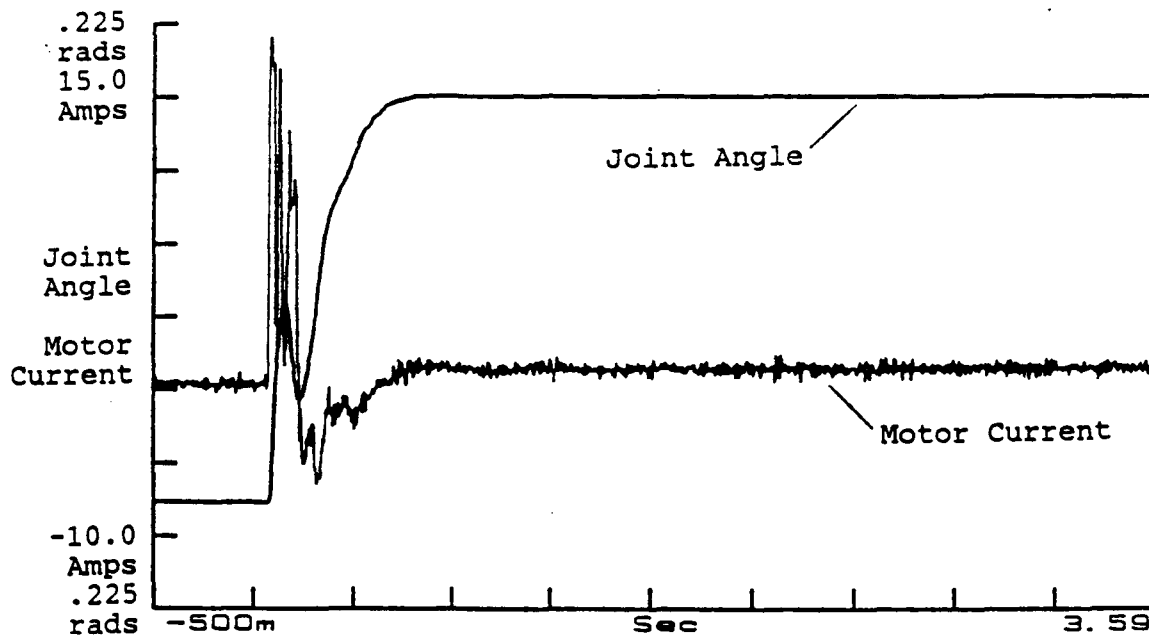
Figure 7-22a. Modal Damping Only, Modal Controller,
Joint Angle/Motor Current Step Response
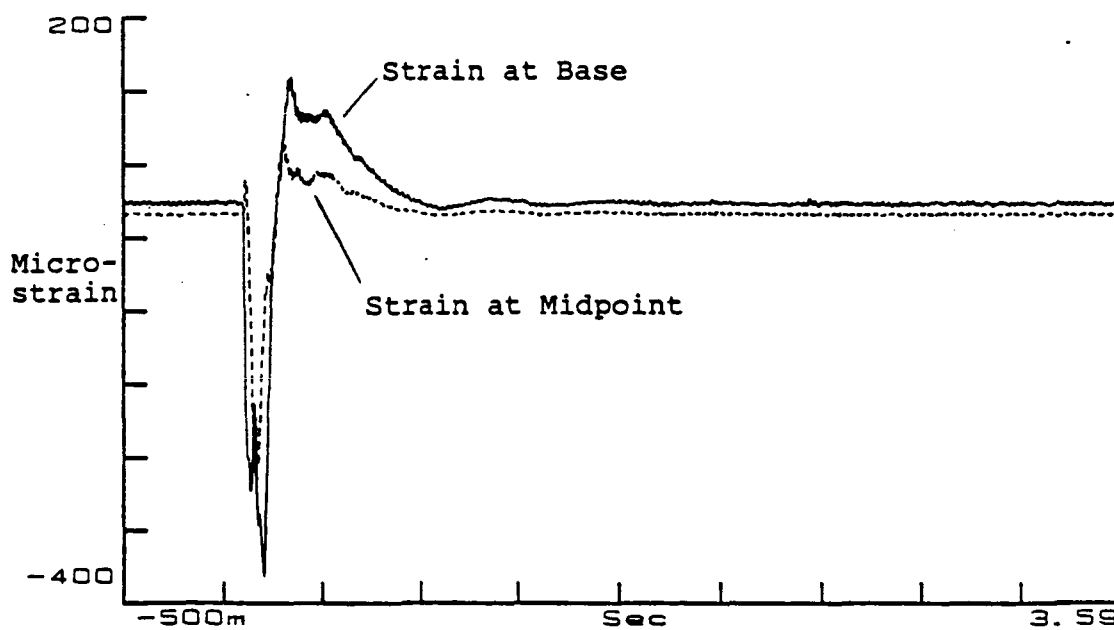
Figure 7-22b. Modal Damping Only, Modal Controller,
Strain at Base/Midpoint Step Response

The second case of damping gain only on the flexible mode coupled with moderate gains on the joint variables is shown in figure 7-23. This time the modal damping gain was increased over the last case, and a pinned-free vibration mode was excited.

Table 7-11. Design Results, Gain Vectors,
Closed Loop Eigenvalues for Figure 7-23

Discrete Gains
F(modal) = 1306.7 -0.0 529.9 -50.0

Continuous Eigenvalues Modal Controller		Discrete Eigenvalues Modal Controller	
-3.13	2.12E-17	.851	-8.67E-19
-2.94	0.0	.985	-9.37E-19
-3.29	+/- 10.7	.983	+/-.050
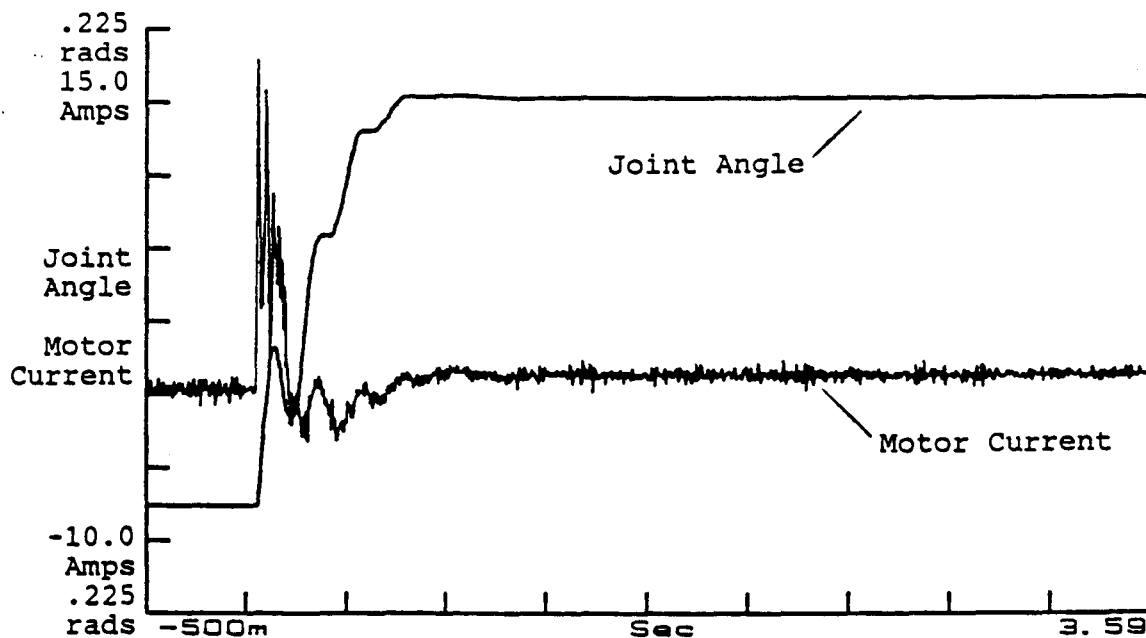
Figure 7-23a. Large Modal Damping, Modal Controller,
Joint Angle/Motor Current Step Response
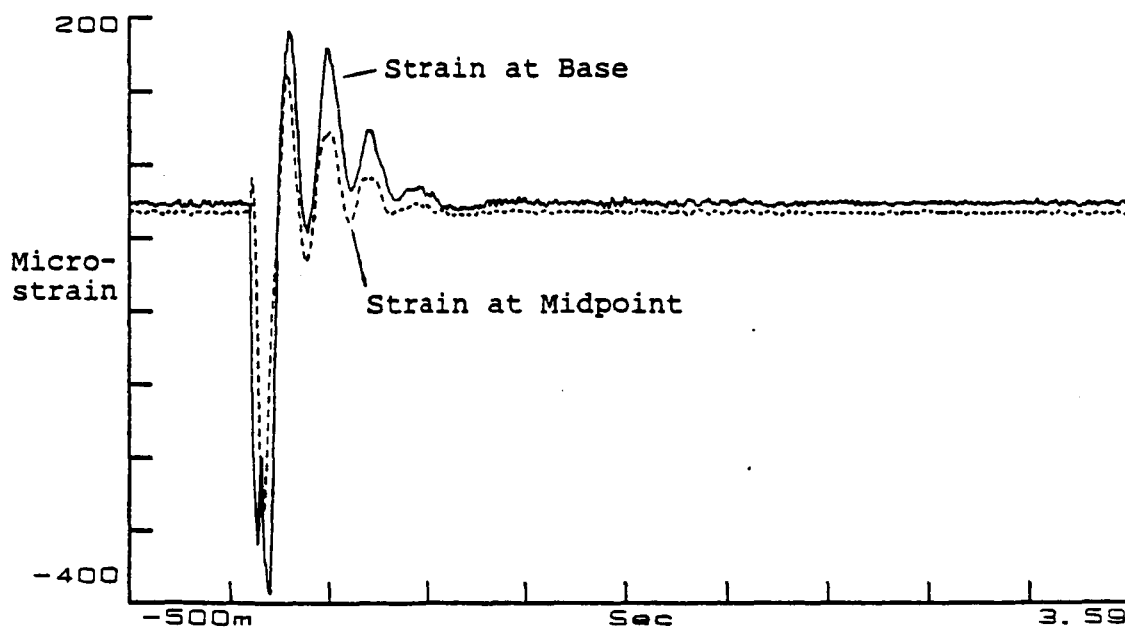
Figure 7-23b. Large Modal Damping, Modal Controller,
Strain at Base/Midpoint Step Response

7.3.4 Disturbance Rejection and Robustness

Two of the modal controllers from the previous section attained results consistent with the aims of the design process. The modal controller with the high prescribed degree of stability in both the rigid mode and the flexible with step response shown in figure 7-18 is examined in this section. Additionally, the controller with a larger prescribed degree of stability in the flexible mode (and higher damping gain than from the design process) with step response figure 7-20 is examined here.

7.3.4.1 Disturbance Impulse Response

An impulse hammer was used to apply a disturbance to the beam at the payload. This would correspond to the arm making contact with a work piece or bracing surface. The amplitude of the impulse was selected to cause a peak disturbance of roughly five to six inches at the payload. The time domain response of the beam was found to be the most revealing measurment, though frequency domain results could be obtained from the hammer impulse signal. Though the signal from the hammer was not utilized in these measurements, the design of the hammer still enhanced the operators control of the impulse delivered to the beam. The disturbance response of the modal controller with a large and equal amount prescribed stability is shown in figure 7-24, and the disturbance response of the controller with a larger degree of prescribed stability in the flexible mode
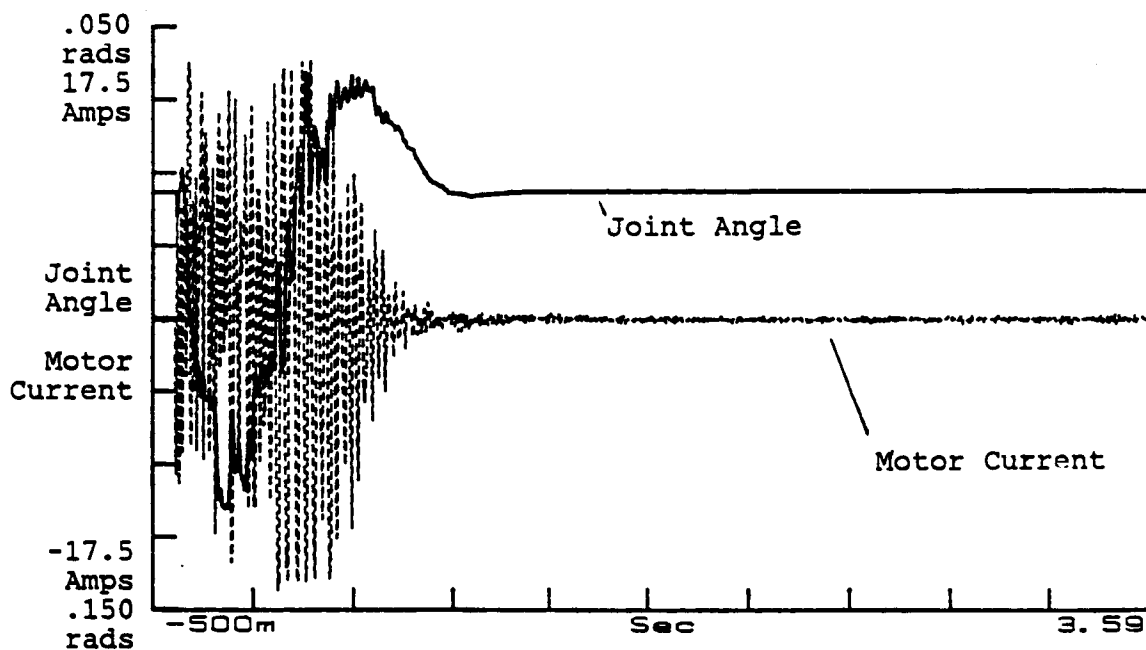
Figure 7-24a. Large α Modal Controller, Disturbance Impulse
Joint Angle/Motor Current Response
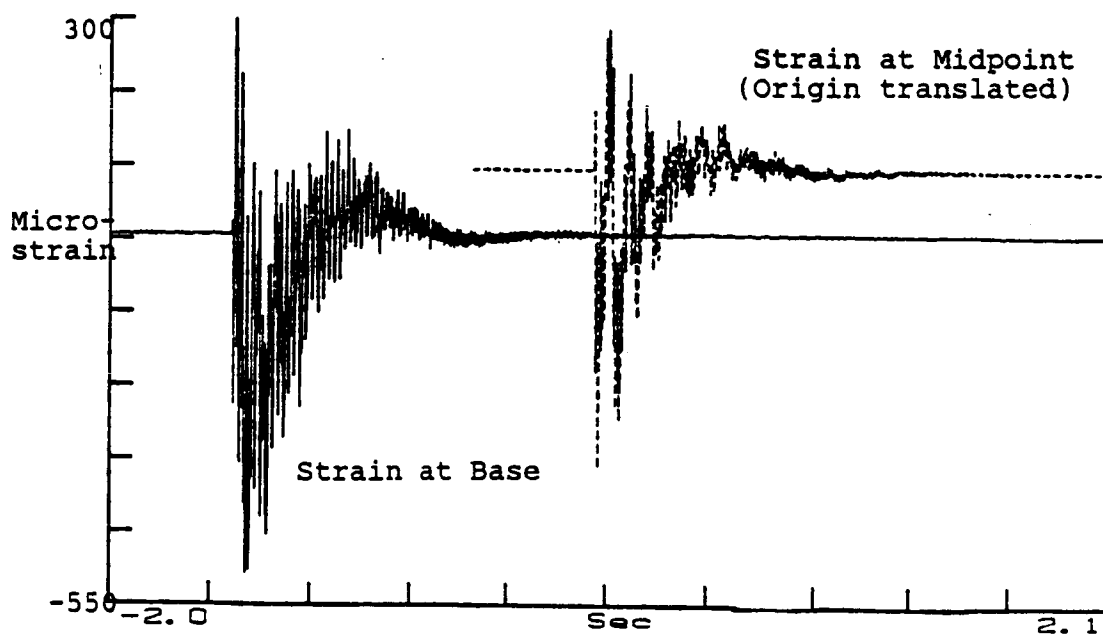
Figure 7-24b. Large α Modal Controller, Disturbance Impulse
Strain at Base/Midpoint Response
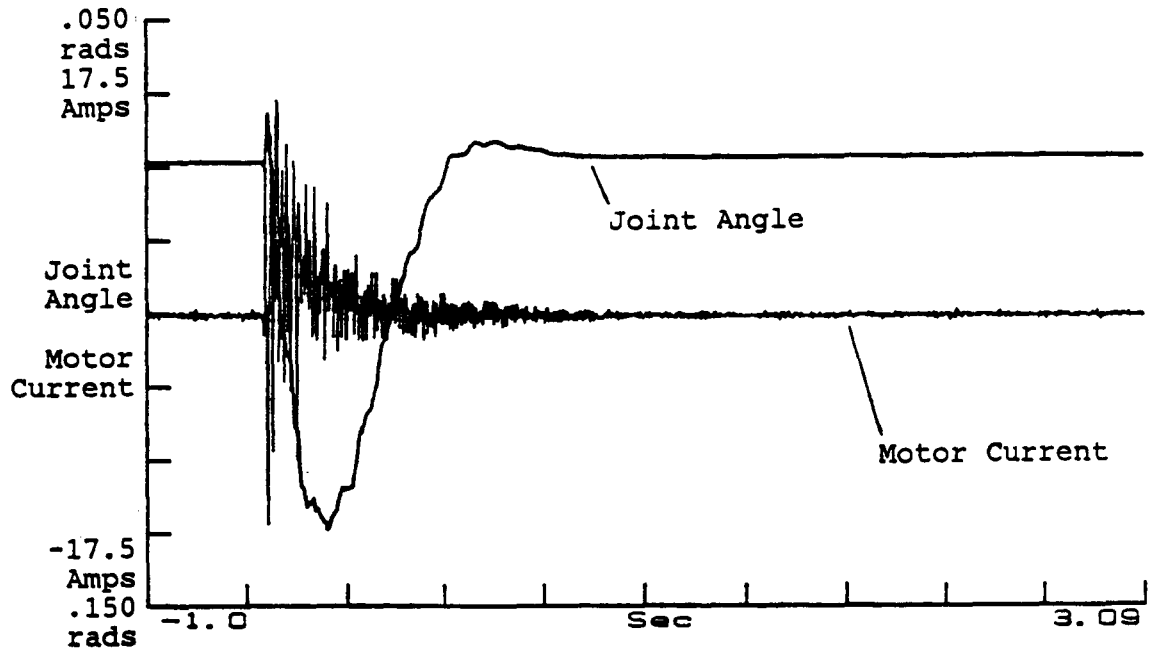
Figure 7-25a. Increased Modal Damping,Modal Controller,
Joint Angle/Motor Current Disturbance Response
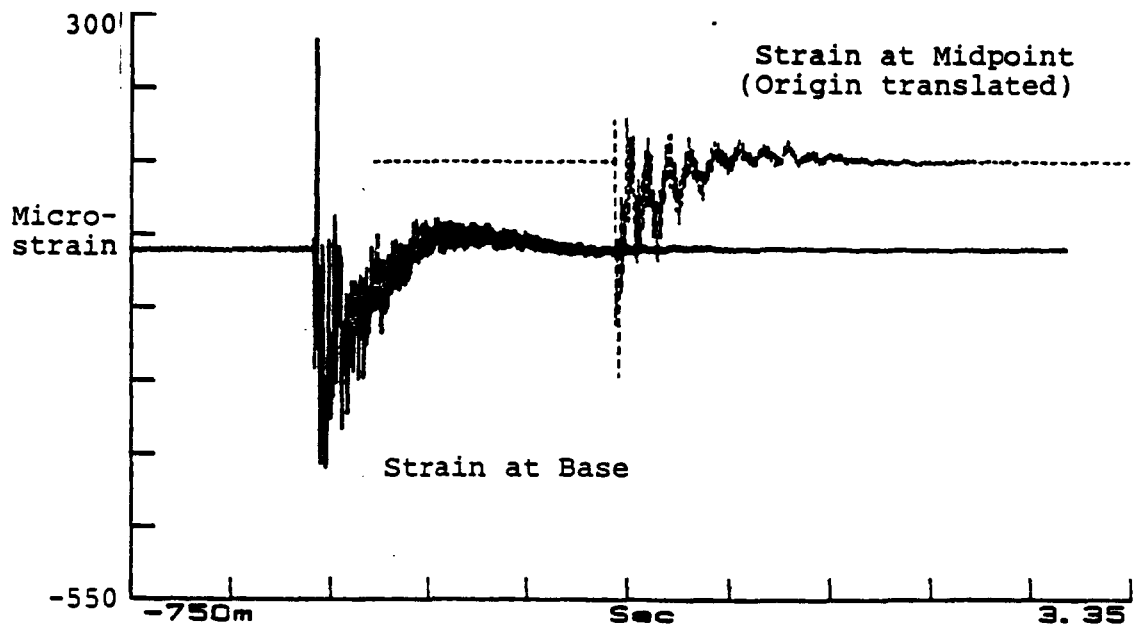
Figure 7-25b.Increased Modal Damping, Modal Controller,
Strain at Base/Midpoint Disturbance Response

is shown in figure 7-25. The large gains associated with prescribing a large degree of stability reduces the disturbance rejection of the system, as seen in the trace.

7.3.4.2 Payload Sensitivity

The payload was increased to a total of four times the design payload. Responses for the two cases are shown in figures 7-26, through 7-27. The increased mass results in the expected overshoot of the rigid mode. The response of the unteated higher flexible modes was generally reduced in the experimental observations. This is thought to result from the increased separation of the modal frequencies. The higher modes approach clamped-pinned shapes while the lower modes do not change significantly.
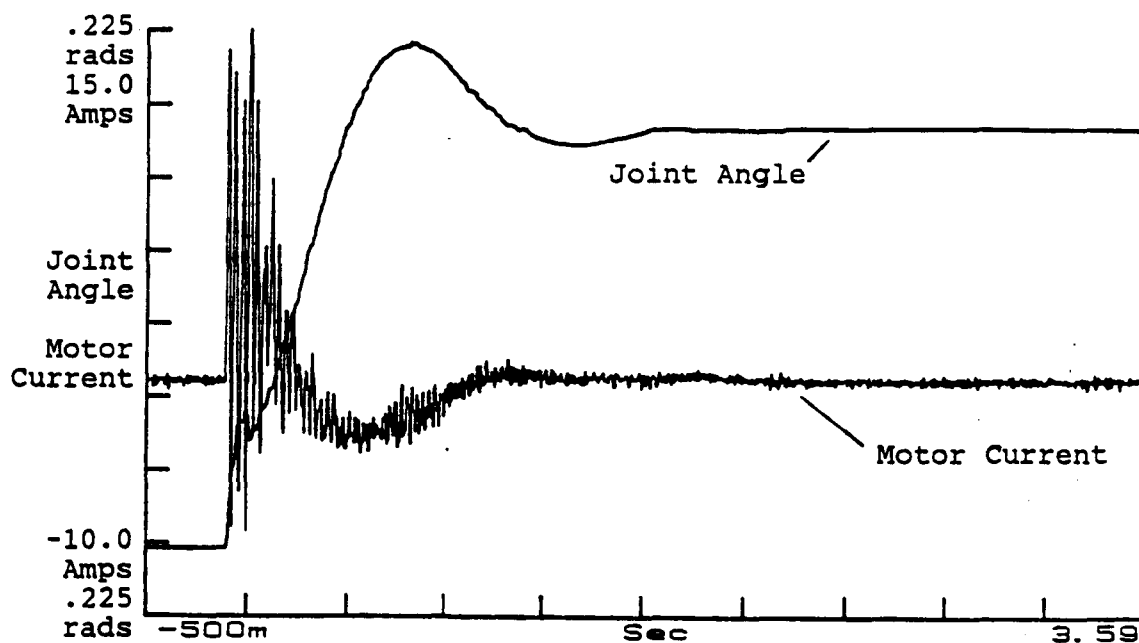
Figure 7-26a. Large α Modal Controller, 4 Times Payload,
Joint Angle/Motor Current Response
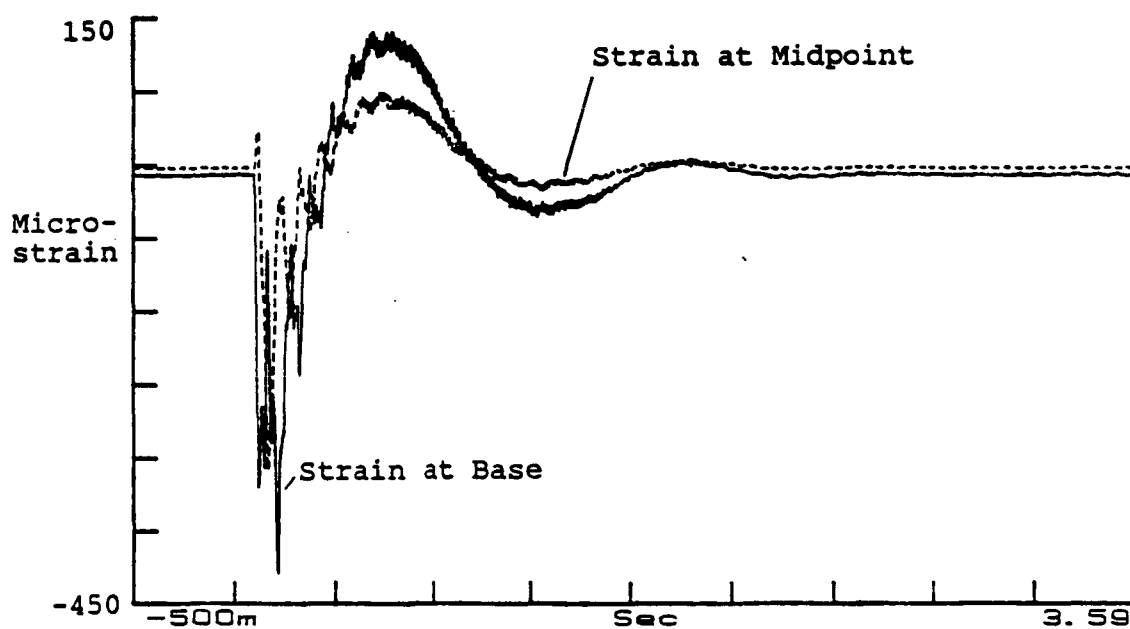
Figure 7-26b. Large α Modal Controller, 4 Times Payload,
Strain at Base/Midpoint Response
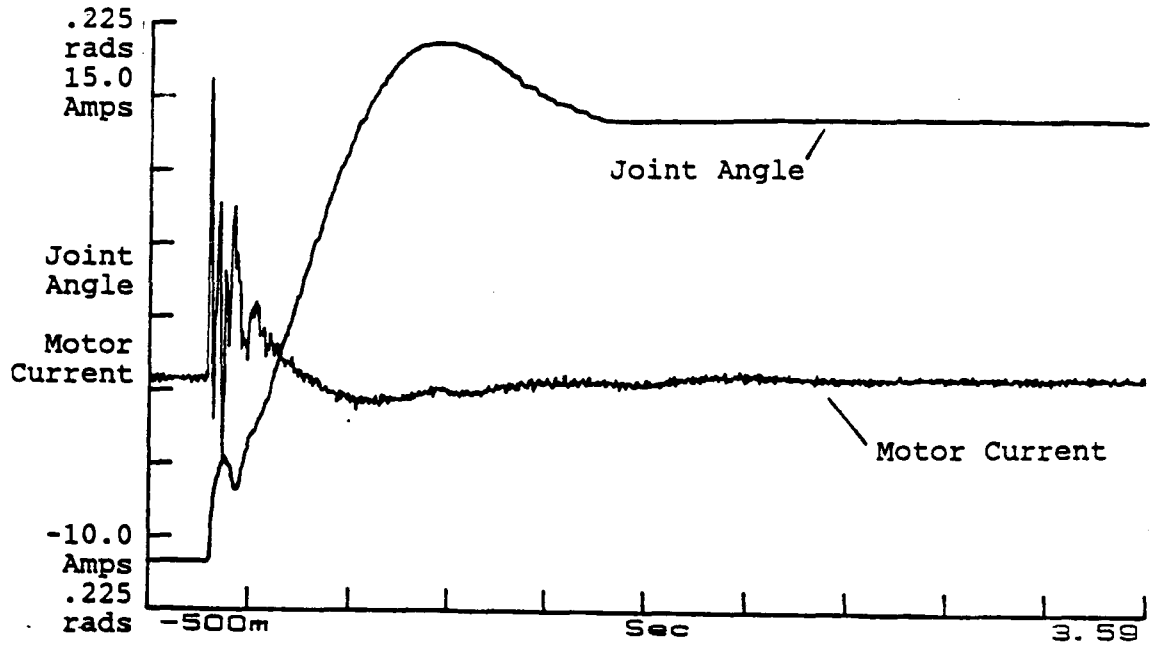
Figure 7-27a. Increased Modal Damping, Modal Controller,
4 Times Payload, Joint Angle/Motor Current Response
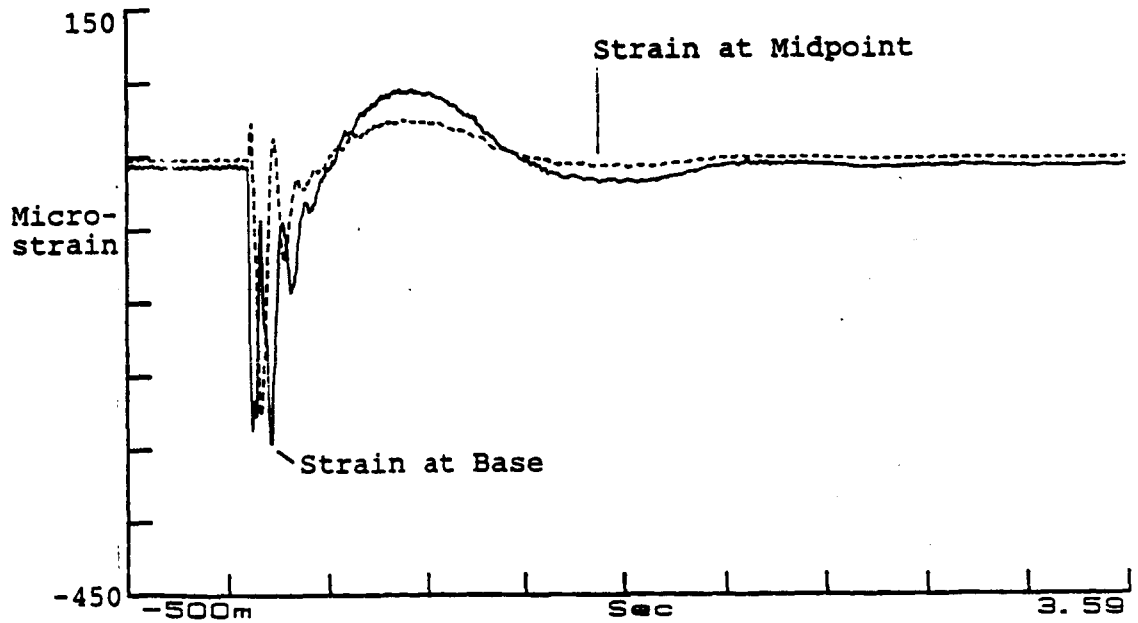
Figure 7-27b. Increased Modal Damping, Modal Controller,
4 Times Payload, Strain at Base/Midpoint Response

7.4 Summary

Control laws designed as linear quadratic regulators did successfully damp and control the vibratory modes included in the system model. The controllers were even successful in the presence of joint friction and measurement noise.

Using the prescribed degree of stability in the regulator design process allowed for rapid and direct placement of the model poles.

Attaining a rapid cycle time for the digital control implementation by neglecting the second flexible mode resulted in an improved response over the inclusion of the second mode.

Even small amounts of modal feedback resulted in more stable systems than collocated controllers, though the stability was added to untreated modes.

Attempts to obtain very short settling times for the system by prescribing large degrees of stability were ineffective. Though the rigid and flexible modes appeared to individually achieve tighter control, coupling between the modes caused the overall time to remain roughly the same. Fast joint rotations caused large modal amplitudes to be occur, and the large modal gains resulting from the large degree of stability required additional joint angle rotations to damp the mode.

The higher gains resulting from large prescribed degrees of stability also resulted in excitation of the higher untreated flexible modes, and poorer disturbance rejection. The best combinations resulted from placing more stability in the flexible mode, than the rigid mode.

Large gains always resulted in the appearance of untreated flexible modes. It was anticipated that trying to move the flexible poles far from the modeled poles would result in reductions of model accuracy. This was indeed the observed result.

CHAPTER VIII

KALMAN FILTER

8.1 Introduction

This section discusses the application of a Kalman Filter to estimate the modeled states. The estimated states are then used to generate control torques for the experimental arm based on a LQR state feedback law.

For a linear system subject to white noise plant disturbances $w(t)$ and white measurement noises $v(t)$,

$$x_{i+1} = Ax_i + Bu_i + w_i \qquad (8.1)$$

$$Y_i = Cx_i + v_i \qquad (8.2)$$

$$u_i = K^T x_i \qquad (8.3)$$
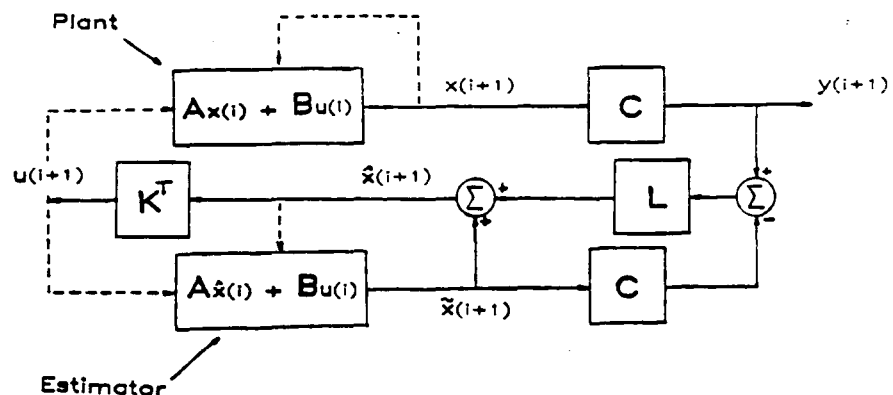
Figure 8-1. Kalman Filter Block Diagram

a filter can be designed with the structure shown in figure 8-1 which minimizes the mean error.

The task is to determine a steady state filter gain, L, which minimizes the performance index,

$$PI = 1/2 \sum [\tilde{e}_i^T M^{-1}{}_i \tilde{e}_i + (y_i - Cx_i)^T R_v^{-1}{}_i (y_i - Cx_i)] \qquad (8.4)$$

M is the covariance of the filter error between the updated estimate, and the plant. R_v is the covariance of the measurement noise. The formulation and solution to this problem is discussed in detail in Appendix D.

8.2 Implementation

The Kalman Filter discussed above was implemented for a model with a rigid mode and one clamped-mass flexible mode. Software for the IBM Series/1 executed at a cycle time of 5.85 milliseconds, slightly faster than that for the two mode observer yet significantly slower than the single mode observer. One of the reasons for the favorable speed compared to the two mode observer is the removal of the reconstruction algorithm. The measurement matrix include the strain measurements directly as shown in equation (8.5).

$$y = [\; \theta, \varepsilon(x=0), \varepsilon(x=1/2), \dot{\theta} \;] \qquad (8.5a)$$

$$x = [\; \theta, q, \dot{\theta}, \dot{q} \;] \qquad (8.5b)$$

$$C = \begin{vmatrix} 1.0 & 0.0 & 0.0 & 0.0 \\ 0.0 & c\dfrac{\partial^2 \phi(0)}{\partial \eta^2} & 0.0 & 0.0 \\ 0.0 & c\dfrac{\partial^2 \phi(.5)}{\partial \eta^2} & 0.0 & 0.0 \\ 0.0 & 0.0 & 1.0 & 0.0 \end{vmatrix} \qquad (8.5c)$$

8.3 Measurement Noise

The measurement gain, L, for the Kalman Filter depends entirely on knowledge of the covariances of the measurement, and plant disturbances. It is difficult to gain a thorough knowledge of the disturbances to the plant, especially in this case where it is hoped that unmodeled plant dynamics may be treated as disturbances. Information about the measurement noise is easier to gain and forms the starting point for this investigation.

The power spectrums for the joint angle, joint angle velocity, strain at the hub, and strain at the midpoint of the beam were captured using a Hewlett Packard 3562A spectrum analyzer.

The noise was thought to be bandlimited by a characteristic time of less than two seconds. The noise variance can be determined to within 10 percent by taking autocorrelation measurements over sampling intervals of at

least 100 seconds as given by;

$$T = \frac{1}{.1^2} \cdot \frac{2}{\beta} \qquad\qquad (8.6)$$

where the .1 represents the needed accuracy, and β the limiting time. This is an approximation for Gauss-Markov correlation functions [VIII1].

The joint angle and beam tip were fixed to prevent rotations and vibration, and the power spectrums averaged over ten periods. Additionally, the sampling time was doubled to avoid wrap around, as suggested in the operating manual for the spectrum analyzer [VIII2]. This required roughly thirty minutes of data collection for each measurement.

The resultant power spectrums were inverse Fourier transformed to obtain the autocorrelation function, and estimate of the variance. The power spectrums for the joint angle, figure 8.2a, and strain at the base, figure 8.2b, are presented as examples of the noise spectrum. The corresponding autocorrelation functions are shown in figures 8.3a, and 8.3b.
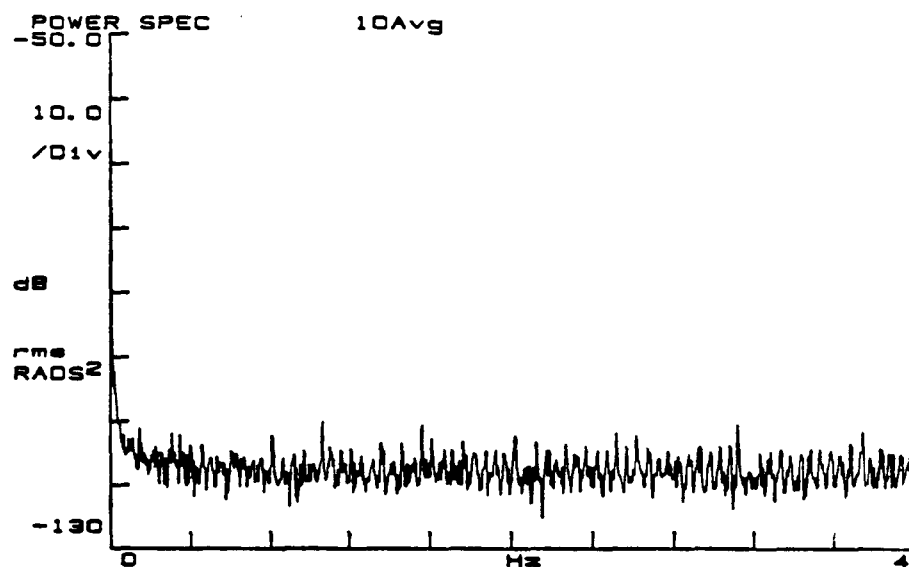
Figure 8.2a. Joint Angle Noise Power Spectrum
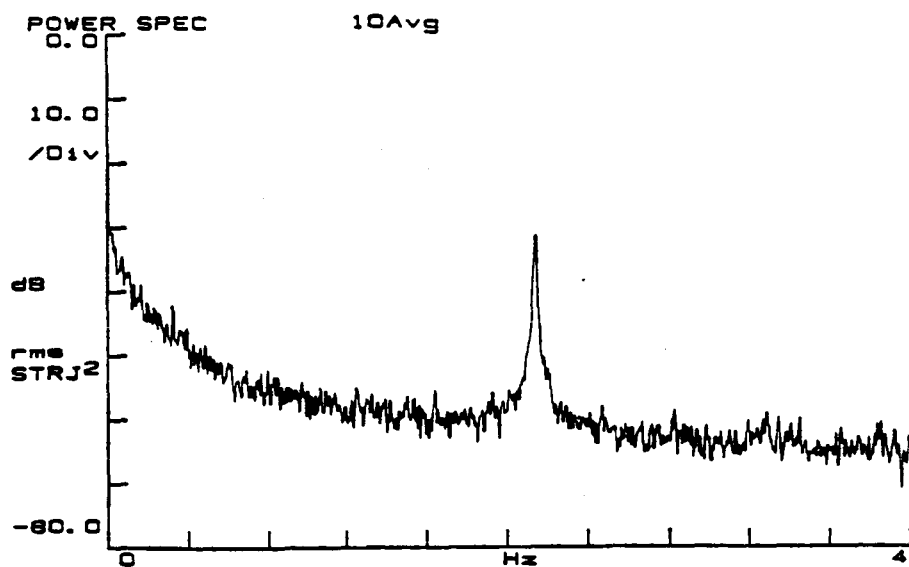
Figure 8.2b. Strain at Base Noise Power Spectrum.
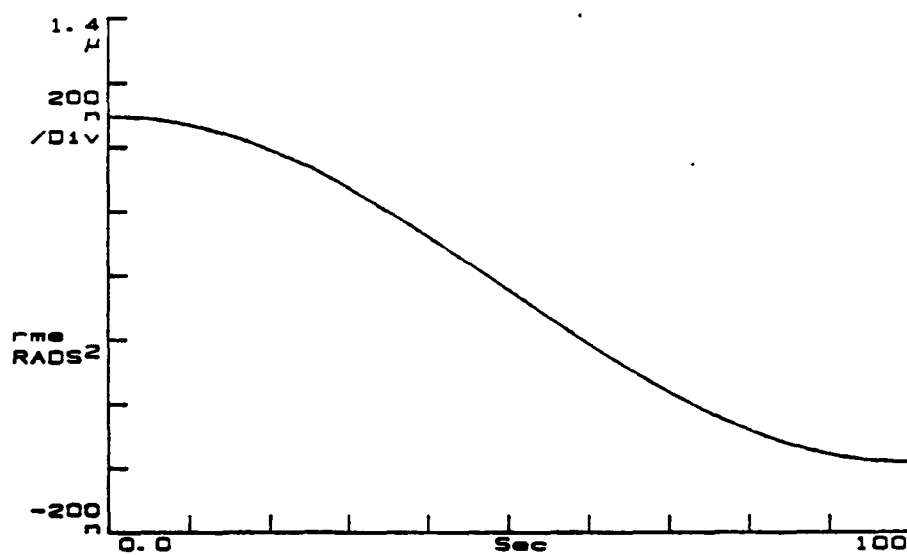
Figure 8.3a. Joint Angle Noise Autocorrelation Function
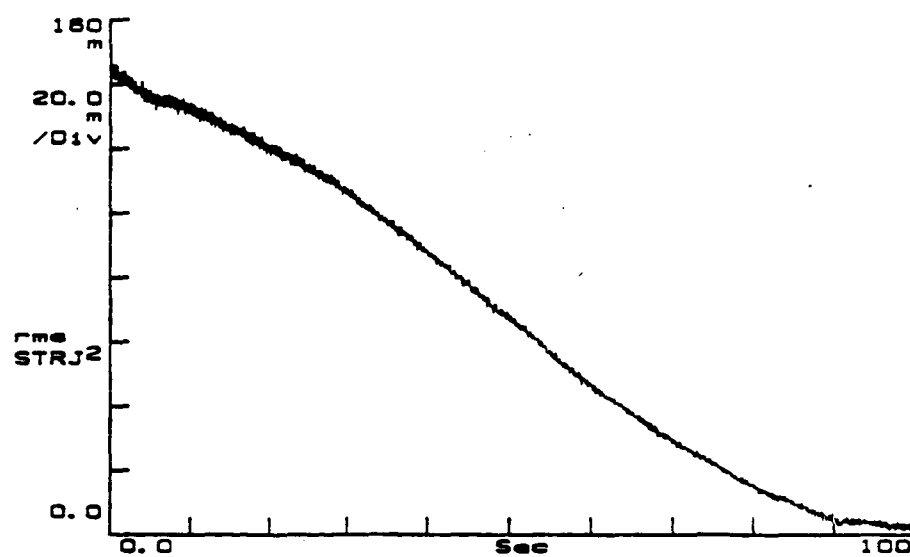
Figure 8.3b. Strain at Base Noise Autocorrelation Function

The estimates of the measurement noise variances based on the autocorrelation functions are shown in table 8.1.

Table 8-1. Noise Variance Estimates Based on
Autocorrelation Measurements

Measurement	Variance Estimate
Joint Angle	$1.1E-6 \; rad^2/sec$
Joint Velocity	$238E-6 \; rad^2/sec^3$
Strain at Base	$141E-9 \; Strain^2/sec$
Strain at Midpoint	$936E-9 \; Strain^2/sec$

8.4 Filter Design

The parameters available to the Kalman Filter designer are the measurement noise specifications, the elements of the disturbance noise distribution matrix, G, and the matrix of disturbance noise intensities I shown in equation (8.6). The covariance of the noise w_i for the digital implementation is determined from the distribution matrix, G, and the continuous noise, w(t) with intensities I, as shown in equation (8.7).

$$\dot{x} = Ax + Bu + Gw \qquad (8.6)$$

$$Q_k = e^{A\Delta t}Q_{k-1}e^{A^T\Delta t} + \int_0^{\Delta t} e^{A\tau}GIG^Te^{A^T\tau}d\tau \qquad (8.7)$$

The character of the distribution matrix, G, and intensity matrix, I, are often extremely difficult to determine [VIII3]. The untreated modes couple to the system

through the mass and stiffness matrices, as well as the control inputs by corrupting the strain measurements.

Attempting to model the untreated modes as noises, and selection of an appropriate distribution matrix, G, for this case results in a tremendous parameter space to search. The following strategy [VIII3] has been suggested as one method for tackling the Kalman Filter design problem, and was partially utilized by Schmitz [VIII4] in his experimental work. A state estimator robust with respect to errors in modeling plant parameters can be obtained. The first step is to assume that the disturbances to the plant are caused by the control and are distributed by the input matrix, B. Next, the covariance of the plant disturbance is assumed to be much greater than the covariance of the measurement noise. This results in a robust state estimator with poles close to the poles of the plant. This strategy was examined experimentally. The parameters and design results are contained in table 8-2.

The control laws resulting from LQR design were oupled with the Kalman Filter estimates of the states to form a closed loop system. Separation of the poles is assured, as shown for the state observer in chapter 6. Use of these control laws additionally provides a point of comparison with the reduced order observer/reconstruction controller discussed in chapter 7.

Table 8-2. Kalman Filter Design Results

State Vector $x_i = [\ \theta,\ q,\ \dot{\theta},\ \dot{q}\ ]$

Measurement Vector $y_i = [\ \theta,\ \varepsilon(0),\ \varepsilon(.5),\ \dot{\theta}\ ]$

Measurement Matrix (strain measured in micro strain)

$$C = \begin{vmatrix} 1.0 & 0.0 & 0.0 & 0.0 \\ 0.0 & 1530.0 & 0.0 & 0.0 \\ 0.0 & 630.0 & 0.0 & 0.0 \\ 0.0 & 0.0 & 1.0 & 0.0 \end{vmatrix}$$

Measurement Noise Covariance Matrix
V = diag[1.09E-6 .145 .939 2.37E-4]

Plant Noise Covariance
Q = 1.0E+6

Measurement Gain

$$L = \begin{vmatrix} 4.318E-2 & -4.238E-5 & -2.621E-6 & 1.914E-3 \\ -3.552E-5 & 2.412E-4 & 1.491E-5 & -8.4341-3 \\ 4.142E-1 & -2.178E-3 & -1.346E-4 & 9.492E-1 \\ -1.322 & 9.902E-3 & 6.122E-4 & -4.416 \end{vmatrix}$$

Discrete Eigenvalues (A-LC)
.2386
.4231
.9773 +2.42E-2
.9773 -2.42E-2

8.5 Experimental Results

Initially the collocated control law of table 7-1 was applied to the Kalman Filter state estimates. This control law was stable for the two mode controller whose cycle time was roughly the same. Coupling this control law to the Kalman Filter resulted in growing oscillations of the third flexible mode during experiments with this control law.

Another control law was designed with a reduced degree of prescribed stability and applied to the estimated states. The step response for this control law is shown in figure 8-4. The closed loop feedback back poles are identified in table 8-3 for the collocated, and modal control law.

Note the slow decay of the 43Hz oscillation, and the overshoot of this controller. The process was repeated with a modal controller with the same prescribed degree of stability. The response for this case is shown in figure 8-5. There is very little alteration of . the response; the Kalman Filter is obviously not tracking the states of the system very well.
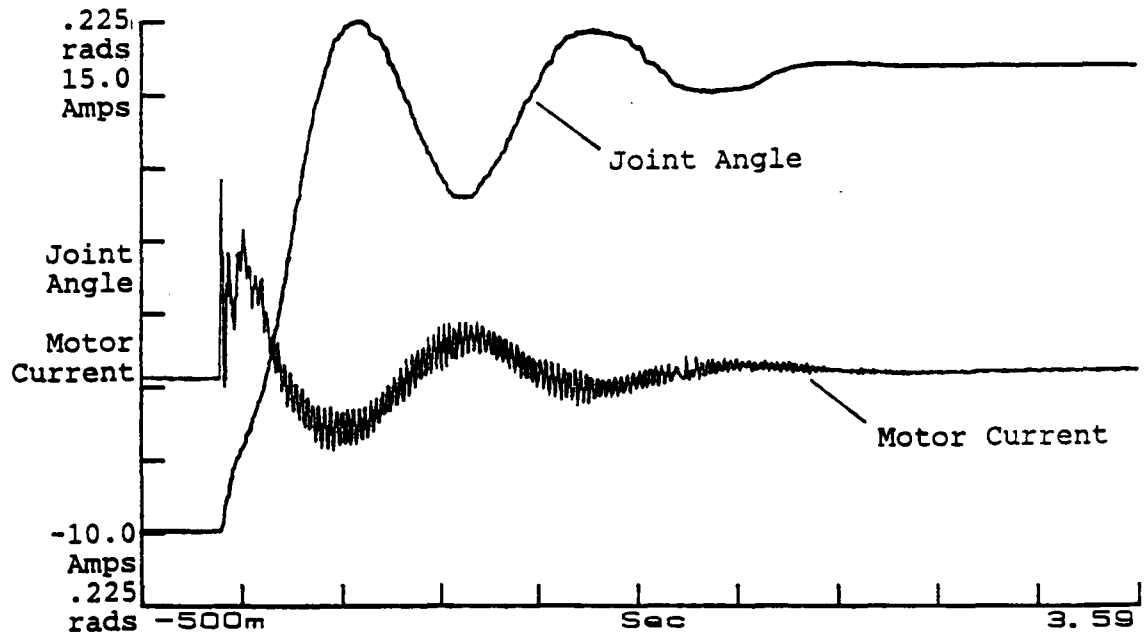
Figure 8-4a. Collocated Control Law, Joint Angle,
and Motor Current Response.
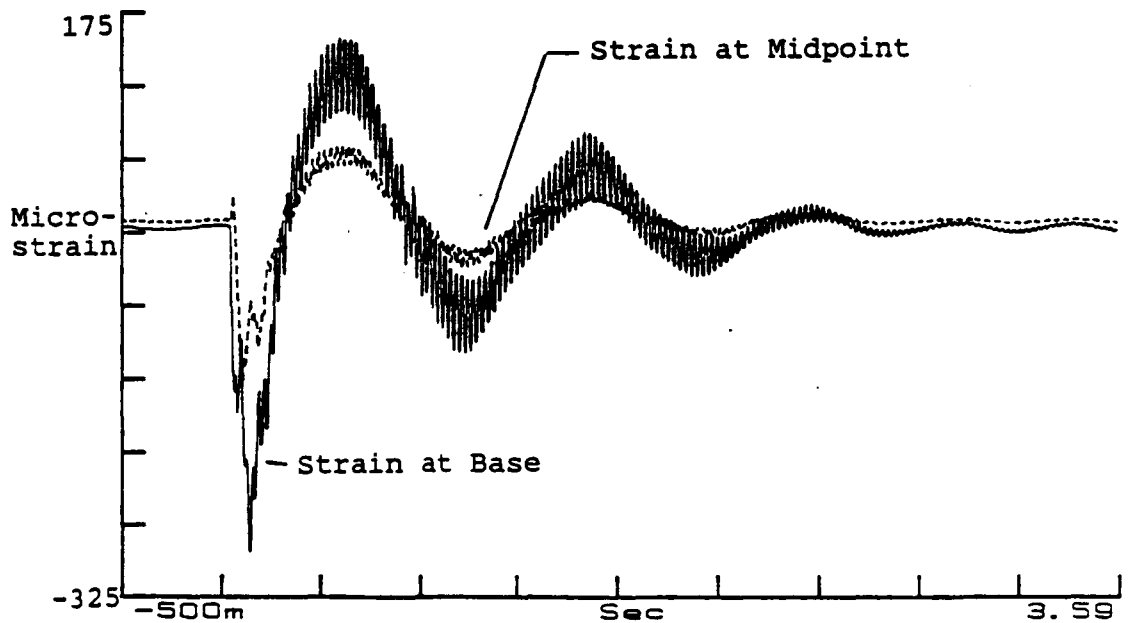
Figure 8-4b. Collocated Control Law, Strain at Base,
Strain at Midpoint Response.

From experience it was apparent that the overshoot could be reduced by forcing the Kalman Filter to track the joint angle more quickly. The element of the gain matrix $L(1,1)$ which is the update of joint angle estimate due to joint angle measurement was increased ten fold. The step response was repeated with the modified measurement gain. The result is recorded in figure 8-6.

Table 8-3. Closed Loop Poles.

Collocated Feedback Law
F = [667.   0.   349. 0.]

Modal Control Law
F = [667. -220. 349. 9.]

Discrete Eigenvalues

Collocated Control Law		Modal Control Law	
.957	3.323E-18	.973	-1.086E-18
.983	-4.381E-18	.978	+3.782E-20
.969 +/-9.700E-02		.970 +/-1.100E-01	
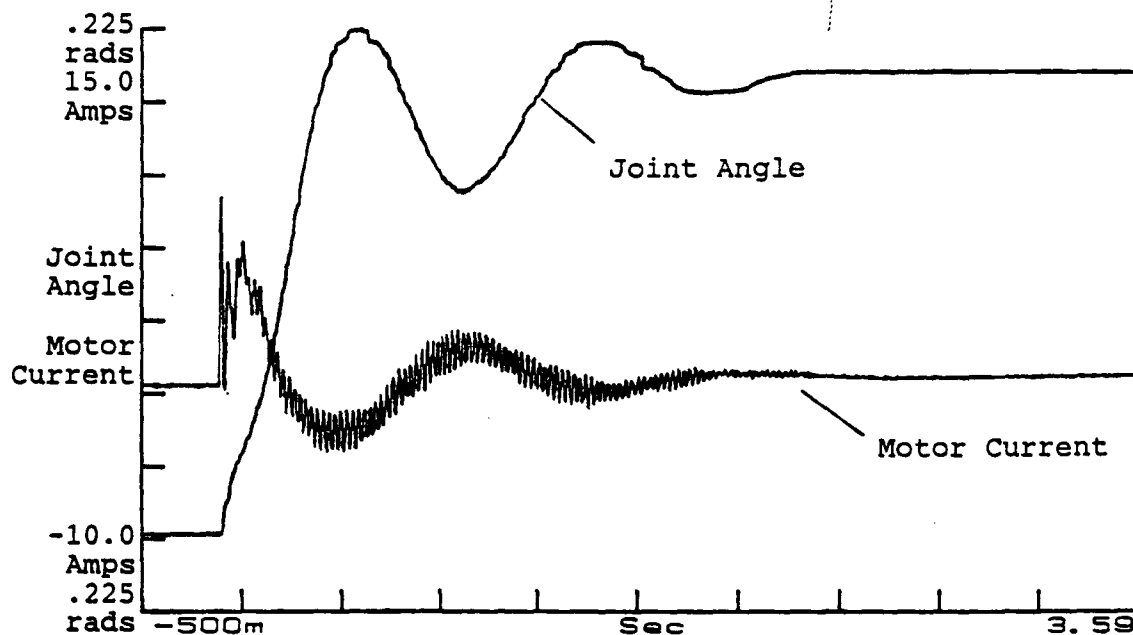
Figure 8-5a. Modal Control Law, Joint Angle,
and Motor Current Response.
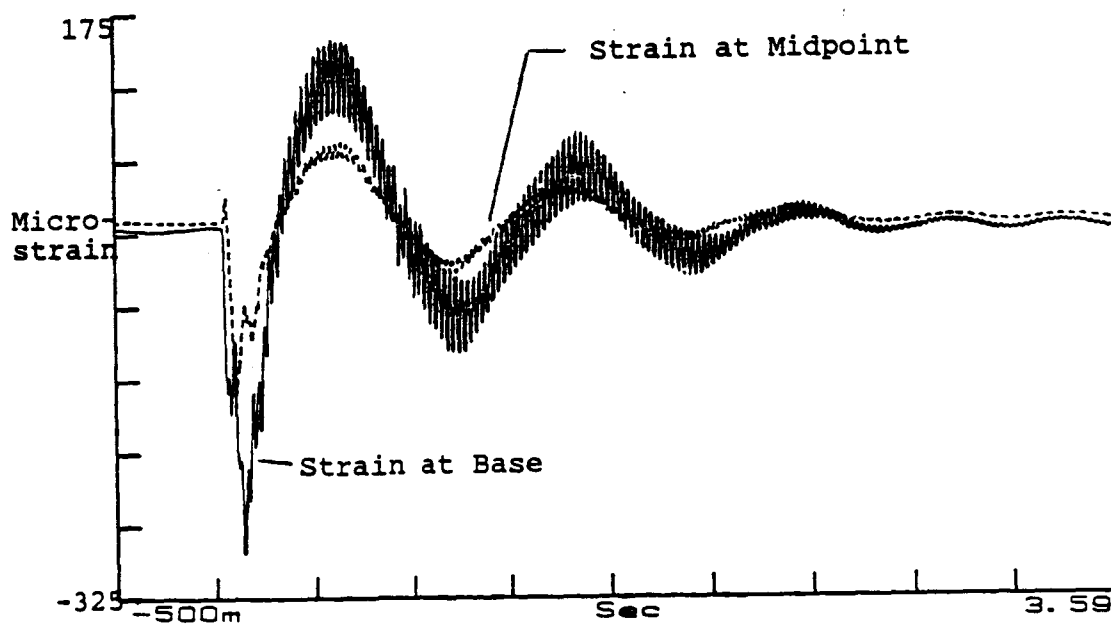
Figure 8-5b. Modal Control Law, Strain at Base,
Strain at Midpoint Response.
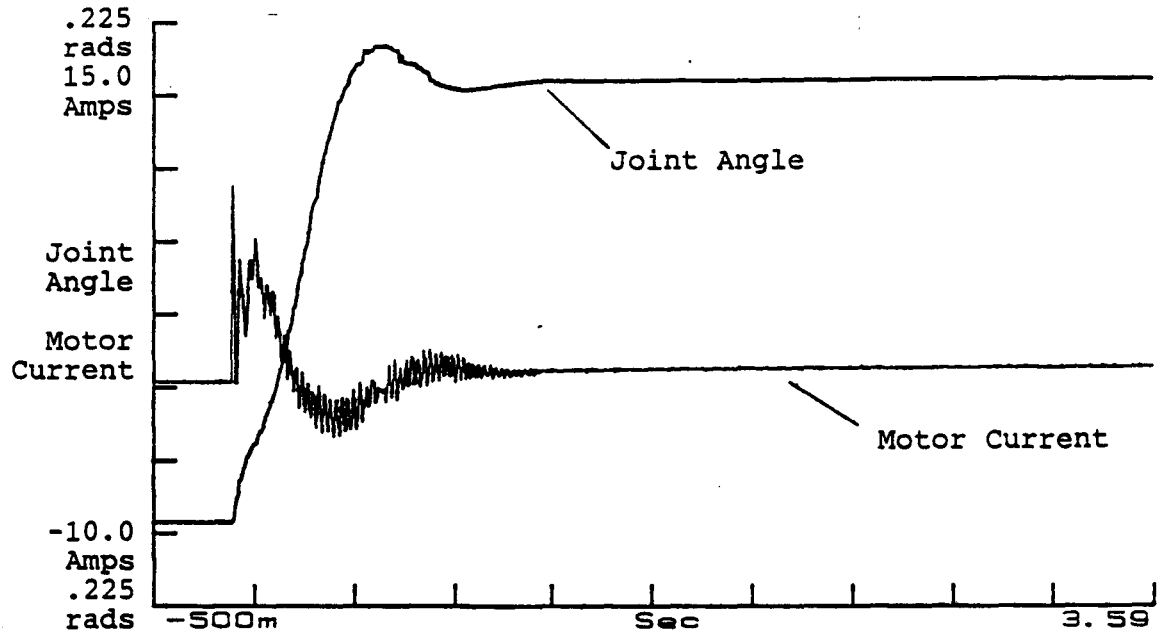
Figure 8-6a. Modified Measurement Gain, Joint Angle,
and Motor Current Response.
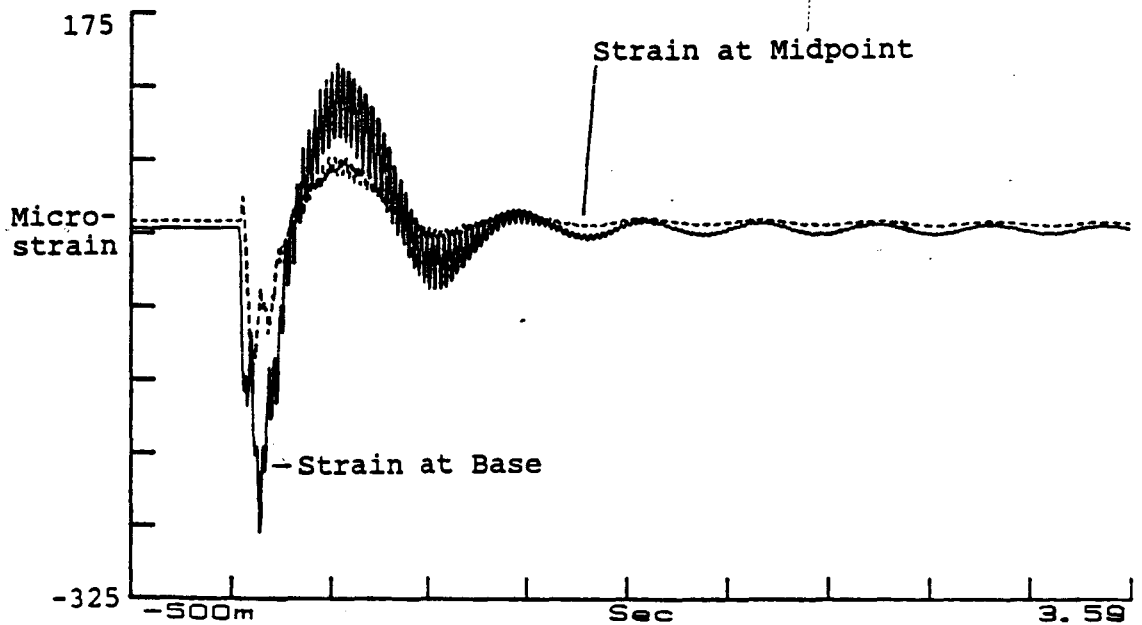
Figure 8-6b. Modified Measurement Gain, Strain at Base,
Strain at Midpoint Response.

The results of this intuitive change in the measurement gain is readily apparent. It much more difficult to cause this type of change through creating "fictitious" noise values in the measurement covariance.

Several other plant covariance values were examined, with similar results. It quickly became apparent that this was not a suitable approach to estimator design.

8.6 Summary

Comparison of the experimentally determined noise covariances to the levels of periodic excitations caused by the truncated higher flexible modes indicates that the control problem is dominated by truncation effects, as opposed to stochastic noise. The experimentally determined noise covariances result in expectations of very small errors from the these sources. This is particularly true in light of the measured content of the untreated flexible modes during the control experiments conducted in chapter 7. Some strain traces presented in chapter 6 contained periodic amplitudes due to the higher flexible modes on the order of 100 microstrain. The joint angle trace in many responses was also significantly corrupted by the higher modes. Thus the impact of the unmodeled modes in the system is far more important than a consideration of the system noise. Additionally, approximation of the impact of the distinct modal frequencies on the system by white noise covariance

estimates is extremely questionable.

For some systems, such as airplanes, modeling flutter of lift surfaces as stochastic disturbances to the craft is more appropriate. The flutter can be measured or rationally approximated, as well as the manner in which the disturbance propagates through the system dynamics. Additionally, the aircraft disturbances are typically at much higher frequencies than the characteristic eigenvalues of the craft [VIII5]. This is not the case for the flexible manipulator.

Work done in chapter 6 indicated that observer poles for the estimation of the modal velocities needed to be much faster than the system poles being estimated. The Kalman Filter design process results in relatively slow poles close to those of the plant being estimated. This is reasonable, as the filter was intended to minimize the mean estimate error when the plant and measurements are subject to white noise. The speed of these poles results in slow convergence to the actual states for initial errors in state estimates and disturbances caused by the untreated modes.

Schmitz[VIII4] had limited success in dealing with this problem by using a higher order model, and generating fictitious estimates of the measurement noises. The fictitious noise estimates were parameterized, and the parameter space examined using root locus techniques to obtained a usable measurement gain, L, for the Kalman

Filter.

Use of the covariance values as a pole placement algorithm was not as direct or successful as the traditional method discussed in chapter 6 for the state observer design process. Use of the Kalman Filter design process to obtain pole placement is also thought to be impractical for future applications because:

- As measurements are added, as in this experimental work or in future multi-link systems, the parameter space becomes extremely large.
- The model is not diagonal, and parameter variations are coupled, thereby making the search of the parameter space even more difficult.

In view of what has been learned form this exercise, direct pole placement techniques, and traditional state observer design methods appear more suitable to the flexible arm problem at its current level of sophistication.

CHAPTER IX

CHRONOLOGY AND ADDITIONAL EXPERIMENTAL OBSERVATIONS

The work contained in the body of this dissertation chapters 1-8 follows a logical, cohesive path that is not completely representative of the course of work required to accomplish these results. This chapter discusses the sequence in which the experiments progressed, and additional interesting experimental observations regarding software, and hardware impacts on the experiments. The narrative and observations would interupt the flow of earlier chapters without adding insight to the results of a particular section yet they may be of interest and assistance to future researchers.

9.1 Experimental Chronology

Once the experimental apparatus had been assembled and verified a winding and broken path through the work described in this thesis began. This section tries to chronicle the sequence of events and comment on matters of possible interest to future investigation which might otherwise go unrecorded.

Initial experiments focused on implementation of a functional observer instead of the observer/regulator combination and the Kalman Filter discussed in earlier

chapters. A functional observer estimates a function of the states, for example a control law, instead of individual states. Functional observation can result in significant computational savings over state estimation, and then computation of the control. The computational savings associated with the functional observer was the source of the early attraction.

Unfortunately, implementation of the functional observer yielded unsatisfactory results and dramatically demonstrated the negative aspects of functional observation when applied to a system with many uncertainties. In trying to analyze the source of the discrepancies between prediction and observation, the functional observer was proved intractable experimentally.

The thesis effort took a dramatic turn at this point, trying to identify clear, functional divisions in the experimental apparatus and control system. Additionally, questions arose concerning the model and methods for it's evaluation. This led to functionally segmenting the system into a reconstruction algorithm, state observation algorithm, and controller as distinct elements.

Following analysis and design of the individual functional elements, the experimental process was initiated again with the observer/optimal regulator combination. Some useful results were obtained, but stability and performance observations were far from expectation. This led to the

sequence followed in the rest of the thesis, closely aligned with the chapter titles;

1. Examination of the Model
2. Examination of the Reconstruction Algorithm
3. Examination of the State Observation
4. Examination of the Optimal Regulator
5. Examination of the Kalman Filter

This evolved into an iterative process of analysis, experiment, and comparison of the two. The process was repeated until confidence was gained that hardware, design software, and controller software bugs had been eliminated. The work reported in the body of thesis could then be conducted.

Often the hardware, and software problems were not easily examined with the state space structure utilized for selecting control laws. As will be discussed in the next section, transfer function analysis was used in assessing the impact of many of the components.

As the work progressed, usually meaning the implementation of higher gains in a specific control design, more faults or problems became apparent. The most aggravating and recurrent problems came from sixty hertz AC power noise picked up by the measurements, measurement phase lag introduced by the Butterworth filters, and short life of the potentiometer. The final limitation to evaluation the proposed control schemes with this experimental system appears to be computational speed.

Sixty hertz noise repeatedly halted progress. It appeared as a distinct harmonic disturbance which at times excited modes in the 40Hz and 80Hz ranges.The sixty hertz AC noise was removed in phases by carefully assuring that the commons for all the signal conditioning devices were the same. Instrumentation methods of grounding and shielding the signal leads were implemented.

Instabilities which were not predicted by the analysis techniques in use at earlier phases of the research were particularly hard to resolve. Analysis discussed in the next section using transfer functions identified the Butterworth filters as the culprit. The filters were implemented initially to act as band pass and band reject devices in the hopes of improving separation between modes. Eventually, after many unsuccessful attempts to compromise between the performance and phase introduction, the filters were removed.

The mounting of the potentiometer used to measure joint angle rotations was a particularly troublesome component. A rubber grommet interfaced the potentiometer shaft to the motor hub. The grommet would wear and loosen, allowing slippage between the motor and potentiometer. The relative slip was of extremely small amplitude, and not noticed from observation of the endpoint position.

The typical onset of the slipping condition was noticed by a reduction in stability of the controller under

observation. The gradual onset of the slipping condition, coupled with the fact that the work was almost always progressing towards a tighter control law or new implementation, made the identification of this problem extremely difficult for the first few occurrences of this malady. The remedy was to replace the grommet.

9.2 Phase Sensitivity

The instabilities introduced by the four pole Butterworth filters were not easily identified by the state space structure used for control law design. At the time the instabilities were occurring, the source of the difficulties was unknown. The model and controller were suspect, as well as the hardware components. To investigate the problem, a simple and thoroughly analyzed collocated controller [IX1-3] was implemented. This would hopefully allow for separation of the hardware issues from the modeling issues.

Perhaps one of the most useful pieces of information available for resolution of the problem came from companion results for the unstable case with a passively damped beam. The passively damped beam showed an increased degree stability, and resultant analysis could be tested against the two cases. Figure 9-1 shows a time response for the experimental beam with collocated gains resulting in unpredicted instabilities. Surprisingly the instabilities are occurring in the second flexible mode. The measurement

is repeated with a passively damped beam, and this time the same gains do not result in instabilities in the second flexible mode as depicted in figure 9-2.

Many components of the system were considered as sources of unmodeled, and hence uncompensated dynamics. These included sample rate (partially analyzed by sample and hold discretization), digitization, torque motor/amplifier dynamics, Butterworth filters, and tachometer. These factors were examined individually and cumulatively for their effect on system performance.

These components as well as the beam were modeled as transfer functions, and assembled into an open loop transfer function, as shown in figure 9-3a, and a collocated feedback function as seen in figure 9-3. The transfer function, T(s) of Figure 9-3b, is the open loop function of 9-3a. The transfer function of the beam was common to the work of several researchers [IX4,5].

The collocated controller was also implemented in analog hardware to eliminate the questions regarding digitizing.
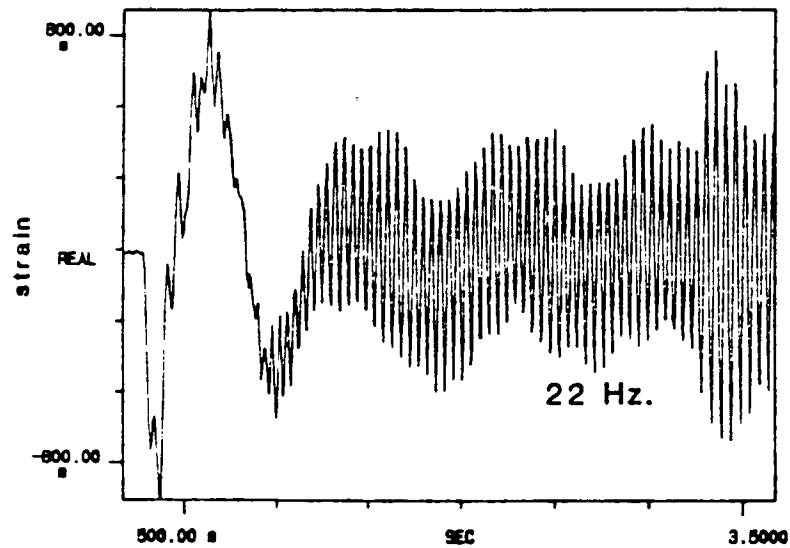
Figure 9-1. Time Response, Experimental Beam.
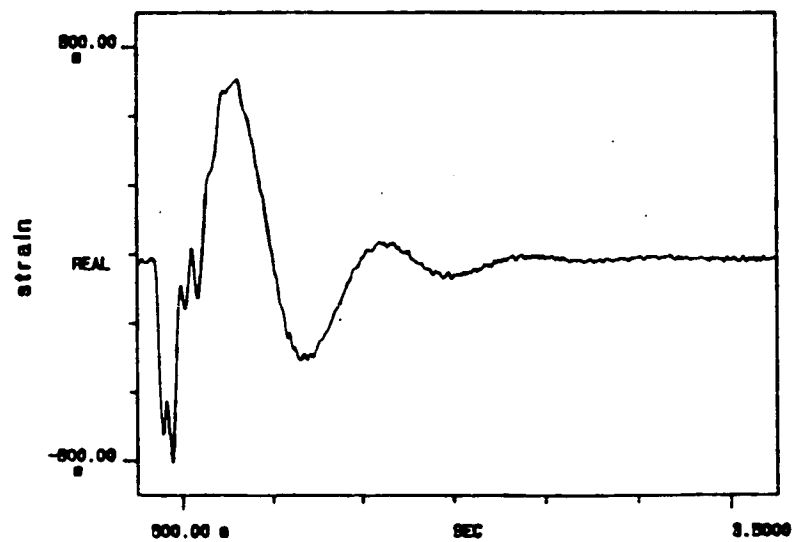
Figure 9-2. Time Response, Passively Damped Beam
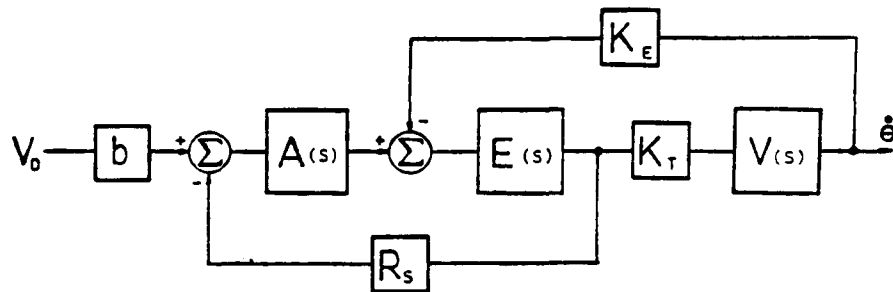
Figure 9-3a. Open Loop Transfer Function Model
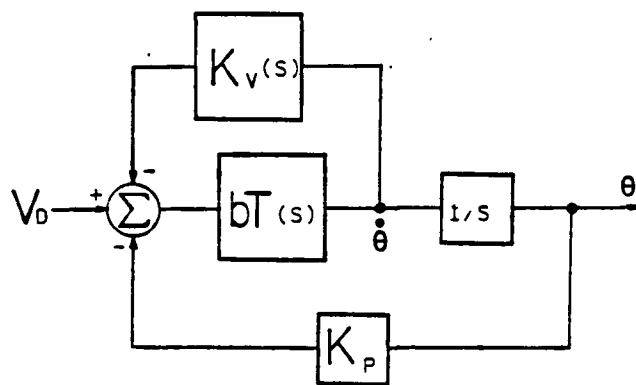
Figure 9-3b. Collocated Transfer Function Model

The various transfer functions utilized in the analysis are identified in table 9-1.

Table 9-1. Transfer Functions

A(s)   Amplifier Transfer Function,
        Voltage In to Voltage Out

E(s)   Motor Electrical Transfer Function,
        Voltage Applied to Current

V(s)   Beam Transfer Function,
        Hub Torque to Joint Velocity

K_e Motor Back Emf Constant

K_t Motor Torque Constant

b   Amplifier Gain

V_d Desired Torque

R_s Current Sense Resistor

K_v Velocity Feedback Transfer Function

K_p Position Feedback Gain

The resultant closed loop transfer function from commanded joint angle to joint angle could then be examined for varying gains by monitoring the closed loop pole locations. Evaluation of the torque motor/amplifier transfer function did not change the expected stable result for collocated feedback shown in figure 9-4.

Analysis of the discretization effects by a sample and hold model did have a slightly destabilizing effect, but did not significantly alter the earlier result for the torque motor amplifier combination, even when examined together.

Inclusion of a four pole low pass Butterworth filter used to filter commutation noise generated by the tachometer did have a drastic effect on the stability results. The drastic change in the departure angle from the open loop poles is depicted in figure 9-5. The analysis is repeated approximating the effect of the passive damping applied to the beam with modal damping values determined from frequency responses of the open loop beam. The plot is also depicted in figure 9-5.

It is apparent from figure 9-5 that the second mode goes unstable at sufficiently large gains. Additionally the frequency at crossover closely approximates the frequency of the instability determined from measurements shown in figure 9-1. This provides some confidence that the transfer function analysis employed is accurately modeling the observed phenomena.

The dramatic effect of the filter poles being driven into the right half plane, even though they are at a frequency roughly 30 times the modal frequency, emphasizes the proximity of the flexible poles to the real axis.
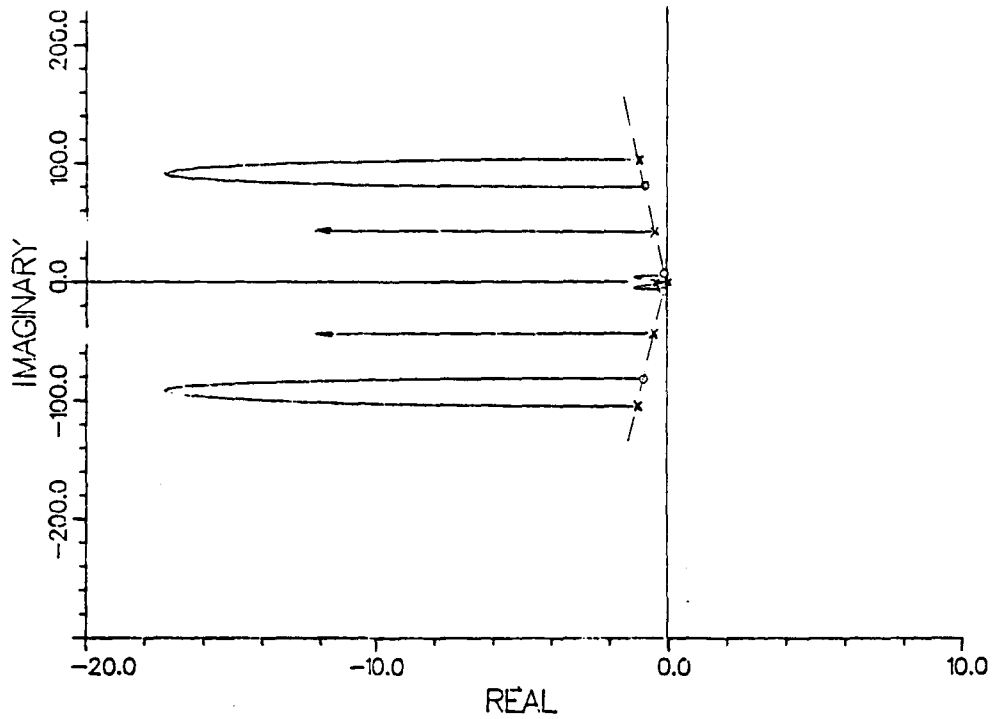
Figure 9-4. Collocated Root Locus, Torque Motor

Amplifier Included
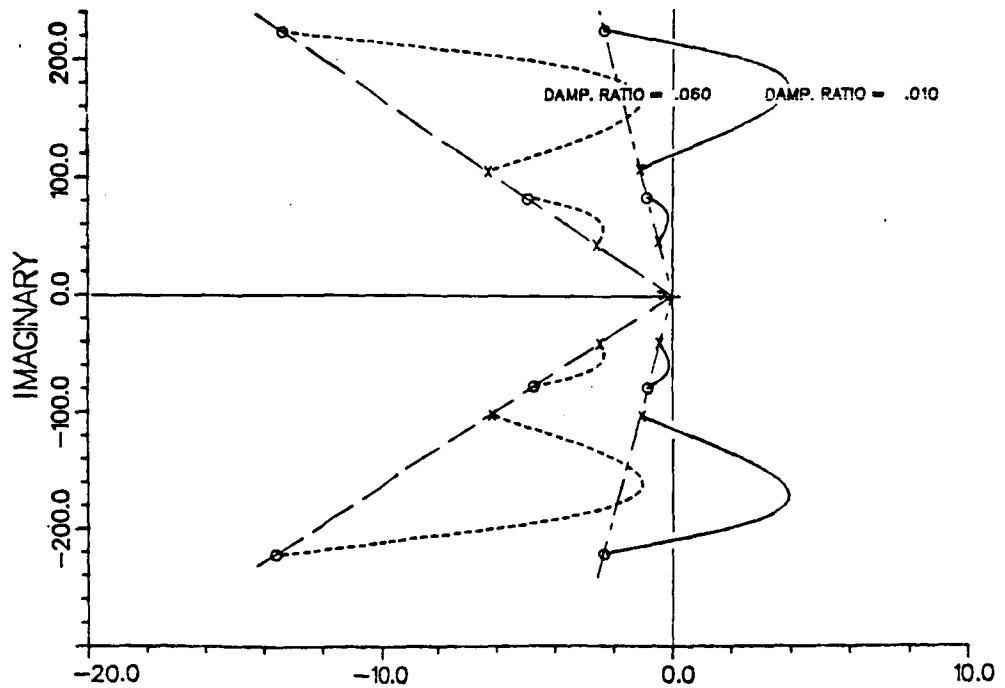
Figure 9-5. Collocated Root Locus, Four Pole

Butterworth Filter Included

CHAPTER X

SUMMARY AND RECOMMENDATIONS

10.1 Summary

This section briefly summarizes the important observations and results of the various sections by topic.

• **Linearized Model** - The linear modeling technique was implemented based entirely upon manipulator design parameters. The responses predicted agreed well with measurements when coupled with appropriate selection of modal candidates and model order. The linear modeling technique was readily adapted for computer generation of models with different modal candidates and orders. The model predicted increased responses of the higher modes than was experimentally observed. The increased response predicted by the model is attributed to inaccurate determination of the damping for the higher modes.

• **Mode Selection** - The application of feedback control laws to the flexible manipulator strongly impacts the resultant flexible vibration modes. It is extremely important to consider the control action in selecting modal candidates. The flexible manipulator's beam exhibits pinned-mass modes without control action, and as seen in chapters 3, 7, and 8 may exhibit clamped-mass, or pinned-mass modes under the action of control laws. Clamped-mass modes were

used in the LQR control implementation.

- **Model Order** - The response of the flexible arm was dominated by the rigid and first flexible modes. The application of large feedback gains and the effects of discretization had a significant impact on the required model order. The faster the cycle time, the less the response of the higher modes. A change in cycle time from 5.8 milliseconds, to 2.0 milliseconds resulted in almost complete elimination of the third flexible mode from the strain traces recorded for step responses obtained with collocated controllers. The speed was even more important than the inclusion of the second mode in the LQR controller.

- **Model Order Reduction** - The application of the method of balanced realizations to the evaluation of model order agreed well with the qualitative evaluation made in chapter 3. Aggregation of the seven highest flexible modes of the ten mode model, (an aggregation level of six), resulted in only a 6.7% increase the performance index used to estimate model order requirements. The inclusion of the first two flexible modes and the rigid body mode brings the performance index to its maximum value of 100%. The method is based upon examining the strengths of the singular values of the linear model being evaluated. Therefore, in this application the method cannot evaluate the accuracy of the model in describing the physical problem. The method does provide a satisfactory estimate of appropriate order for a

selected model.

· **Measurement and Reconstruction** - This technique was particularly successful when utilized for the single mode model. The evaluation for the two mode model is less certain due to experimental limitations. Measurement of strain due to the vibrations of the higher flexible modes truncated from the model was a particular problem. Measurement of the higher modes definitely contributed to the control actions exciting the third clamped-mass mode at 41Hz when large gains were applied.

· **Reduced Order Observation** - The modal observers were successfully applied to the flexible manipulator. The most significant factor in the design process was to insure that the estimator was fast enough to accurately track the flexible mode amidst initial offsets and measurements of the higher modes. Slow observers, while successfully providing an estimate of the velocity, tended to excite the higher modes truncated from the model when used in feedback control laws.

· **Linear Quadratic Regulators** - The application of LQR controllers to the control of vibratory modes occurring in flexible manipulators was successful in damping the vibratory modes of the system, as well as control the rigid orientation. The modal controllers were successful even in the presence of measurement noise and hardware imperfections, such as joint friction.

The joint friction makes collocated controllers ineffective for precise control of the manipulator. Once the joint is close to the desired final state the applied torques become smaller than the torque required to overcome friction. At this point the system becomes uncontrollable for the collocated controller. Additionally, the beam vibrates in cantilevered modes without joint rotation and the vibratory modes are unobservable by the joint measurements.

The fastest settling times were achieved with the single flexible mode controller designed with high modal damping. The settling times achieved with this design were on the order of one second for step changes in the desired angle of .35 radians. This settling time corresponds to roughly twice the period of oscillation of the first clamped-mass flexible mode. The quickest closed loop poles indicated by the model for the single mode LQR controller with a high prescribed degree of stability were -7.5 +/- .005i and -7.5 +/-19.13i radians/sec. If each of these pole pairs were considered as separate second order systems they would both correspond to a settling time,(to within 2% of the final states), of .533 sec.: The prescribed degree of stability design technique yielded poles with the same negative real parts. The response for the total system with these eigenvalues, settling times of 1.2-1.3 sec., was roughly twice the the time for the individual poles.

Experimental attempts to shorten the settling time by increasing the prescribed degree of stability in the control law design yielded instabilities in the flexible modes truncated from the model.

· **Kalman Filter** - The application of Kalman Filters is not recommended for design of estimators to be used in controlling flexible manipulators. Estimates of the noise covariances yielded expectation of noise signals in the strain traces 40-50 Db below the strains caused by the neglected modes.

The Kalman Filter designs yielded estimator poles close to those of the plant poles being estimated, much slower than indicated by the earlier results on modal velocity observation. Placement of the estimator poles by creating "fictitious" noise estimates and input distribution matrices was difficult and less direct than traditional methods.

10.2 Discussion

The most appropriate work for comparison is that conducted by Schmitz [X1] at the Guidance and Control Laboratory associated with Stanford University. This section will compare the experimental equipment, and results for the two efforts.

Schmitz experimentally examined endpoint position control of a flexible manipulator structure. The endpoint

position of the experimental manipulator was sensed by an optical sensor mounted external to the manipulator which viewed the intended objective for the endpoint motion.

Schmitz employed a manipulator constructed with sidewalls made from aluminum sheets joined at regular intervals along the length by braces. The construction employed by Schmitz is similar to the light weight truss structures favored by aerospace engineers [X2-3]. The first three cantilevered modes of the manipulator structure were 0.554, 2.781, 7.468Hz. Schmitz experimentally determined damping ratios for these modes in the range of .015-.020. The manipulator structure was complex, and difficult to model. Schmitz assumed a decoupled modal form for the system dynamics and then executed identification algorithms experimentally.

The aim of the work presented in this thesis was to construct a modal controller which determined and controlled the vibratory modes of the system, as well as the orientation in space. The objective of the sensor system implemented in in this study was to not require apriori knowledge of the final configuration of the manipulator. The controller and sensor system can be active over the full range of motions insuring control over the quality of motion and peak stresses.

The continuous beam used for this thesis is representative of lightweight manipulators receiving

attention for industrial [X4] and aerospace [X5] applications. The first three cantilevered modes of the beam are 2.08, 13.92, 41.38Hz with measured damping ratios in the range of .007-.015.

Schmitz achieved better agreement between his model and experiment, than was obtained in this work. This is not suprising as Schmitz used a higher order model,(three flexible modes and a rigid mode), and experimentally identified all the parameters of the system.

Schmitz obtained endpoint position step responses with settling times of one second roughly half the period of oscillation of the first cantilevered mode. This compares favorably to the rough guideline established by Book [X6]. Book limits the upper response of a collocated controller to half the first cantilevered mode. The modal controller in this work obtained modeled settling times of .533 for each state, roughly the period of oscillation of the clamped-mass mode. The controller which tried to regulate both states with a single control input was half as fast.

Part of Schmitz success in obtaining quick responses is attributed to use of endpoint position as the primary control. Additionally, the computation speed required by Schmitz is roughly one third that required in this work based on the ratio of flexible mode frequencies. The additional damping found in Schmitz's structure increases the stability of the system, as was found with the passive

damping treatment discussed in chapter nine.

Schmitz considered that the upper time response limit attainable with endpoint control was caused by non-minimum phase zeroes associated with a time delay observed in his experiments from when torque is applied until tip motion occurs, (roughly 120 milliseconds for his apparatus). The modal controller developed in this work obtained strain measurements from the base of the beam and observed strain responses were effectively instantaneous with respect to the applied torques. The primary limitation encountered in this work was computational speed which limited model order.

These two works are not contradictory, or mutually exclusive, and in most phases they are complimentary. The observed trends in stability and difficulties of obtaining a good dynamic model in the two efforts were in complete accord. The selection of approach for future work might well be driven by the chosen application, or even hybrid schemes investigated, (the possibilities for hybridization was also recognized by Schmitz).

10.3 Recommendations

It appears clear at this point that the selection of the flexible vibratory modes is extremely important in generation of a useful model. Additionally, identification of the manipulator structure is not the answer, as the application of feedback control laws alter the modes

observed in closed loop form of the system. It seems appropriate, then, that methods be sought which incorporate the feedback law into the modeling process, (Majette [X7] considered this problem for manipulators with small motions about an equilibrium). These methods are thought to come from iterative processes between beam solution techniques and Lagrangian dynamics.

Future flexible manipulators consisting of serial links and complex geometrical configurations will require the inclusion of many more modes in the model. These modes arise from torsion and bending in more than one plane for each link. Models including modal series consisting of a large number of terms may never be realizable in available real-time controllers. Based on this experimental history it is doubtful that blind truncation of model order will yield successful results when high performance of the manipulator is required.

Methods need to be adapted which account for the higher mode's responses even when designing for a lower order controller. Frequency domain methods [X8] promise to accommodate the feedback boundary conditions in the model as well as robust controller design. The research issues facing the frequency domain approaches lie in merging the physical measurements with the frequency domain description and computational requirements of practical implementations.

Balas [X9] proposed phase-locked loop filtering for the rejection of the untreated higher modes from the control or the measurement. Filters which remove information about the truncated modes from the measurement is still an appealing technique for research, although the attempt in this work with analog butterworth filters, as discussed in chapter 10, was. disappointing.

Design of structures which inherently reduce the response of the higher modes should be pursued. This type of structure would greatly reduce the control problems encountered in this work. Combining attempts at designing "lossy" joints, and beams, such as passive damping [X3] treatments, may result in successful high performance hybrid active/passive schemes.

APPENDIX A

FORMULATION OF DYNAMIC EQUATIONS

This section describes the generation of a dynamic model via application of Lagrange's equations to the flexible system [A1,A2].

A.1 Coordinates

The first step in this process is to select a suitable set of coordinates. The approach utilized selects one rigid body coordinate associated with the joint rotation, and flexible transverse displacements from a set of axes attached to the joint. This is depicted in figure A-1. Then
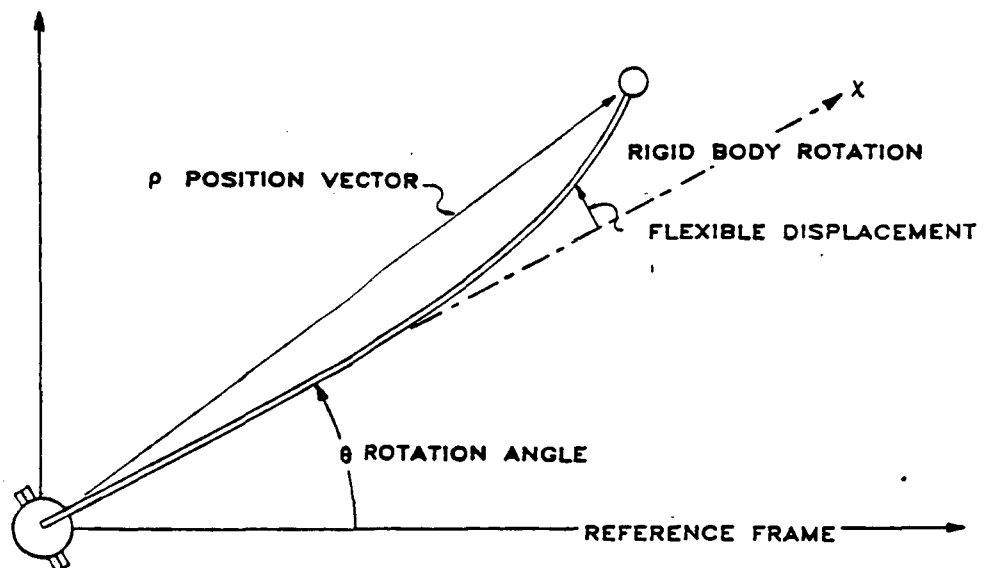
Figure A-1. Coordinate Definition

a position vector R to every point of the system can be can be constructed;

$$\dot{R} = x\hat{i} + w(x,t)\hat{j} \qquad (A.1)$$

The absolute velocity of the position vector;

$$\dot{R} = \frac{\partial R}{\partial t} + \dot{\theta}\hat{k}x\hat{R} \qquad (A.2a)$$

$$\dot{R} = x\hat{i} + \frac{\partial w(x,t)}{\partial t}\hat{j} + \dot{\theta}x\hat{j} - \dot{\theta}w(x,t)\hat{i}] \qquad (A.2b)$$

A.2 Kinetic and Potential Energies

The kinetic energy of the system KE, can then be computed by integrating this expression over the entire mass of the flexible system M_s;

$$KE = \frac{1}{2} \int \dot{R}\cdot\dot{R}dm \qquad (A.3a)$$

$$\dot{R}\cdot\dot{R} = [\frac{\partial w(x,t)}{\partial t}]^2 + 2\dot{\theta}\frac{\partial w(x,t)}{\partial t}x + \dot{\theta}^2[x^2 + w^2(x,t)] \qquad (A.3b)$$

$$KE = \frac{1}{2} \int \{[\frac{\partial w(x,t)}{\partial t}]^2 + 2\dot{\theta}\frac{\partial w(x,t)}{\partial t}x + \qquad (A.3c)$$

$$\dot{\theta}^2[x^2 + w^2(x,t)]\}dx$$

Next, introduce the assumed mode series representation for the transverse deflections $w(x,t)$;

$$w(x,t)=\sum \phi_i(x)q_i(t) \quad , \text{ for } i=1,2...n \qquad (A.4)$$

where $\eta = x/L$ a normalized length variable. Substitution for the transverse deflections results in;

$$KE = \frac{1}{2} \int \{ \sum \phi_i(\eta)\frac{dq_i}{dt}(t) \sum \phi_j(\eta)\frac{dq_j}{dt}(t) + \qquad (A.5a)$$

$$2\dot{\theta}\eta \sum \phi_i(\eta)\frac{dq_i}{dt}(t) + \dot{\theta}^2[(L\eta)^2 + \sum \phi_i(\eta)q_i(t) \sum \phi_j(x)q_j(t)]\}dm$$

This integral can be separated into three integrals over the primary components of the beam, joint mass, beam mass, and payload. Evaluation of equation A.5a over the joint mass results in;

$$KE_m = \frac{1}{2} J_0 [\sum \frac{d\phi_i}{d\eta}(0)\frac{dq_i}{dt}(t) \sum \frac{d\phi_j}{d\eta}(0)\frac{dq_j}{dt}(t) + \dot{\theta}^2] \qquad (A.5b)$$

Evaluation of equation (A.5a) over the mass of the beam results in;

$$KE_b = \frac{1}{2}J_b\dot{\theta}^2 + \frac{1}{2}A_b\rho L \int \{ \sum \phi_i(\eta)\frac{dq_i}{dt}(t) \sum \phi_j(\eta)\frac{dq_j}{dt}(t) + \qquad (A.5c)$$

$$2\dot{\theta}\eta L \sum \phi_i(\eta)\frac{dq_i}{dt}(t)\}d\eta$$

Notice that in evaluating;

$$\frac{1}{2}A_b\rho L \int [\dot{\theta}^2\eta^2 + \sum \phi_i(\eta)q_i(t) \sum \phi_j(\eta)q_j(t)]d\eta \qquad (A.6)$$

the squared flexible deflections was assumed negligible compared to the axial dimension squared. This linearization step can be postponed to until the equations of motion are formed, but this results in applying the same assumption to

multiple terms. Finally the integral is evaluated over the mass of the payload as;

$$KE_p = \frac{1}{2}[M_p L^2 + J_p]\dot{\theta}^2 + \frac{1}{2}M_p \sum \phi_i(1)\frac{dq_i}{dt}(t) \sum \phi_j(1)\frac{dq_j}{dt}(t) + \quad (A.7)$$

$$1/2 J_p M_p \sum \frac{d\phi_i}{d\eta}(\eta)\frac{dq_i}{dt}(t) \sum \frac{d\phi_j}{d\eta}(\eta)\frac{dq_j}{dt}(t)$$

Next, it is convenient to introduce an orthonormal condition on the spatial mode functions.

$$\frac{1}{2}A_b \rho L \int \{ \sum \phi_i(\eta)\frac{dq_i}{dt}(t) \sum \phi_j(\eta)\frac{dq_j}{dt}(t) + \quad (A.8)$$

$$\frac{1}{2} M_p \sum \phi_i(1)\frac{dq_i}{dt}(t) \sum \phi_j(1)\frac{dq_j}{dt}(t) +$$

$$\frac{1}{2}J_p M_p \sum \frac{d\phi_i}{d\eta}(\eta)\frac{dq_i}{dt}(t) \sum \frac{d\phi_j}{d\eta}(\eta)\frac{dq_j}{dt}(t) = \begin{matrix} 1, & \text{for } i=j \\ 0, & \text{for } i=j \end{matrix}$$

The potential energy, PE, for the system is evaluated by the following integral expression;

$$PE = \frac{1}{2}EI \int [\sum \frac{d^2\phi_i}{dx^2}(\eta)q_i(t) \sum \frac{d^2\phi_j}{dx^2}(\eta)q_j(t)]dx \quad (A.9)$$

Applying the orthogonality condition on the mode functions, and substituting the normalized length variable yields;

$$PE = \frac{1}{2}\frac{EI}{L^3} \int \{ \sum [\frac{d^2\phi_i}{d\eta^2}(\eta)]^2 q_i(t)\}d\eta \quad (A.10)$$

Notation in the following sections can be greatly simplified if the following definitions are made for a "modal stiffness", K_i, for equation (A.10), and "moment of modal

mass", W_i, for the last integrand in equation (A.5b) as;

$$K_i = \frac{1}{2}\frac{EI}{L^3}\int_L [\frac{d^2\phi_i}{d\eta^2}(\eta)]^2 d\eta \qquad (A.11)$$

$$W_i = \frac{1}{2}A_b\rho L \int \eta L \phi_i(\eta)d\eta \qquad (A.12)$$

The kinetic energy for the system can be expressed as;

$$KE = \frac{1}{2}\dot{\theta}^2[J_0+J_p+M_pL^2] + \dot{\theta}\int\frac{dq_i}{dt}(t)[W_i+LM_p\phi(1) + \qquad (A.13)$$

$$LJ_p\phi(1)] + \frac{1}{2}\int[\frac{dq_i}{dt}(t)]^2$$

A.3 Lagrange's Equations

To generate the dynamic equations the Lagrangian of the energy expressions are formed, where the q_i are the coordinates, and Q_i represents the work done by the input torque at the joint by each coordinate. The resultant equations can then be organized in matrix form;

$$\frac{d}{dt}\left|\frac{\partial KE}{\partial \dot{\xi}_i}\right| - \frac{\partial PE}{\partial \xi_i} = Q_i \qquad (A.14)$$

$$[M]\ddot{z} + [K]z = [Q] \qquad (A.15)$$

$$z = [\theta, q_1(t), q_2(t), \ldots, q_n(t)] \qquad (A.16)$$

$$M = \qquad\qquad\qquad\qquad\qquad\qquad\qquad\qquad\qquad\qquad (A.17)$$

$$\begin{vmatrix} J_0 + J_b + J_p + M_p L^2 & W_1 + LM_p \phi_1(1) + J_p \frac{d\phi}{d\eta}1(1) & W_2 + LM_p \phi_2(1) + J_p \frac{d\phi}{d\eta}2(1) & \cdots \\ W_1 + LM_p \phi_1(1) + J_p \frac{d\phi}{d\eta}1(1) & 1 & 0 & \cdots \\ W_2 + LM_p \phi_2(1) + J_p \frac{d\phi}{d\eta}2(1) & 0 & 1 & \cdots \\ \vdots & \vdots & \vdots & \ddots \end{vmatrix}$$

$$K = \begin{vmatrix} \cdot & \cdot & \cdot & \cdot \\ 0 & K_1 & 0 & \cdot\cdot \\ 0 & 0 & K_2 & \cdot\cdot \\ \vdots & \vdots & \vdots & \cdot \end{vmatrix} \qquad Q = \begin{vmatrix} 1 \\ \frac{d\phi}{d\eta}1(0) \\ \frac{d\phi}{d\eta}2(0) \\ \vdots \end{vmatrix} \qquad \begin{matrix} (A.18) \\ (A.19) \end{matrix}$$

This system is easily organized into a linear state-space model as shown in figure A-2.

$$\begin{vmatrix} \dot\theta \\ \dot q_1 \\ \dot q_2 \\ \vdots \\ \ddot\theta \\ \ddot q_1 \\ \ddot q_2 \\ \vdots \end{vmatrix} = \begin{vmatrix} 0 & \vdots & I \\ \hline & M^{-1}K & \quad 0 \end{vmatrix} \begin{vmatrix} \theta \\ q_1 \\ q_2 \\ \vdots \\ \dot\theta \\ \dot q_1 \\ \dot q_2 \\ \vdots \end{vmatrix} + \begin{vmatrix} 0 \\ \hline M^{-1}Q \end{vmatrix} |u|$$

Figure A-2. State Space Representation.

APPENDIX B

BERNOULLI-EULER BEAM EQUATIONS

This section describes the development of a frequency determinant from Bernoulli-Euler beam theory which was used to derive candidate mode frequencies and the associated shapes. The homogeneous differential equation is presented first, followed by a discussion of the boundary conditions utilized. Lastly the frequency determinant is derived.

B.1 Differential Equation

The transverse displacement of the beam, $w(x,t)$, shown in figure A-1 is a function of both the spatial variable along the beam, and time. Following the analysis attributed to Bernoulli and Euler gives rise to following fourth order partial differential equation.

$$EI\frac{\partial^4 w(\eta,t)}{\partial\eta^4} - A_b L^4 \frac{\partial^2 w(\eta,t)}{\partial t^2} = 0 \qquad (B.1)$$

where: $\eta=x/L$ The next step applies the separability of equation (1) to obtain the following result;

$$EI\frac{d^4\phi(\eta)}{d\eta^4}q(t) - \rho A_b L^4 \phi(\eta)\frac{dq(t)}{dt^2} = 0 \qquad (B.2)$$

Searching for periodic time functions of the form $q(t)= e^{i\omega t}$ leads to the following formulation;

$$EI[\frac{d\phi^4(\eta)}{d\eta} - \rho L^4 A_b \phi(\eta)\omega^2]q(t) = 0 \qquad (B.3a)$$

This implies that the term in brackets must be equal to zero for all time t. This is expressed as:

$$\frac{d\phi^4(\eta)}{d\eta} - \beta^4 \phi(\eta) = 0 \qquad (B.3b)$$

where the new parameter,

$$\beta^4 = \rho L^4 A_b \omega^2 \qquad (B.4)$$

has been substituted. This is readily solved for $\phi(\eta)$:

$$\phi(\eta) = A\sin(\beta\eta) + B\cos(\beta\eta) + C\sinh(\beta\eta) + D\cosh(\beta\eta) \qquad (B.5)$$

The solution for the spatial mode function $\phi(\eta)$ requires four independent boundary conditions be provided. The first and most obvious results from noting that there cannot be transverse displacement at the pinned joint, this takes the form;

$$\phi(\eta) = 0 \text{ , for } \eta = 0 \qquad (B.6)$$

The second condition is provided from a moment balance at joint, this is expressed as;

$$\frac{d^2\phi(\eta)}{d\eta^2} = -\frac{J_0 \beta^4 d\phi(\eta)}{\rho A_b L^3 d\eta} \quad \text{for } \eta = 0 \qquad (B.7)$$

where the following substitution was made to eliminate the dependence on the frequency;

$$\omega^2 = \frac{\beta^4 EI}{\rho A_b L^4} \qquad (B.8)$$

Using this boundary condition results in pinned mode shapes for small joint inertias. Additionally, clamped mode shapes can be determined by inputing very large joint inertias. This provides more programming versatility than supplying one formulation of the frequency determinant for each type of boundary condition. The third boundary condition is derived by resolving the shear force at the end of the beam against the inertial forces of the payload mass. This takes the following form;

$$\frac{d^3\phi(\eta)}{d\eta^3} = -\frac{M_p\beta^4\phi(\eta)}{\rho A_b L^3} \text{ , for } \eta = 1 \qquad (B.9)$$

The last boundary condition arises from a moment balance against the angular inertial forces of the payload.

$$\frac{d^2\phi(\eta)}{d\eta^2} = -\frac{J_0\beta^4 d\phi(\eta)}{\rho A_b L^3 d\eta} \quad \text{for } \eta = 1 \qquad (B.10)$$

B.2 Frequency Determinant

Application of the boundary conditions to the solution for $\phi(\eta)$ will result in a frequency determinant for the eigenvalues β. Application of the first boundary condition for transverse displacement at the joint relates two of the constants in the solution;

$$B = -D \qquad (B.11)$$

The second boundary condition balancing the moment at the joint forms a relation between three of the of the

constants;

$$2DJ_0 = -\rho A_b L^3 \beta^3 (A+C) \qquad (B.12)$$

The shear force balance at the payload relates all the constants of the solution;

$$A(M_p \frac{\beta \sin\beta}{A_b L} - \cos\beta) + B(\sin\beta + M_p \frac{\beta \cos\beta}{A_b L}) + \qquad (B.13)$$

$$C(M_p \frac{\beta \sinh\beta}{A_b L} + \cosh\beta) + D(\sinh\beta + M_p \frac{\beta \cosh\beta}{A_b L}) = 0$$

The moment balance at the payload forms a similar relation;

$$-A(\sin\beta + J_p \frac{\beta^3 \cos\beta}{A_b L^3}) + B(J_p \frac{\beta^3 \sin\beta}{A_b L^3} - \cos\beta) + \qquad (B.14)$$

$$C(\sinh\beta - J_p \frac{\beta^3 \cosh\beta}{A_b L^3}) + D(-J_p \frac{\beta^3 \sinh\beta}{A_b L^3} + \cosh\beta) = 0$$

The expressions (B.11- B.14) involve only the constants from the solution for the mode function and the parameter β. This can be configured in matrix form as;

$$F(\beta) \left| \begin{matrix} A \\ D \end{matrix} \right| = 0 \qquad (B.15)$$

$$F11 = \sin\beta + \sinh\beta + J_{p*} \beta^3 (\cos\beta - \cosh\beta) \qquad (B.16)$$

$$F12 = \sin\beta - \sinh\beta + \frac{2\cosh\beta}{J_{0*}\beta^3} + M_{p*}\beta(\cos\beta - \cosh\beta) + \qquad (B.17)$$

$$\frac{2\sinh\beta}{J_{0*}\beta^3}$$

$$F21 = \cos\beta + \cosh\beta - M_{p*}\beta(\sin\beta - \sinh\beta) \qquad (B.18)$$

$$F22 = -\cos\beta - \cosh\beta + 2\frac{\sinh\beta}{J_{0*}\beta^3} + J_{p*}\beta^3(\sinh\beta-\sin\beta)- \quad \text{(B.19)}$$

$$2J_{p*}\frac{\cosh\beta}{J_{0*}\beta^3}$$

Where the starred subscripts indicate modification by the appropriate area and length terms. The roots of the frequency determinant $\det[F(\beta_i)] = 0$ yield the characteristic values for the mode functions $\phi_i(\eta)$, and associated frequencies ω_i.

APPENDIX C

LINEAR QUADRATIC REGULATOR

This appendix discusses the design and implementation of deterministic Linear Quadratic Regulators (LQR). The first section formulates the governing equations for the continuous case and applies the sweep method to obtain the Ricatti equation. This presentation is a compilation of the material contained in Bryson and Ho's text [C1] on optimal control. The section discussing controller design with a prescribed degree of stability follows Moore [C2]. The last section considers the necessary adaptations required for the experimental sampled data system.

C.1 Continuous System

The earlier sections discussed the development of the state-space equations for the flexible manipulator system. This system can be represented by the general expression;

$$\dot{x} = f(x,u,t) \tag{C.1}$$

The model for the flexible manipulator does not require explicit expression of the time variable and $f(x,u,t)$ has the following linear form;

$$\dot{x} = f(x) = A_c x + B_c u \tag{C.2}$$

The goal of the process is to determine a gain vector , K^T, which determines the input function, u(t), as a linear combination of the states, x(t), in an optimal manner. The gain vector, K^T, will be "optimal" in the sense of a specific performance measure. The measures of performance are called Performance Indices (PI), and for LQR controllers the PI is defined in the following manner;

$$PI = \frac{1}{2}\int [x^T Q x + u^T R u]dt \qquad (C.3)$$

Q and R represent weighting matrices which selectively penalize the various states, x, and input, u, during the process. The next step is to adjoin the system dynamic equations (C.2) to the performance index by the use of the time varying functions $\lambda(t)$;

$$PI = \frac{1}{2}\int \{x^T Q x + u^T R u + \lambda^T[f - \dot{x}]\}dt \qquad (C.4)$$

Integrating the adjoined performance index by parts yields;

$$PI = \lambda^T x \Big|_{t_0}^{t_f} + \frac{1}{2}\int [x^T Q x + u^T R u + \lambda^T f + \dot{\lambda}^T x]dt \qquad (C.5)$$

Notation can be simplified by defining a "Hamiltonian"[C1] function H(x,u) for the system as;

$$H(x,u) = x^T Q x + u^T R u + \lambda^T f \qquad (C.6)$$

Substitution into equation (C.5) yield the more compact expression;

$$PI = \lambda^T x \Big|_{t_0}^{t_f} + \frac{1}{2}\int [H(x,u) + \dot{\lambda}^T x]dt \tag{C.7}$$

To find the minimizing functions, variational principles are applied to the performance index. Small perturbations about the optimal solution are considered;

$$\delta PI = \lambda^T \delta x \Big|_{t_0}^{t_f} + \frac{1}{2}\int \{[\frac{\delta H(x,u)}{\partial x} + \dot{\lambda}^T]\delta x + \frac{\delta H \delta u}{\partial x}\}dt \tag{C.8}$$

The optimal solution $x(t)$, $u(t)$ is an extremum for the PI and therefore the variations must be zero. The task is now to find the functions $x(t)$, $u(t)$ which satisfy this condition.

C.2 Modification for Solution

Solving the set of equations (C.8) can be simplified by noting that for a regulator the initial and final states are known, and choosing the multiplier functions û ;

$$\delta x = 0 \text{ , for } t=t_0, \text{ and } t=t_f \tag{C.9}$$

$$\dot{\lambda}^T = \frac{\partial H}{\partial x} \tag{C.10}$$

The variation in the PI can now be expressed as;

$$\delta PI = \frac{1}{2}\int \frac{\delta H \delta u}{\delta u}dt \tag{C.11}$$

The variation in the performance index must be zero for arbitrary variations in the control function u. This can

only be true for;

$$\frac{\delta H}{\partial u} = 0 \qquad (C.12)$$

Equations (C.9,10,12) are known as "Euler-Lagrange Equations"[C1] for the system.

C.3 Sweep Method

The "sweep method" will be presented in the next section as one approach to obtain the Ricatti equation. First a solution, $S(t)$, relating the states, $x(t)$, to the multiplier functions, $\lambda(t)$, with the following form is assumed;

$$\lambda^T = Sx \qquad (C.13)$$

Substitution into equation (C.10) yields;

$$\frac{\partial (Sx)}{\partial t} = -(Qx + \lambda^T A_c) \qquad (C.14a)$$

or carrying out the indicated partial differentiation, and substituting equation (C.13) for λ;

$$\dot{S}x + S\dot{x} = -(Qx + A_c^T Sx) \qquad (C.14b)$$

Next, the differentiation indicated in equation (C.12) is carried out, and the resulting expression examined in more detail;

$$\frac{\partial H}{\partial u} = 0 = u^T R + \lambda^T B_c \qquad (C.15)$$

This can be formulated for the input function $u(t)$ as;

$$u = -R^{-1}B^T\lambda \qquad (C.16)$$

This result can be substituted into equation (C.2) to obtain;

$$\dot{x} = A_c x - B\bar{R}^1\ \overset{T}{B}\ Sx \qquad (C.17)$$

Equations (C.14,17) can be combined to form the "Matrix Ricatti Equation" for the system.

$$[\dot{S} + SA_c - SBR^{-1}B^TS + Q + A_c^TS]x = 0 \qquad (C.18a)$$

This expression must hold true for arbitrary x, therefore the expression inside the brackets must be zero;

$$\dot{S} + SA_c - SBR^{-1}B^TS + Q + A_c^TS = 0 \qquad (C.18b)$$

The "sweep method" is so named because the usual solution technique for this problem is to sweep backward in time from the final condition to the start. Regulators are designed by finding the steady state solution, dS/dt equals zero, by finding the solution matrix S of;

$$SA_c - SBR^{-1}B^TS + Q + A_c^TS = 0 \qquad (C.19)$$

C.4 Prescibed Degree of Stability

In this section modification of the LQR regulator problem to include specification of minimum stabitility in the design process. The objective of this modification is to design the optimal control law in such a was that the closed

loop eigenvalues have negative real parts less than a value (-a). This technique was first studied by Anderson and Moore [C2], and discussed for application to flexible manipulators by Sangveriphusiri [C3].

The modification starts by considering the following definitions.

$$x'(t) = e^{at} x(t) \qquad (C.20)$$

$$u'(t) = e^{at} u(t) \qquad (C.21)$$

From these definitions, it is clear that x't) and u'(t) will be stable (i.e. x'(t) or u'(t) $\to$ 0 as t $\to$ ∞) only if x(t) and u(t) decay faster than e^{-at}. This is equivalent to requiring the closed loop system to have a degree of stability of at least -a.

Differention of equation (C.20) yields,

$$\dot{x}' = a \, e^{at} x + e^{at} \dot{x} \qquad (C.22)$$

Substituting equation the linearized form of the state space model, equation (C.2), for x(t) into equation (6.20), the modified system equation can be written as follows:

$$\dot{x}' = (A+aI)x' + B \, u' \qquad (C.23)$$

The function inside the integral sign of the cost function is modified to

$$u'^T R \, u' + x'^T Q \, x' = e^{2at}(u^T R \, u + x^T Q \, x) \qquad (C.24)$$

Instead of solving the previous regulator problem, equation (C.2), one solves the modified system of equation (C.23) with the following modified performance index is

$$\int_0^t (x'^T Q x' + u'^T R u')dt \qquad (C.25)$$

A similar form of solution will be expected. The control u'(t) is the linear function of state, i.e.

$$u' = -Kx' \qquad (C.26)$$

and the matrix-valued function, K, can be evaluated from

$$K = R^{-1}B^T S \qquad (C.27)$$

where S is the solution of the Riccati equation.

Next, it can be shown that a feedback control law for the modified problem readily yields a feedback control law for the original problem. Substituting the definitions of equations (C.20) and (C.21) into equation (C.26),

$$u = -e^{at} u' = -e^{-at}K(e^{at}x) = -K x \qquad (C.28)$$

So that, the optimal feedback gain of the modified regulator problem can be selected as the control law of the original problem and the closed loop system of the original problem will have a degree of stability of at least -a.

C.5 Sampled Data System

This section discusses translating the continuous LQR design problem to the sampled data case which approximates the digital implementation employed for the experiments.

The approach taken will be transform the dynamic equations and the weighting matrices to the discrete domain and then reformulate the problem for solution.

Inputs to the plant from the micro-processor controller are "held" constant between cycles of the controller. This type of sampled data control system has an equivalent discrete dynamic equation to the continuous plant dynamic equation (C.2) which is the solution for continuous equation over the time interval. The solution is given by;

$$x_{i+1} = A_d x_i + Bdu_i \qquad (C.29a)$$

where the subscript i indicates a particular sampled time, and i+1 indicates the next, and;

$$A_d = \exp(A_c \Delta t) \qquad (C.29b)$$

$$B_d = \int \exp(A_c \tau) B_c u_i d\tau \qquad (C.29c)$$

The goal of this process is to design a feedback control K_d which determines the input sequence u_i as a function of the state vector sequence x_i;

$$u_i = K_d^T x_i \qquad (C.29d)$$

The performance index expressed by equation (C.3) is transformed from an integral into a sequence of responses over the sampling interval Δt.

$$PI = \sum \int \{ [\exp(A_c \tau) x_i + (\int \exp(A_c \xi) B_c u_i) d\xi]^T Q \qquad (C.30)$$

C-3

$$[\exp(A_c\tau)x_i + (\int \exp(A_c\xi)B_c u_i)d\xi]) + u_i{}^T R u_i\}d\tau$$

This expression can be formulated with almost a direct correspondence to the terms of equation (C.3);

$$PI = \sum(x_i{}^T Q_d x_i + x_i{}^T W_d u_i + u_i{}^T R_d u) \qquad (C.31a)$$

where;

$$Q_d = \int \exp(A_c\xi)^T Q \exp(A_c\xi)d\xi \qquad (C.31b)$$

$$W_d = 2\int \exp(A_c\tau)^T Q[\int \exp(A_c\xi)B_c u_i)d\xi]d\tau \qquad (C.31c)$$

$$R_d = \int \{R + [\int \exp(A_c\xi)B_c u_i)d\xi]Q[\int \exp(A_c\xi)B_c u_i)d\xi]\}d\tau$$

$$(C.31d)$$

Without the cross terms associated with W_d in Equation (C.31a) the sampled data representation would be directly analogous to equation (C.3). A pre-filter gain F can be chosen to eliminate the cross terms;

$$F = \tfrac{1}{2}R^{-1}W_d \qquad (C.32)$$

Another input sequence can be defined utilizing the pre-filter gain F as;

$$v_i = Fx_i + u_i \qquad (C.33)$$

such that;

$$x_{i+1} = A_d'x + B_d v_i \qquad (C.34a)$$

where;

$$A_d' = A_d - B_d F \qquad (C.34b)$$

Making one last transformation for the state penalty matrix Qd;

$$Q_d' = Q_d - \tfrac{1}{2}W_d F \qquad (C.35)$$

yields the desired equivalent form of the performance index for the sampled data system.

$$PI = \Sigma(x_i^T Q_d' x_i + v_i^T R_d v_i) \qquad (C.36)$$

The solution of this problem subject to the dynamics of equation (C.34a) will yield a solution vector K_d' which coupled with the pre-filter gain F yields the desired gain vector K_d for the original sampled regulator;

$$K_d = K_d' + F \qquad (C.37)$$

The variational approach, and Sweep Method presented for the continuous case carry through for the sampled data regulator by direct analogy using sequences instead of continuous functions. The process is extremely straightforward and will not be presented here. The resultant form of the steady state Ricatti equation for the sampled data regulator is;

$$S_d A_d' - S_d B_d R_d^{-1} B_d^T S_d + Q_d' + A_d'^T S_d = 0 \qquad (C.38)$$

C.6 Ricatti Equation Solution

The Newton-Raphson, and other methods have been formulated for this problem repeatedly, and software is readily available. Two implementations were utilized for this work to provide cross checking. Routines extracted from the ORACLS[C4], and Control-C[C5] software packages were executed on the flexible arm model.

APPENDIX D

KALMAN FILTER DEVELOPMENT

This section discusses the development of a Linear Quadratic Gaussian Regulator (LQGR) this is more commonly referred to as a Kalman Filter [D1-2]. The basic relations and solution technique will be discussed as was done in appendix C for the deterministic regulator. For brevity only the sampled data case will be developed here.

D.1 Governing Equations

Consider the dynamic equations for the system now subject to the introduction of a zero mean gaussian noise w_i to the plant and v_i to the measurement y_i.

$$x_{i+1} = Ax_i + Bu_i + w_i \qquad (D.1)$$

$$y_i = Cx_i + v_i \qquad (D.2)$$

The noises are uncorrelated and have covariances given by;

$$E[w_i w_j^T] = R_w \qquad (D.3)$$

$$E[v_i v_j^T] = R_v \qquad (D.4)$$

The objective of this formulation is to select the measurement gains for the full state observer depicted in figure D-1 in an optimal manner.

Many notational definitions are required to form a tractable formulation of the Kalman Filter equations [D3].

The definitions are summarized in table D-1 for easy reference.

Table D-1. Summary of Kalman Filter Notation

Symbol	Comment
x	Plant state vector
$\hat{x}$	Estimate of the Plant state with measurement update
$\tilde{x}$	Estimate of the Plant without measurement update
$\hat{e}$	Error between plant state and estimate $\hat{e} = (x - \hat{x})$
$\tilde{e}$	Error between plant state and estimate $\tilde{e} = (x - \tilde{x})$
M	Covariance of error $\tilde{e}$ $M = E[\tilde{e}\tilde{e}^T]$
P	Covariance of error $\hat{e}$ $P = E[\hat{e}\hat{e}^T]$
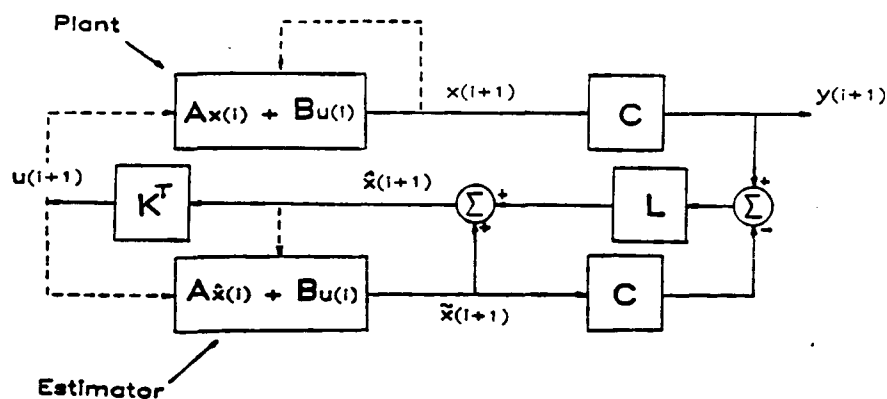
Figure D-1. Block Diagram for Kalman Filter

Consider the error $\tilde{e}$ for an estimator constructed with actual plant dynamics;

$$\tilde{e}_{i+1} = x_{i+1} - \tilde{x}_{i+1} = A_d(x_i - \hat{x}_i) + B_d w_i \qquad (D.5)$$

Then the covariance of the error without the measurement update M_{i+1} is;

$$M_{i+1} = E[A_d \hat{e}_i \hat{e}_i{}^T A_d{}^T + B_d w_i w_i{}^T] \qquad (D.6a)$$

Or in more compact notation;

$$M_{i+1} = A_d P_i A_d{}^T + B_d R_w B_d{}^T \qquad (D.6b)$$

Consider a performance index for the system with the following form;

$$PI = 1/2\Sigma[\tilde{e}_i{}^T M^{-1}{}_i \tilde{e}_i + (y_i - Cx_i)^T R_v{}^{-1}{}_i (y_i - Cx_i)] \qquad (D.7)$$

The task is again to find the sequences which minimize the performance index, therefore, we wish to find the conditions which will yield the sequences. Examining the effect of small arbitrary variations in the state vector x_i;

$$\delta PI = \delta x_i [M^{-1}{}_i \tilde{e}_i + C^T Rv^{-1}{}_i (y_i - Cx_i)] \qquad (D.8)$$

For the sequences to minimize the index the coefficient of the variation must vanish;

$$M^{-1}(x_i - \tilde{x}_i) + C^T R_v{}^{-1}{}_i (y_i - Cx_i) = 0 \qquad (D.9)$$

This can be organized in terms of the plant state;

$$(M^{-1}{}_i + C^T R_v{}^{-1}{}_i C)x_i = M^{-1}{}_i \tilde{x} + C^T R_v{}^{-1}{}_i y_i \qquad (D.10)$$

forming the the feedback grouping $y_i - C\tilde{x}_i$ results in;

$$(M^{-1}{}_i + C^T R_v^{-1}{}_i C) x_i = (M^{-1}{}_i + C^T R_v^{-1}{}_i C) \tilde{x}_i + \qquad (D.11)$$

$$C^T R_v^{-1} (y_i - C\tilde{x}_i)$$

Dividing through by the coefficient of the state, x_i, provides a relation between the estimate without update, $\tilde{x}_i$, the measurement, and the state which minimizes the performance index.

$$x_i = \tilde{x}_i + L_i (y_i - C\tilde{x}_i) \qquad (D.12a)$$

where a Kalman gain, L, has been introduced;

$$L_i = (M^{-1}{}_i + C^T R_v^{-1}{}_i C)^{-1} C^T R_v^{-1}{}_i \qquad (D.12b)$$

Thus an optimal estimate, $\hat{x}_i$, of the state can be formed using the measurement, y_i, and the estimate without update, $\tilde{x}_i$, which satisfies the same conditions;

$$\hat{x}_i = \tilde{x}_i + L_i (y_i - C\tilde{x}_i) \qquad (D.13)$$

It is of interest to separate the terms forming the Kalman gain as;

$$L_i = P^*{}_i C^T R_v^{-1}{}_i \qquad (D.14a)$$

where the grouping;

$$P^*{}_i = (M^{-1}{}_i + C^T R_v^{-1}{}_i C)^{-1} \qquad (D.14b)$$

has been formed. It will now be shown that the grouping shown in equation (D.14b) is in fact the covariance matrix, P_i. The error for the estimate with update, $\hat{e}$, can be written as;

$$e_i = x_i - \hat{x}_i = x_i - \hat{x}_i + \qquad (D.15a)$$

$$P^*_i C^T R_v^{-1}{}_i [v_i - C(x_i - \tilde{x}_i)]$$

Rearranging terms, and using the notation $\tilde{e}_i$ for the error before measurement update;

$$\hat{e}_i = (I + P^*_i C^T R_v^{-1}{}_i C)\tilde{e}_i + P^*_i C^T R_v^{-1}{}_i v_i \qquad (D.15b)$$

Then the expected values can be determined;

$$P_i = (I + P^*_i C^T R_v^{-1}{}_i C) M_i (I + P^*_i C^T R_v^{-1}{}_i C)^T + L_i R_{vi} L_i{}^T \qquad (D.16)$$

Next, consider the inverse of equation (D.14b);

$$P^*_i{}^{-1} = M^{-1}{}_i + C^T R_v^{-1}{}_i C \qquad (D.17)$$

Premultiplication of equation (D.17) by P^*_i, followed by postmultiplication with M_i yields;

$$M_i = P^*_i + P^*_i C^T R_v^{-1}{}_i C M_i \qquad (D.18a)$$

or;

$$(I + P^*_i C^T R_v^{-1}{}_i C) M_i = P^*_i \qquad (D.18b)$$

The result, equation (D.18b) can be substituted into equation (D.16) to eliminate the M_i term;

$$P_i = P^*_i (I + P^*_i C^T R_v^{-1}{}_i C)^T + L_i R_{vi} L_i{}^T \qquad (D.19)$$

This can be regrouped using equation (D.14a) for the Kalman gain twice;

$$P_i = P^*_i (I + L_i C)^T + (P^*_i C^T R_v^{-1}{}_i) R_{vi} L_i{}^T \qquad (D.20a)$$

,finally after some simplification;

$$P_i = P^*_i - P^*_i C^T L_i{}^T + P^*_i C^T L_i{}^T \qquad (D.20b)$$

This yields the needed result;

$$P_i = P^*_i \qquad\qquad (D.20c)$$

Now the Kalman gain, L_i, can be expressed in terms of the covariance P_i;

$$L_i = P_i C^T R_v^{-1}{}_i \qquad\qquad (D.21)$$

This completes the derivation of necessary Kalman Filter equations. The next section will discuss a method for solution of the steady state gain gain L.

D.2 Solution Method

Iterative solutions using expressions for P_i and M_{i+1} converge very slowly for discretizations of the plant for short time intervals. Formulation of the problem into a Ricatti equation suitable for the same Newton-Raphson algorithm employed for the deterministic regulator covered in appendix C is very desirable in terms of convergence properties and software usage.

To achieve this goal, equation (D.15) is rewritten;

$$\hat{e}_{i+1} = (A_d - L_i C)\hat{e} + L_i v_i + B_d w_i \qquad\qquad (D.22)$$

The expected value can then be determined;

$$P_{i+1} = (A_d - L_i C)P_i(A_d - L_i C)^T + L_i R_v L_i^T + B_d R_w B_d^T \qquad (D.23)$$

Steady state is reached when P_{i+1} is the same as P_i, this gives the necessary form;

$$P = (A_d - L_i C)P_i(A_d - L_i C)^T + L_i R_v L_i^T + B_d R_w B_d^T \qquad (D.24)$$

Combining this with expression (D.21) for the Kalman gain completes the process.

APPENDIX E

EXPERIMENTAL APPARATUS

This section of the thesis describes the the experimental manipulator system. Manufacturers, specifications, experimental measurements made to assure the performance parameters of key components, and detail diagrams identifying the actual electrical connections are presented.

The experimental hardware is separated into five functional areas, and identification and description of the hardware components will proceed sequentially through the functional groups. Electrical schematics for components will be given presented in the functional groups, but interconnections for subsytems will conclude the appendix.

The following list identifies the functional hardware groupings:

- Flexible Manipulator
- Sensors/Signal Conditioning
- Analog to Digital Conversion
- Micro-Processor System/Digital to Analog Conversion
- Torque Motor/Servo-Amp

The microprocessor is discussed in appendix F with the controller software.

E.1 Flexible Manipulator

The first piece of hardware to be discussed is the actual flexible link, and payload. This component sets the scale for the experiment. The arm is a four foot aluminum beam with the section oriented so that axis of increased flexibility is in the horizontal plane. The manipulator mounted in its base with sensors is shown in figure E-1.

The payload is provisioned for the addition of weights giving it a range of five to one in increments of one quarter of the base amount. Table E-1 lists physical properties, and dimensions for the beam, and payload.
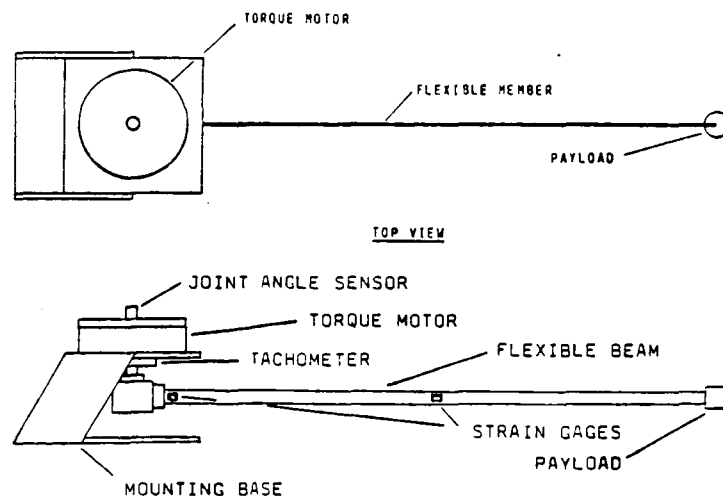
Figure E-1. Manipulator with Sensors.

E.2 Sensors

The manipulator and base are equipped with several sensors to obtain information about the state of the flexible system. This section discusses the individual measurement systems.

E.2.1 Joint Angle Sensor

Rotation of the joint is measured by the use of a rotational potentiometer connected to a high impedance signal amplifier. This is depicted in figure E-2. Ninety degrees of rotation is scaled to +/-5 volts DC by use of the signal amplifier.

E.2.2 Joint Angle Velocity

An Inland motor tachometer is utilized to measure the angular velocity of the joint. The tachometer is also connected to a signal amplifier, this provides analog signal scaling and isolates the tachometer from line loads, as well as reducing noise.

Table E-1. Physical Properties of the Beam
and Payload

```
Beam
Length = 48 in.
Section: 3/16 x 3/4 in.    EI Product= 4120
Material:Aluminum          Alloy: 6065-T6


Payload
Material: Aluminum         Alloy: 6065-T6
Diameter= 1.25 in.         Thickness= .75 in.
```
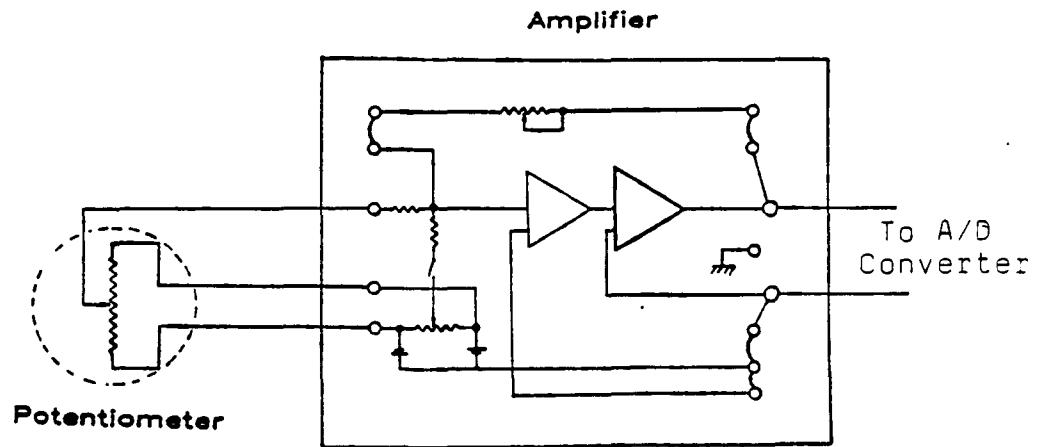
Figure E-2. Angle Sensor.
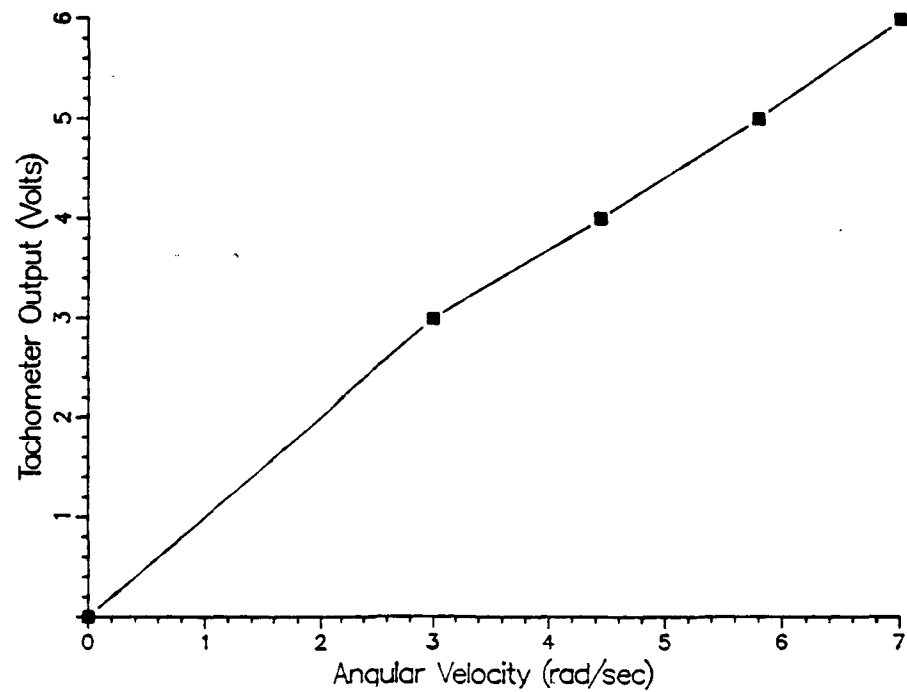
Figure E-3. Measured Tachometer Performance.

The manufacturers specifications for the tachometer are listed in table E-2. Measurements were made of the tachometer to verify the manufactures voltage/speed constant. The joint was rotated at a constant velocity for several revolutions, the output voltage measured, and the velocity computed. The data is presented in figure E-3. Computation of the slope provides a constant,.9volt-sec/radian, relatively close to the specified amount, 1.0volt-sec/rad.

E.2.3 Strain gages

State feedback using modal variables obtained from reconstruction (chapter V), and estimation (chapter VI) is based on measurement of strain due to bending at the surface of the beam. Strain at a point on the surface of the beam has contributions from axial stress, torsional stress, and out of plane bending. Additionally, strain gages generate low level signals, and are sensitive to temperature.

The specific implementation for this experiment consisted of a four active element bridge commonly used to measured planar bending of beams [E1]. This configuration is much less sensitive to stresses due to torsion, extension, transverse bending and provides higher signal levels in bending than an individual gage. Temperature is also compensated.

Figure E-4 depicts the mounting arrangement for the active gages in the bridge at a single measurement point.

The performance of the bridges was examined by locking the joint and deflecting the endpoint in fixed increments. The result is shown figure E-5. This result was compared against linear elastic theory, allowing for calibration of the bridge, and amplifiers in one step.

The gages are driven by a constant voltage bridge control circuit (Honeywell Accudata 105), and the resultant change in output is amplified (Honeywell Accudata 122) before being connected to the by the analog to digital converter.
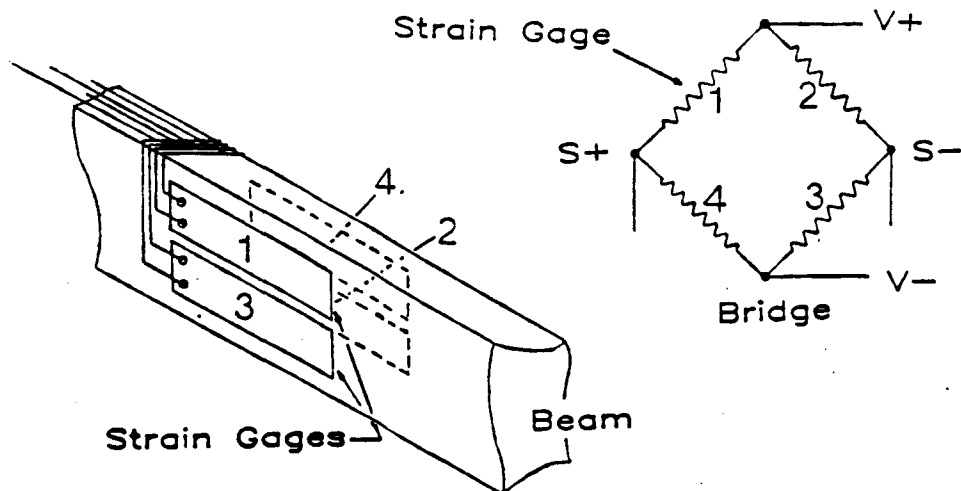
Figure E-4. Strain Gage Implementation.
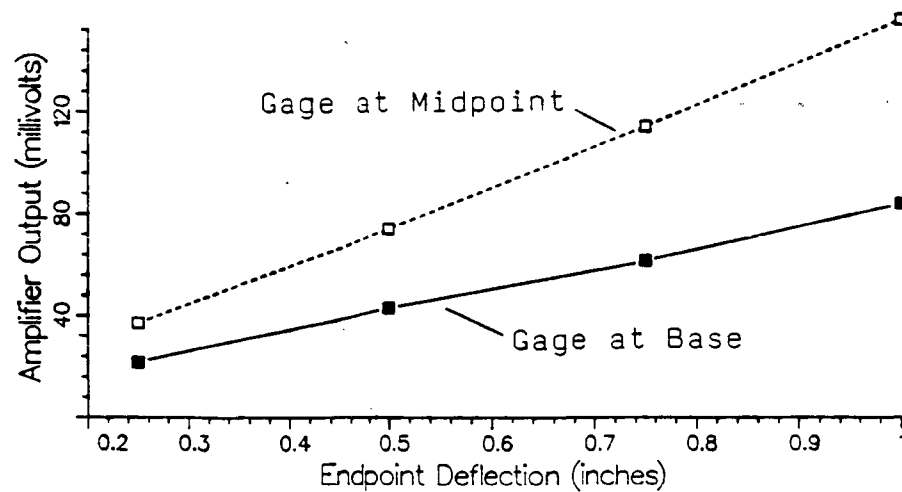
Figure E-5. Bridge/Amplifier Response.

Hardware Identification
Table E-2

Device	Function	Manufacturer	Specifications
Potentiometer	Joint Angle Sensor	Bourns Part no. 658-S-1-502	5 kohm, 1 turn, Cermet resistive element
Amplifier	Scaling/Isolation of Joint Angle Signal	KEPCO Model no. BOP36-15M	2.0amp, 36 volt Unity gain crossover 300khz
Tachometer	Joint Angle Velocity Sensor	Inland Motor Model no. TG-2139A	.9 volt-sec/rad max speed 77 rad/sec
Amplifier	Scaling/Isolation Joint Velocity	Hewlett Packard Model no. 6823A	1amp, 20volt
Strain Gage	Dynamic Strain Measurement	Micro-Measurement Systems Part no. EA-13-250-350W	Two gages per element, 250 ohms, solder tabs
Bridge	Drive Strain Gage Bridge	Honeywell Model no. Accudata 105	Four active element, 5-10 volts DC excitation
Amplifier	Scaling Strain Signal	Honeywell Model no. Accudata 122	Variable gain, .02-5000
Motor	Joint Torque	Inland Motor Model no. T-5730-M	Peak torque = 85 in-lbs, peak current= 15 amps
Power Amp	Motor Current	KEPCO Part no. BOP15-20M	20amp, 15 volt 300khz crossover
Resistor	Motor Current Sense	Ohmite	Variable Resistor, .0-.5 ohms.

E.3 Torque Motor/Servo-Amp

The digital to analog converter generated voltage signals proportional to the desired motor torque. The commutated DC torque motor was driven by a servo-amp configured in current mode. This meant that a current was driven through the amplifier load (DC torque motor) proportional to the input voltage. This implementation uses a sense resistor on the output terminal of the motor to monitor current. The connections and configuration for this mode of operation are shown in figure E-6.
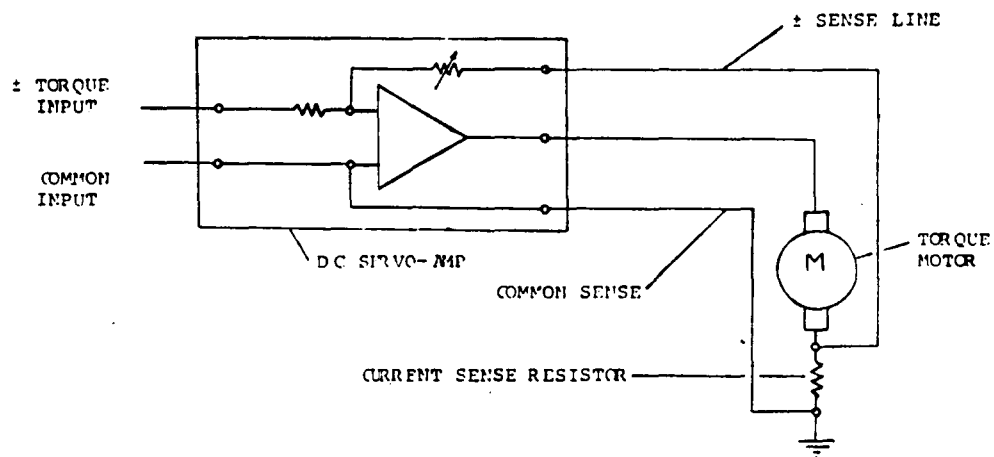
Figure E-6. Motor/Amplifier Current Mode Configuration.

APPENDIX F

CONTROLLER IMPLEMENTATION

This section covers the issues and structures of the real time controller implementation, key hardware elements, and software. Specific features, and methods written into the software which were particularly useful for this system are discussed. Additionally, the actual code utilized on the IBM Series/1 to implement the LQR controller designs of chapter 7 in real time is presented here as an example for future programmers. The basic system structure and utilities are described as well as the process required to compile, link, and execute the software.

F.1 Software Development

The software evolved over the course of the controller implementations into a compromise between initial objectives, and performance requirements. Throughout the software design the following goals were used as guides:

- Intelligibility - easily understandable source code, high level of documentation, High level language.
- Modularity - Separation of code into distinct functional modules, subroutines etc., common to multiple controllers.
- Operator Input/Output - Terminal supported parameter adjustment.

- Speed - Fast execution times, resulting in short cycle times which reduce the impact of discretization

Applying these goals to a real-time implementation can not be accomplished in an abstract form. Specific features of the hardware, and available software compatible with the hardware become extremely important in making software generation.

Initially the controllers were implemented in Fortran, this is a high level language familiar to most engineering students. Difficulties were encountered by the vary system transparency afforded by a high level language. System overhead primarily due to provisions for multi-level, multi-tasking options resulted in execution speeds far short of processor capabilities. Additionally special features of the analog input and output, and terminal devices were not easily accessed. The combination of these factors led to abandonment of Fortran as the language for implementation.

The second generation of control software was written in IBM's system language, Event Driven Language (EDL). EDL is a moderately high level language providing IF-THEN, DO-WHILE structures, as well as subroutines support, yet closely resembles assembly language statements. EDL is also tailored to the specific hardware elements providing full use the device features. The difficulty encountered in this iteration of the controllers was primarily speed of

execution. Although EDL provided better access to the hardware devices, system overhead was still extensive and execution times were still much slower than indicated by summing processor instruction times.

The third generation of software was a hybrid of EDL and Assembly languages. EDL was utilized for controlling the system interfaces, and the computations were executed in assembly language routines. The execution times for this software hybrid came close to realizing the capabilities of the processor. This compromise leaned more to the performance requirements and modularity goals for the software, and less toward the intelligibility goal. However, with alot of annotation, the time required for familiarization is minimized.

F.2 Hardware Features

Special hardware functions were found to be extremely helpful in implementation of the control laws. Hardware floating point computations were used throughout the controller implementations. Depending upon the control law design procedure and the input quantities being investigated at any one time, the state gains varied a full order of magnitude. Use of floating point instructions avoided extensive rescaling required with integer computations to retain high accuracy and resolution.

Another feature found to be extremely useful in

investigating control strategies, was static screen support for menu driven parameter adjustment using the terminal. Many parameters needed to be input to the system and updated for the various controllers. Static screens supported menu type data entry providing easy access, and verification of the memory locations holding key parameters.

F.3 IBM Series/1

The IBM Series/1 utilized for the experiments is a micro-processor based computing system supporting several processors, and a wide variety of peripheral devices. For a complete list of processors, cards, and subsystems supported refer to "Series/1 Digest"[F1]. Only the specific configuration used in the experiment will be discussed here.

There are several unique features to the Series/1 in addition to the floating point hardware and terminal support mentioned above. These additional features were not required for the sequential implementation of the controllers, but will be mentioned to provide reference to the available resources. The processor has separate I/O, and memory channels, 213 programable interrupts from the I/O channel, and four hardware levels for rapid execution interrupt processes.

The capabilities, and hardware of the Series/1 utilized for the experiments are summarized in table F-1.

Table F-1. Series/1 Configuration

Micro-processor	Model 4955-F, 16 bit
Cycle Time	220 nano-sec
Instruction set	160 basic set
Storage	512 kilo-byte
Floating Multiply	19 micro-sec
I/O Channel	256 addressable, 1.65 mega-byte/sec throughput.
Mass Storage	Model 4964
Hard Disk	64 mega-byte
Floppy	256 kilo-byte
Input and Output	Sensor I/O no. 4982
Analog Input	Solid State 16 differential points,9600 samples/sec Reed Relay 8 differential points,200 samples/sec
Analog Output	Solid State 2 differential points, 20 micro-sec settling time.
Digital I/O	Isolated, 16 points Non-Isolated, 16 points
Communications	
Serial Async.	8 ports, ASCII, EBCDC

F3.1 Utilities and Program Preparation

The Series/1 supports an IBM programming language/operating system called the Event Driven Executive, which refers to its ability to identify and service interrupt requests. This comes with a lot of useful utility programs for system generation, diagnostics, and data management. Additionally, editing, compiling, linking, and

interactive debugging is well supported.

All the utility programs can be executed individually using the relocating loader routine $L, or a "mothering" program, $SMMAIN, which provides menu driven interfaces with which the utility routines can be invoked. Documentation on the utility programs and there use is contained in "Operator commands and Utilities Reference"[F2]. An example of the procedure for compiling will be given with each program, and a linking procedure will follow the source codes for each controller.

F.4 Deterministic Regulator

The source code for the regulator is broken into several assembly language subroutines joined together.by a driver/initialization routine written in IBM's Event Driven Language EDL. The routines, their names, and functions are summarized below:

LUENEDX(EDL)	Drive parameter initialization menus, call the assembly level subroutines, provide interrupt capability
CONV(ASM)	onvert input values, reconstruct modal variables.
UPDATE(ASM)	Update state estimate.
CNTRL(ASM)	Execute control law and convert output
EST(ASM)	Estimate state variables.

F.5 Program Generation

This section discusses the process required to generated executable code for the Series/1. These steps are straightforward, typical of all processors, but may be less transparent on the Series/1 than some programmers are familiar with. The steps consist of source code generation using a line or screen editor. The Series/1 provides a reasonable screen editor $FSE which can be loaded directly, or via the system manager. Fortran, EDL, and Assembly code source code can all be generated with this editor. The source modules must be compiled individually into object code. The system is provisioned with compilers for all three languages, $FORT for Fortran, $EDXASM for EDL, and $S1ASM for the Assembly source code which can again be invoked directly at the system prompt, or with the session manager.

The compiled objects must be linked with each other, and system library files into a relocatable module for execution. The modules are linked with the utility program, $EDXLINK, which as with the other system utilities can be loaded directly or with the session manager.

The program generation sequence is summarized in table F-2, for the case of the deterministic regulator. The source files, temporary holding files set aside for the object modules, and linking instructions are included.

Table F-2. Program Generation Sequence

Step 1. Generate Source Code Modules (Editor - $FSE,EDX003)
        Event Driven Language Driver - LUENEDX,GORDON
        Assembly Code Modules - CONV1,GORDON
                              - UPDATE,GORDON
                              - CNTRL,GORDON
                              - EST,GORDON

Step 2. Assemble Object Modules
        Event Driven Language Modules (Compiler - $EDXAS
M,EDX003)
                        . Compile LUENEDX,GORDON to ASMWK1,GORDON
        Assembly Language Modules (Compiler - $S1ASM,EDX003)
                        Compile CONV1,GORDON   to ASMWK2,GORDON
                                UPDATE,GORDON   ASMWK3,GORDON
                                CNTRL, GORDON   ASMWK4,GORDON
                              . EST,GORDON   ASMWK5,GORDON

Step 3. Link Executable Module (Linker - $EDXLINK,EDX003)
        Assembled Object Modules
                        Include ASMWK1,GORDON
                        Include ASMWK2,GORDON
                        Include ASMWK3,GORDON
                        Include ASMWK4,GORDON
                        Include ASMWK5,GORDON

        Access System Library
                        Autocall $AUTO,ASMLIB

        Perform Linkage
                        Link EXEC,GORDON Replace End

Step 4. Execute Program
        At System Prompt Utilize Relocating Loader on
        Executable Module
                        $L EXEC,GORDON
        Then Provide Input, and Output Data Files at Prompts
                        IN10,GORDON
                        IN10,GORDON (Write Modifications to Same
                        File)

F.5.1 Routine LUENEDX
        This file can be compiled using the utility routine
$EDXASM. This routine is most easily accessed through the
program preparation facility of $SMMAIN. One word of
caution, destination files for the compiled objects must be
allocated prior to compilation, or the object will not be
stored. To avoid generation of excess object files on the
hard disk, ASMWK1 on volume CONTROL was allocated as the

```
        typical destination for the compilation of LUENEDX.
        (START OF FILE LUENEDX)
        ***********************************************************
        *****                                                   ***
        * EDX DRIVER PROGRAM WITH INITIALIZATION ROUTINE,AND I/O ***
        *****                                                   ***
        ***********************************************************
        *
        REDOO    PROGRAM   START,DS=((INPUT,??),(OUTPUT,??)),FLOAT=YES
        *
        *   KEYBOARD INTERUPT ROUTINE DEFINITION TO STOP CONTROLLER
        *
                 ATTNLIST    (X,QUIT)
        QUIT     MOVE        FLAG,1
                 ENDATTN
                 EXTRN       EST,CONV,UPDATE,CNTRL
                 EXTRN       $IMOPEN,$IMDEFN,$IMPROT
        TERM     IOCB        SCREEN=STATIC
        *
        ***********************************************************
        *     DEFINE THE ANALOG INPUT AND OUTPUT PORTS
        *     THETA,STRAIN1,STRAIN2,VELOCITY
        ***********************************************************
        *
        *            ANGLE SENSOR
        *
             IODEF      AI1,ADDRESS=63,POINT=0,RANGE=5V

        *            STRAIN GAGES
        *
             IODEF      AI2,ADDRESS=63,POINT=1,RANGE=500MV
             IODEF      AI3,ADDRESS=63,POINT=2,RANGE=500MV
        *
        *            VELOCITY SENSOR
        *
             IODEF      AI4,ADDRESS=63,POINT=3,RANGE=5V
        *
        *.   THE DESIRED END POINT INPUT
        *
             IODEF      AI5,ADDRESS=63,POINT=4,RANGE=5V
        *
        *   DITHER SIGNAL
        *
             IODEF      AI6,ADDRESS=63,POINT=5,RANGE=5V
        *
        *    THE TORQUE OUTPUT A/D DEVICE
        *
             IODEF      AO1,ADDRESS=64,POINT=0
        *
        *    SIGNAL OUTPUT PORT
        *
```

```
          IODEF          AO2,ADDRESS=64,POINT=1
*
***********************************************************
*
*     MAIN MENU DRIVER
*
***********************************************************
*
*     CALL THE PREPARED SCREEN IMAGE
*
START     EQU            *
LMENU     CALL           $IMOPEN,(DSNAME1),(DISKBUF),(TERMTYPE)
          ENQT           TERM
          CALL           $IMPROT,(DISKBUF),(FTABLE)
          TERMCTRL       DISPLAY
*
*     READ THE SELECTION INTEGER CHOICE
*
          PRINTNUM       ZERO,FORMAT=(1,0,I),LINE=16,SPACES=26
          PRINTEXT       LINE=16,SPACES=26
          TERMCTRL       DISPLAY
          WAIT           KEY
          GETVALUE       CHOICE,FORMAT=(1,0,I),LINE=16,SPACES=26
          IF             (CHOICE,EQ,1),GOTO,LINPUT
          IF             (CHOICE,EQ,2),GOTO,LGAIN
          IF             (CHOICE,EQ,3),GOTO,LOBSVR
          IF             (CHOICE,EQ,4),GOTO,LINCOEF
          IF             (CHOICE,EQ,5),GOTO,LUPDATE
          IF             (CHOICE,EQ,6),GOTO,LZERO
          IF             (CHOICE,EQ,7),GOTO,LOUTPT
          IF             (CHOICE,EQ,8),GOTO,LXQT
          IF             (CHOICE,EQ,9),GOTO,LEND
          GOTO LMENU
*
*     ROUTINE TO INPUT DATA SET OF PARAMETERS
*            CALL THE PREPARED SCREEN
*
LINPUT    CALL           $IMOPEN,(DSNAME3),(DISKBUF),(TERMTYPE)
          ENQT           TERM
          CALL           $IMPROT,(DISKBUF),(FTABLE)
          TERMCTRL       DISPLAY
*
*     READ THE INPUT DATA SET NAME AND VOLUME
*
          READ           DS1,DATBUF,2
          MOVE           FN,DATBUF,(256,BYTES)
          GOTO           LMENU
*
*     ROUTINE VIEW/ALTER GAIN VECTOR
*            CALL THE PREPARED SCREEN
*
```

```
LGAIN     CALL          $IMOPEN,(DSNAME2),(DISKBUF),(TERMTYPE)
          ENQT          TERM
          CALL          $IMPROT,(DISKBUF),(FTABLE)
          TERMCTRL      DISPLAY
*
*     FILL IN THE DEFAULT VALUES
*
   PRINTNUM FN+56,FORMAT=(12,6,E),TYPE=F,LINE=3,SPACES=40
   PRINTNUM FN+60,FORMAT=(12,6,E),TYPE=F,LINE=5,SPACES=40
   PRINTNUM FN+64,FORMAT=(12,6,E),TYPE=F,LINE=7,SPACES=40
   PRINTNUM FN+68,FORMAT=(12,6,E),TYPE=F,LINE=9,SPACES=40
   PRINTNUM FN+72,FORMAT=(12,6,E),TYPE=F,LINE=11,SPACES=40
   PRINTNUM FN+76,FORMAT=(12,6,E),TYPE=F,LINE=13,SPACES=40
*
*     POSITION THE CURSOR,WAIT FOR THE ENTER KEY, GET THE
*                 VALUE
*
   PRINTEXT      LINE=14,SPACES=33
   TERMCTRL      DISPLAY
   WAIT          KEY
   GETVALUE FN+56,FORMAT=(12,6,E),TYPE=F,LINE=3,SPACES=40
   GETVALUE FN+60,FORMAT=(12,6,E),TYPE=F,LINE=5,SPACES=40
   GETVALUE FN+64,FORMAT=(12,6,E),TYPE=F,LINE=7,SPACES=40
   GETVALUE FN+68,FORMAT=(12,6,E),TYPE=F,LINE=9,SPACES=40
   GETVALUE FN+72,FORMAT=(12,6,E),TYPE=F,LINE=11,SPACES=40
   GETVALUE FN+76,FORMAT=(12,6,E),TYPE=F,LINE=13,SPACES=40
   GOTO          LMENU
*
*     ROUTINE TO VIEW/ALTER OBSERVOR PARAMETERS
*
LOBSVR    ENQT          TERM
          TERMCTRL      BLANK
          DEQT
          CALL          $IMOPEN,(DSNAME4),(DISKBUF),(TERMTYPE)
          ENQT          TERM
          CALL          $IMPROT,(DISKBUF),(FTABLE)
          TERMCTRL      DISPLAY
   PRINTNUM FN,FORMAT=(12,6,E),TYPE=F,LINE=7,SPACES=4
   PRINTNUM FN+4,FORMAT=(12,6,E),TYPE=F,LINE=7,SPACES=21
   PRINTNUM FN+24,FORMAT=(12,6,E),TYPE=F,LINE=7,SPACES=49
   PRINTNUM FN+28,FORMAT=(12,6,E),TYPE=F,LINE=9,SPACES=4
   PRINTNUM FN+32,FORMAT=(12,6,E),TYPE=F,LINE=9,SPACES=21
   PRINTNUM FN+52,FORMAT=(12,6,E),TYPE=F,LINE=9,SPACES=49
   PRINTNUM FN+8,FORMAT=(12,6,E),TYPE=F,LINE=13,SPACES=8
   PRINTNUM FN+12,FORMAT=(12,6,E),TYPE=F,LINE=13,SPACES=25
   PRINTNUM FN+16,FORMAT=(12,6,E),TYPE=F,LINE=13,SPACES=42
   PRINTNUM FN+20,FORMAT=(12,6,E),TYPE=F,LINE=13,SPACES=59
   PRINTNUM   FN+36,FORMAT=(12,6,E),TYPE=F,LINE=15,SPACES=8
   PRINTNUM   FN+40,FORMAT=(12,6,E),TYPE=F,LINE=15,SPACES=25
   PRINTNUM   FN+44,FORMAT=(12,6,E),TYPE=F,LINE=15,SPACES=42
   PRINTNUM   FN+48,FORMAT=(12,6,E),TYPE=F,LINE=15,SPACES=59
```

```
          PRINTEXT   LINE=19,SPACES=30
          TERMCTRL   DISPLAY
          WAIT       KEY
          GETVALUE    FN,FORMAT=(12,6,E),TYPE=F,LINE=7,SPACES=4
          GETVALUE    FN+4,FORMAT=(12,6,E),TYPE=F,LINE=7,SPACES=21
          GETVALUE    FN+24,FORMAT=(12,6,E),TYPE=F,LINE=7,SPACES=49
          GETVALUE    FN+28,FORMAT=(12,6,E),TYPE=F,LINE=9,SPACES=4
          GETVALUE    FN+32,FORMAT=(12,6,E),TYPE=F,LINE=9,SPACES=21
          GETVALUE    FN+52,FORMAT=(12,6,E),TYPE=F,LINE=9,SPACES=49
          GETVALUE    FN+8,FORMAT=(12,6,E),TYPE=F,LINE=13,SPACES=8
          GETVALUE   FN+12,FORMAT=(12,6,E),TYPE=F,LINE=13,SPACES=25
          GETVALUE   FN+16,FORMAT=(12,6,E),TYPE=F,LINE=13,SPACES=42
          GETVALUE   FN+20,FORMAT=(12,6,E),TYPE=F,LINE=13,SPACES=59
          GETVALUE    FN+36,FORMAT=(12,6,E),TYPE=F,LINE=15,SPACES=8
          GETVALUE   FN+40,FORMAT=(12,6,E),TYPE=F,LINE=15,SPACES=25
          GETVALUE   FN+44,FORMAT=(12,6,E),TYPE=F,LINE=15,SPACES=42
          GETVALUE   FN+48,FORMAT=(12,6,E),TYPE=F,LINE=15,SPACES=59
          DEQT
          GOTO       LMENU
LUPDATE   ENQT       TERM
          TERMCTRL   BLANK
          DEQT
          CALL       $IMOPEN,(DSNAME5),(DISKBUF),(TERMTYPE)
          ENQT       TERM
          CALL       $IMPROT,(DISKBUF),(FTABLE)
          TERMCTRL   DISPLAY
       PRINTNUM  FN+148,FORMAT=(12,6,E),TYPE=F,LINE=13,SPACES=8
       PRINTNUM  FN+152,FORMAT=(12,6,E),TYPE=F,LINE=15,SPACES=8
       PRINTNUM FN+156,FORMAT=(12,6,E),TYPE=F,LINE=13,SPACES=25
       PRINTNUM FN+160,FORMAT=(12,6,E),TYPE=F,LINE=15,SPACES=25
       PRINTNUM FN+164,FORMAT=(12,6,E),TYPE=F,LINE=13,SPACES=42
       PRINTNUM FN+168,FORMAT=(12,6,E),TYPE=F,LINE=15,SPACES=42
       PRINTNUM FN+172,FORMAT=(12,6,E),TYPE=F,LINE=13,SPACES=59
       PRINTNUM FN+176,FORMAT=(12,6,E),TYPE=F,LINE=15,SPACES=59
       PRINTEXT LINE=19,SPACES=30
          TERMCTRL   DISPLAY
          WAIT  ·    KEY
          GETVALUE   FN+148,FORMAT=(12,6,E),TYPE=F,LINE=13,SPACES=8
          GETVALUE   FN+152,FORMAT=(12,6,E),TYPE=F,LINE=15,SPACES=8
          GETVALUE FN+156,FORMAT=(12,6,E),TYPE=F,LINE=13,SPACES=25
          GETVALUE FN+160,FORMAT=(12,6,E),TYPE=F,LINE=15,SPACES=25
          GETVALUE FN+164,FORMAT=(12,6,E),TYPE=F,LINE=13,SPACES=42
          GETVALUE FN+168,FORMAT=(12,6,E),TYPE=F,LINE=15,SPACES=42
          GETVALUE FN+172,FORMAT=(12,6,E),TYPE=F,LINE=13,SPACES=59
          GETVALUE FN+176,FORMAT=(12,6,E),TYPE=F,LINE=15,SPACES=59
DEQT
     GOTO       LMENU
*
*    ROUTINE TO VIEW/ALTER INPUT COEFFICIENTS
*
LINCOEF  ENQT       TERM
```

```
            TERMCTRL    BLANK
            DEQT
            CALL        $IMOPEN,(DSNAME6),(DISKBUF),(TERMTYPE)
            ENQT        TERM
            CALL        $IMPROT,(DISKBUF),(FTABLE)
            TERMCTRL    DISPLAY
*
*     FILL IN THE DEFAULT VALUES
*
     PRINTNUM    FN+80,FORMAT=(12,6,E),TYPE=F,LINE=5,SPACES=25
     PRINTNUM    FN+84,FORMAT=(12,6,E),TYPE=F,LINE=7,SPACES=25
     PRINTNUM    FN+88,FORMAT=(12,6,E),TYPE=F,LINE=9,SPACES=25
     PRINTNUM    FN+92,FORMAT=(12,6,E),TYPE=F,LINE=11,SPACES=25
     PRINTNUM    FN+96,FORMAT=(12,6,E),TYPE=F,LINE=13,SPACES=25
     PRINTNUM   FN+100,FORMAT=(12,6,E),TYPE=F,LINE=15,SPACES=25
     PRINTNUM   FN+104,FORMAT=(12,6,E),TYPE=F,LINE=17,SPACES=25
     PRINTNUM   FN+108,FORMAT=(12,6,E),TYPE=F,LINE=19,SPACES=25
     PRINTEXT LINE=21,SPACES=34
     TERMCTRL DISPLAY
            WAIT        KEY
     GETVALUE    FN+80,FORMAT=(12,6,E),TYPE=F,LINE=5,SPACES=25
     GETVALUE    FN+84,FORMAT=(12,6,E),TYPE=F,LINE=7,SPACES=25
     GETVALUE    FN+88,FORMAT=(12,6,E),TYPE=F,LINE=9,SPACES=25
     GETVALUE    FN+92,FORMAT=(12,6,E),TYPE=F,LINE=11,SPACES=25
     GETVALUE    FN+96,FORMAT=(12,6,E),TYPE=F,LINE=13,SPACES=25
     GETVALUE   FN+100,FORMAT=(12,6,E),TYPE=F,LINE=15,SPACES=25
     GETVALUE   FN+104,FORMAT=(12,6,E),TYPE=F,LINE=17,SPACES=25
     GETVALUE   FN+108,FORMAT=(12,6,E),TYPE=F,LINE=19,SPACES=25
     TERMCTRL    BLANK
     DEQT
            GOTO        LMENU
*
*     ROUTINE TO OUTPUT SELECTED PARAMETERS
*
LOUTPT      ENQT        TERM
            TERMCTRL    BLANK
            DEQT
            CALL        $IMOPEN,(DSNAME8),(DISKBUF),(TERMTYPE)
            ENQT        TERM
            CALL        $IMPROT,(DISKBUF),(FTABLE)
            TERMCTRL    DISPLAY
            MOVE        DATBUF,FN,(256,BYTES)
            WRITE       DS2,DATBUF,2
            DEQT
            GOTO        LMENU
*****************************************************************
******
******          SYSTEM INITIAL ZEROING  ROUTINE
******
*****************************************************************
LZERO       CALL        $IMOPEN,(DSNAME7),(DISKBUF),(TERMTYPE)
```

```
                    ENQT          TERM
                    CALL          $IMPROT,(DISKBUF),(FTABLE)
                    TERMCTRL      DISPLAY
ZZZZ        SBIO          AI1,AN
            SBIO          AI2,AN+2
            SBIO          AI3,AN+4
            SBIO          AI4,AN+6
*
*     CALL THE CONVERSION ROUTINE TO TRANSFORM THE INPUTS
*
            USER          CONV,PARM=(AN,FN)
      PRINTNUM  FN+112,FORMAT=(12,6,E),TYPE=F,LINE=4,SPACES=30
      PRINTNUM  FN+124,FORMAT=(12,6,E),TYPE=F,LINE=6,SPACES=30
      PRINTNUM   AN+2,FORMAT=(6,0,I),LINE=8,SPACES=30
      PRINTNUM AN+4,FORMAT=(6,0,I),LINE=10,SPACES=30
                    PRINTNUM      ZERO,FORMAT=(1,0,I),LINE=12,SPACES=31
                    PRINTEXT      LINE=12,SPACES=31
                    TERMCTRL      DISPLAY
                    WAIT          KEY
                    GETVALUE      ZM1,FORMAT=(1,0,I),LINE=12,SPACES=31
                    IF            (ZM1,EQ,1),GOTO,LMENU
                    GOTO          ZZZZ
LXQT        DEQT
STRCN       CALL          $IMOPEN,(DSNAME9),(DISKBUF),(TERMTYPE)
                    ENQT          TERM
                    CALL          $IMPROT,(DISKBUF),(FTABLE)
                    DEQT
****************************************************************
*****
*****   REDUCED DYNAMIC ORDER LUENBERGER OBSERVER/CONTROLLER
*****
****************************************************************
*
*       THE SECTION WHICH READS THE ANALOG INPUT VALUES
*
LOOP1       SBIO          AI1,AN
            SBIO          AI2,AN+2
            SBIO          AI3,AN+4
            SBIO          AI4,AN+6
            SBIO          AI5,AN+10
            SBIO          AI6,AN+12
*
*       CALL THE ASEMBLER VERSION OF THE ESTIMATOR AND THE
*       CONTROLLER
*
            USER          CONV,PARM=(AN,FN)
            USER          UPDATE,PARM=(AN,FN)
            USER          CNTRL,PARM=(AN,FN)
            SBIO          AO1,AN+8
            USER          EST,PARM=(AN,FN)
            IF            (FLAG,NE,0),GOTO,RTN
```

```
               GOTO       LOOP1
RTN            SBIO       AO1,ZERO
               MOVE       FLAG,0
               ENQT       TERM
               TERMCTRL   BLANK
               GOTO       LMENU
LEND           PROGSTOP
*
*************************************************************
*
FLAG           DATA       F'0'
ZERO           DATA       F'0'
CHOICE         DATA       F'0'
ZM1            DATA       F'0'
INL            DATA       F'0'
AN             DATA       12F'0'
INSC           DATA       F'125'
*JOINT     EQU     AN
*STRAIN1   EQU     AN+2
*STRAIN2   EQU     AN+4
*VEL       EQU     AN+6
*TORQ      EQU     AN+8
*DESANGLE          AN+10
*DITHER SIGNAL     AN+12
*                  AM+14
FN             DATA       64E'0.0'
*F11  EQU    FN      OBSERVER VELMOD1 DEPENDENCE LAST VELMOD1
*F12  EQU    FN+4      "        "         "        "  VELMOD2
*G11  EQU    FN+8      "        "         "        "  ANGLE
*G12  EQU    FN+12     "        "         "        "  MOD1
*G13  EQU    FN+16     "        "         "        "  MOD2
*G14  EQU    FN+20     "        "         "        "  JOINTVEL
*B1   EQU    FN+24     "        "         "        "  TORQUE
*F21  EQU    FN+28 OBSERVOR VELMOD2 DEPENDENCE LAST VELMOD1
*F22  EQU    FN+32     "        "         "        "  VELMOD2
*G21  EQU    FN+36     "        "         "        "  ANGLE
*G22  EQU    FN+40     "        "         ".        "  MOD1
*G23  EQU    FN+44     "        "         "        "  MOD2
*G24  EQU    FN+48     "        "         "        "  JOINTVEL
*B2   EQU    FN+52     "        "         "        "  TORQUE
*K1   EQU    FN+56   JOINT ANGLE GAIN
*K2   EQU    FN+60   MOD 1 AMPLITUDE GAIN
*K3   EQU    FN+64   MOD 2 AMPLITUDE GAIN
*K4   EQU    FN+68   JOINT VELOCITY GAIN
*K5   EQU    FN+72   MOD 1 VELOCITY GAIN
*K6   EQU    FN+76   MOD 2 VELOCITY GAIN
*CONV1 EQU    FN+80    JOINT ANGLE INPUT CONVERSION
*CONV2 EQU    FN+84    STRAIN 1 MOD1 INPUT CONVERSION
*CONV3 EQU    FN+88    STRAIN 2 MOD1 INPUT CONVERSION
*CONV4 EQU    FN+92    STRAIN 1 MOD2 INPUT CONVERSION
*CONV5 EQU    FN+96    STRAIN 2 MOD2 INPUT CONVERSION
```

```
*CONV6 EQU     FN+100   TACHOMETER INPUT CONVERSION
*CONV7 EQU     FN+104   TORQUE OUTPUT CONVERSION
*CONV8 EQU     FN+108   INPUT SIGNAL CONVERSION
*FTHET EQU     FN+112   JOINT ANGLE FLOATING POINT
*FMOD1 EQU     FN+116   AMPLITUDE MODE1 FLOATING POINT
*FMOD2 EQU     FN+120   AMPLITUDE MODE2 FLOATING POINT
*FOMEG EQU     FN+124   JOINT VELOCITY FLOATING POINT
*ESTV1 EQU     FN+128   ESTIMATED MOD1 VELOCITY FLOATING POINT
*ESTV2 EQU     FN+132   ESTIMATED MOD2 VELOCITY FLOATING POINT
*TORQ  EQU     FN+136   TORQUE FLOATING POINT
*OUTPT EQU     FN+140
*ZERO  EQU     FN+144
*      EQU     FN+148   UPDATE GAIN L1
*      EQU     FN+152     "     "   L2
*      EQU     FN+156     "     "   L3
*      EQU     FN+160     "     "   L4
*      EQU     FN+164     "     "   L5
*      EQU     FN+168     "     "   L6
*      EQU     FN+172     "     "   L7
*      EQU     FN+176     "     "   L8
*      EQU     FN+180
*      EQU     FN+184
DATBUF BUFFER  256,BYTES
BDS    BUFFER  258,BYTES
DISKBU BUFFER  1024,BYTES
FTABLE BUFFER  15,WORDS
RDAT1  BUFFER  512,BYTES,INDEX=INDX1
INSET  TEXT    LENGTH=20
OUTSET TEXT    LENGTH=20
DSNAME1 TEXT    'MENUSCR,GORDON'
DSNAME2 TEXT    'GAINSCR,GORDON'
DSNAME3 TEXT    'INPUTSCR,GORDON'
DSNAME4 TEXT    'OBSVRSCR,GORDON'
DSNAME5 TEXT    'UPDATSCR,GORDON'
DSNAME6 TEXT    'COEFSCR,GORDON'
DSNAME7 TEXT    'ZEROSCR,GORDON'
DSNAME8 TEXT    'OUTPTSCR,GORDON'
DSNAME9  TEXT    'LUENSCR,GORDON'
TERMTYPE DATA   C'4978'
MEAS     DATA   4F'0'
         ENDPROG
         END
(END OF FILE LUENEDX)
```

F.5.2 Routine CONV

This routine is compiled using the utility routine $S1ASM.
The program preparation facility accessed via $SMMAIN is the
easiest method for its execution. The file ASMWK2 on volume

CONTROL of the harddisk was reserved as the destination file

for the compiled object.

(START OF FILE CONV)
```
**********************************************************
*****
*****     INPUT CONVERSION/RECONSTRUCTION ROUTINE  ---------
*****
**********************************************************
          START
          EXTRN       RETURN
          ENTRY       CONV
CONV      EQU         *
          FMVC        2(R1,0)*,FR3              :STRAIN1
          FM          84(R1,2)*,FR3            :CONV2*STRAIN1
          FMVC        4(R1,0)*,FR2              :STRAIN2
          FM          88(R1,2)*,FR2            :CONV3*STRAIN2
          FA          FR2,FR3                   :MODE1
          FMV         FR3,116(R1,2)*            :SAVE MODE1
          FMVC        2(R1,0)*,FR2              :STRAIN1
          FM          92(R1,2)*,FR2            :CONV4*STRAIN1
          FMVC        4(R1,0)*,FR1              :STRAIN2
          FM          96(R1,2)*,FR1            :CONV5*STRAIN2
          FA          FR1,FR2                   :MODE2
          FMV         FR2,120(R1,2)*            :SAVE MODE2
          FMVC        (R1,0)*,FR1               :THETA
          FM          80(R1,2)*,FR1            :CONV1*THETA
          FMV         FR1,112(R1,2)*            :SAVE FTHETA
          FMVC        6(R1,0)*,FR1              :OMEGA
          FM          100(R1,2)*,FR1           :CONV6*OMEGA
          FMV         FR1,124(R1,2)*            :SAVE FOMEGA
          ABI         4,R1
          B           RETURN
          END
```
(END OF FILE CONV)

F.5.3 Routine UPDATE

This routine is compiled using the utility routine $S1ASM.
The program preparation facility accessed via $SMMAIN is the
easiest method for its execution. The file ASMWK3 on volume
CONTROL of the harddisk was reserved as the destination file
for the compiled object.

```
(START OF FILE UPDATE)
**************************************************************
*****
*****     UPDATE   FOR   LUENBERGER OBSERVER     ---------
*****
**************************************************************
          START
          EXTRN     RETURN        :DISPLACEMENT LISTING IN M2SO
          ENTRY     UPDATE
UPDATE    EQU       *
*
** UPDATE ESTIMATE OF MODE ONE VELOCITY
*
          FMV       112(R1,2)*,FR3        :FTHETA
          FM        148(R1,2)*,FR3        :UPDATE L1*FTHETA
          FMV       116(R1,2)*,FR1        :FMODE1
          FM        156(R1,2)*,FR1        :UPDATE L3*FMOD1
          FA        FR1,FR3               :ADD TO UPDATE Z1
          FMV       120(R1,2)*,FR1        :FMODE2
          FM        164(R1,2)*,FR1        :UPDATE L5*FMODE2
          FA        FR1,FR3               :ADD TO UPDATE Z1
          FMV       124(R1,2)*,FR1        :FOMEGA
          FM        172(R1,2)*,FR1        :UPDATE L7*FOMEGA
          FA        FR1,FR3               :ADD TO UPDATE Z1
          FA        128(R1,2)*,FR3        :ADD EST VEL MODE1
          FMV       FR3,128(R1,2)*        :SAVE UPDATE Z1
*
** BEGIN UPDATE ESTIMATE OF MODE TWO VELOCITY
*
          FMV       112(R1,2)*,FR3        :FTHETA
          FM        152(R1,2)*,FR3        :UPDATE L2*FTHETA
          FMV       116(R1,2)*,FR1        :FMODE1
          FM        160(R1,2)*,FR1        :UPDATE L4*FMOD1
          FA        FR1,FR3               :ADD TO UPDATE Z2
          FMV       120(R1,2)*,FR1        :FMODE2
          FM        168(R1,2)*,FR1        :UPDATE L6*FMODE2
          FA        FR1,FR3               :ADD TO UPDATE Z2
          FMV       124(R1,2)*,FR1        :FOMEGA
          FM        176(R1,2)*,FR1        :UPDATE L8*FOMEGA
          FA        FR1,FR3               :ADD TO UPDATE Z2
          FA        132(R1,2)*,FR3        :ADD EST VEL MODE1
          FMV       FR3,132(R1,2)*        :SAVE UPDATE Z2
          ABI       4,R1
          B         RETURN
          END
```

F.5.4 Routine CNTRL

This routine is compiled using the utility routine $S1ASM.

The program preparation facility accessed via $SMMAIN is the

easiest method for its execution. The file ASMWK3 on volume

CONTROL of the harddisk was reserved as the destination file

for the compiled object.

(START OF FILE CNTRL)
```
****************************************************************
*****
*****     CONTROL LAW FOR LUENBERGER/KALMAN FILTER ---
*****
****************************************************************
          START
          EXTRN        RETURN       :DISPLACEMENT LISTING IN M2SO
          ENTRY        CNTRL
CNTRL     EQU          *
          FMV          112(R1,2)*,FR3        :FTHETA
          FM           56(R1,2)*,FR3         :K1*FTHETA
          FMV          116(R1,2)*,FR1        :FMODE1
          FM           60(R1,2)*,FR1         :K2*FMOD1
          FA           FR1,FR3               :ADD TO CONTROL
          FMV          120(R1,2)*,FR1        :FMODE2
          FM           64(R1,2)*,FR1         :K3*FMODE2
          FA           FR1,FR3               :ADD TO CONTROL
          FMV          124(R1,2)*,FR1        :FOMEGA
          FM           68(R1,2)*,FR1         :K4*FOMEGA
          FA           FR1,FR3               :ADD TO CONTROL
          FMV          128(R1,2)*,FR1        :EST VEL MODE1
          FM           72(R1,2)*,FR1         :K5*EST VEL MODE1
          FA           FR1,FR3               :ADD TO CONTROL
          FMV          132(R1,2)*,FR1        :EST VEL MODE2
          FM           76(R1,2)*,FR1         :K6*EST VEL MODE2
          FA           FR1,FR3               :ADD TO CONTROL
          FMVC         10(R1,0)*,FR1         :DESIRED ANGLE
          FM           108(R1,2)*,FR1        :SCALE ANGLE
          FA           FR1,FR3               :ADD
          FMV          FR3,136(R1,2)*        :SAVE TORQ
          FMVC         12(R1,0)*,FR1         :DITHER SIGNAL
          FM           108(R1,2)*,FR1        :SCALE
          FA           FR1,FR3               :
          FM           104(R1,2)*,FR3        :CONVERT TORQ
          FMVC         FR3,8(R1,0)*          :SAVE INTEGER TORQ
          ABI          4,R1
          B            RETURN
          END
```
(END OF FILE CNTRL)

F.5.5 Routine EST

This routine is compiled using the utility routine $S1ASM.

The program preparation facility accessed via $SMMAIN is the
easiest method for its execution. The file ASMWK4 on volume
CONTROL of the harddisk was reserved as the destination file
for the compiled object.

```
(START OF FILE EST)
***************************************************************
*****
*****     LUENBERGER OBSERVOR FOR MODAL VELOCITIES  ----------
*****
***************************************************************
          START
          EXTRN      RETURN     :DISPLACEMENT LISTING IN
*                               LUENEDX
          ENTRY      EST
EST       EQU        *
          FMV        128(R1,2)*,FR3   :START EQN1 GET VELMOD1
          FM         0(R1,2)*,FR3     :F11*VELMOD1
          FMV        132(R1,2)*,FR2   :GET*MODE2
          FM         4(R1,2)*,FR2     :F12*MODE2
          FA         FR2,FR3          :SUM TERMS FOR EQN 1
          FMV        112(R1,2)*,FR2   :GET FTHETA
          FM         8(R1,2)*,FR2     :G11*FTHETA
          FA         FR2,FR3          :SUM TERMS FOR EQN 1
          FMV        116(R1,2)*,FR2   :GET MOD1
          FM         12(R1,2)*,FR2    :G12*MOD1
          FA         FR2,FR3          :SUM TERMS FOR EQN 1
          FMV        120(R1,2)*,FR2   :GET MOD2
          FM·        16(R1,2)*,FR2    :G13*THETA
          FA         FR2,FR3          :SUM TERMS FOR EQN 1
          FMV        124(R1,2)*,FR2   :GET FOMEGA
          FM         20(R1,2)*,FR2    :G14*FOMEGA
          FA         FR2,FR3          :SUM TERMS FOR EQN 1
          FMV        136(R1,2)*,FR2   :GET FTORQ
          FM         24(R1,2)*,FR2    :B1*TORQ
          FA         FR2,FR3          :COMPLETE EQN 1
          FMV        128(R1,2)*,FR2   :START EQN2 GET VELMOD1
          FM·        28(R1,2)*,FR2    :F21*VELMOD1
          FMV        132(R1,2)*,FR1   :GET*MODE2
          FM         32(R1,2)*,FR1    :F22*MODE2
          FA         FR1,FR2          :SUM TERMS FOR EQN 2
          FMV        112(R1,2)*,FR1   :GET FTHETA
          FM         36(R1,2)*,FR1    :G21*FTHETA
          FA         FR1,FR2          :SUM TERMS FOR EQN 2
          FMV        116(R1,2)*,FR1   :GET MOD1
          FM         40(R1,2)*,FR1    :G22*MOD1
          FA         FR1,FR2          :SUM TERMS FOR EQN 2
          FMV        120(R1,2)*,FR1   :GET MOD2
```

```
        FM          44(R1,2)*,FR1    :G23*THETA
        FA          FR1,FR2          :SUM TERMS FOR EQN 2
        FMV         124(R1,2)*,FR1   :GET FOMEGA
        FM          48(R1,2)*,FR1    :G24*FOMEGA
        FA          FR1,FR2          :SUM TERMS FOR EQN 2
        FMV         136(R1,2)*,FR1   :GET FTORQ
        FM          52(R1,2)*,FR1    :B2*TORQ
        FA          FR1,FR2          :COMPLETE EQN 2
        FMV         FR3,128(R1,2)*   :SAVE EST VEL MODE1
        FMV         FR2,132(R1,2)*   :SAVE EST VEL MODE2
        ABI         4,R1
        B           RETURN
        END
(END OF FILE EST)
```

BIBLIOGRAPHY

I1. F.T. Brown,"On the Dynamics of Distributed Systems", Applied Mechanics Reviews, vol. 17, no. 5, 1964, pp 353-357.

I2. R.E. Andeen, "Stabilizing Flexible Vehicles", Journal of Astronautics and Aeronautics, August 1964, pp 38-44.

I3. M.A. Murray-Lasso, "The Modal Analysis and Synthesis of Linear Distributed Systems with Distributed Feedback", PhD Thesis, MIT, Nov. 1966.

I4. L.A. Gould, and M.A. Murray-Lasso, "On the Modal Control of Distributed Systems with Distributed Feedback", IEEE Trans. on Automatic Control, AC-11, no. 4, Oct. 1966.

I5. J.H. Wykes, and A.S. Mori, "An Analysis of Flexible Aircraft Structural Mode Control", Part 1, North American Adviation Technical Report, AFFDL-TR-65-190, June 1966.

I6. D.R. Vaughan, "Application of Distributed Parameter Concepts to Dynamic Analysis and Control of Bending Vibrations", ASME Journal of Basic Engineering, June 1968, pp 157-166.

I7. V. Komkov, "The Optimal Control of Transverse Vibration of a Beam", SIAM Journal on Control, vol. 6, no. 3, August 1968.

I8. J. Neto, "Automatic Control of a Vibrating Flexible Beam", M.S. Thesis, MIT, January 1972.

I9. W.J. Book, "Model, Design, and Control of Flexible Manipulator Arms", PhD Dissertation, MIT, April 1974.

I10. O. M. Neto, "Modal Analysis and Control of Flexible Manipulator Arms", PhD Dissertation, MIT, September 1974.

I11. D.B. Schaechter, "Hardware Demonstrartion of Flexible Beam Control", Journal of Guidance, vol. 5. no. 1, February 1982, pp 48-53.

I12. G.D. Martin, "On Control of Flexible Systems", PhD Thesis, Stanford University, 1978.

I13. M. J. Balas, "Modal Control of Certain Flexible Dynamic Systems", SIAM Journal Control Opt. 16, 1978, pp 450-462.

I14. W.J. Book, M. Majette, "The Distributed Systems Analysis Package and its Application to Modelling Flexible Manipulators", Georgia Institute of Technology, July 1979.

I15. P. Hughes, "Dynamics of a Chain of Flexible Bodies", Journal of Astronautical Sciences, Vol. 27, No.4 October-December 1979.

I16. M. J. Balas, "Finite Element Models and Feedback Controlof Flexible Aerospace Structures", Proc. Joint Automation Control Conference, San Fransisco, California, 1980.

I17. N. Fujii, " Feedback Stabilization of DPS by a Functional Observer", SIAM J. Control Opt. 18, 1980.

I18. A. Trukenbrodt, "Modelling and Control of Flexible Manipulator Structures", Proceedings of the 4th CISM-IFToMM

Symposium, Theory and Pratice of Robots and Manipulators, 1981.

I19. M. J. Balas, "Toward a More Practical Control Theory for Distributed Parameter Systems", Control and Dynamic Systems: Advances in Theory and Practice, Vol. 18, 1982, pp 361-421.

I20. W. Sunada, S. Dubowsky, "On the Dynamic Analysis and Behavior of Industrial Robotic Manipulators with Elastic Memebers", ASME Design and Production Engineering Technical Conference, Washington D.C., Sept. 1982.

I21. R. Cannon, E. Schmidtz, "Initial Experiments on the End-Point Control of a Flexible One Link Robot", The International Journal of Robotics Research, MIT Press, Cambridge Mass., vol.3, no.3, 1984.

I22. E. Schmidtz," Experiments on the End-point Position Control of a Very Flexible One-Link Manipulator", Stanford University, SUDAAR 548, June 1985.

I23. A. Zalucky, D. Hardt, "Active Control of Robot Structure Deflections", Journal of Dynamic Systems, Measurement and Control, Vol. 106, March 1984, pp 63-69.

I24. D. Turic, A. Midha, "Generalized Equations of Motion for the Dynamic Analysis of Elastic Mechanism Systems", Journal of Dynamic Systems, Measurement and Control, Vol. 106, March 1984, pp 243-248.

I25. D. Turic, A. Midha, J. Bosnik, "Dynamic Analysis of Elastic Mechanism Systems. Part II: Experimental Results", Journal of Dynamic Systems, Measurement and Control, Vol.

106, March 1984, pp 255-260.

I26. C. Weeks, " Static Shape Determination and Control for Large Space Structures: I. The Flexible Beam", <u>Journal of Dynamic Systems, Measurement and Control,</u> Vol. 106, March 1984, pp 261-266.

I27. D. S. Bodden and J. L. Junkins, "Eigenvalue Optimization Algrithms for Structural/Controller Design Iterations", American Control Conference, San Diego, CA, June 1984.

I28. D. Rew, J. L. Junkins, "In Search of the Optimal Quadratic Regulator", Proc. 5th VPI&SU/AIAA Symposium, Blacksburg, Va, June 1985.

I29. L. Meirovitch, H. Baruh, "On Implementation of Modal Filters for Control of Structures", Porc. of AIAA Guidance and Control Conference, Seattle, Washington, Aug. 1984

I30. V. Sanbveraphusiri, " The Optimal Control and Design of a Flexible Manipulator Arm", PhD Dissertation, Georgia Institute of Technology, May 1984.

I31. C.S. Major, E. B. Shain, "An Experiment fo Demonstrate Active and Passive Control of a Flexible Structure", American Control Conference, San Diego, CA, June 1984.

I32. C.S. Major, E. B. Shain, "Demonstration of Vibration Control of a Flexible Truss Structure", Proc. 5th VPI&SU/AIAA Symposium, Blacksburg, Va, June 1985.

I33. W. Book, "The Bracing Strategy for Robot Operation". Joint IFToMM-CISM Symposium on the Theory of Robots and

Manipulators, Udine, Italy, June 1984.

I34. J.S. Lane, S.L. Dickerson,"Contribution of Passive Damping to the Control of Flexible Manipulators", Proc. ASME Conf. International Computers in Engineering, Vol 1., Las Vegas, Nevada, August 1984.

I35. T. Alberts, G. Hastings, W. Book, S. Dickerson, "Experiments in Optimal Control of a Flexible Arm with Passive Damping", VPI&SU/AIAA Symposium on Dynamics and Control of Large Flexible Structures, Blacksburg, Va, June 1985.

I36. J. Maples,"Force Control of Robotic Manipulators with Structural Flexibility", PhD Thesis, Stanford Univ. Dept. Elec. Eng., June 1985.

I37. G. Naganathan, A.H. Soni, "Non-Linear Flexibility Studies for Spatial Manipulators" Proc. IEEE Robotics Automation Conference, San Fransisco, CA, April 1986.

II1. T.R. Wilson, " The Design and Construction of a Flexible Manipulator", M.S. Thesis, Georgia Institute of Technology, March 1986.

II2. P. Nguyen, R. Ravindran, R. Carr, D. Gossain, "Structural Flexibility of the Shuttle Remote Manipulator System Mechanical Arm", Proc. Guidance and Control Conf., AIAA paper No. 82-1536, August 1982.

III1. L. Meirovitch, "Elements of Vibration Analysis", McGraw Hill, 1975.

III2. See reference I12, Martin.

III3. F.H. Chu, B.P. Wang, "Experimental Determination of Damping in Materials and Structures", Damping Applications and Vibration Control, ASME, AMD, Vol 38., 1980, pp 113-122.

III4. W.T. Thompson, "Theory of Vibration with Applications", second edition, Prentice Hall, 1981.

IV1. G. Golub, C. Van Loan, "Matrix Computations", John Hopkins Univ. Press, 1983, pp 16-29.

IV2. G. Toullinos, J. Dorsey, J. Meyers, S. Goodwin, "Estimating Order Reduction for Dynamic Equivalents", Proc. IEEE/PES Winter Meeting, New York, New York, February 1985.

IV3. Strang, Gilbert, "Linear Algebra and its Applications", Academic Press, Inc., London, 1980.

IV4. R. A. Schlueter, U. Ahn, and H. Modir, "Modal Analysis Equivalents Derived Based on the RMA Coherency Measure", Proc. IEEE Winter Meeting, 1979, IEEE Publication 79CH 1418-C.

IV5. R. Brockett, "Finite Dimensional Systems", John Wiley and Sons, 1970.

IV6. B. C. Moore, "Singular Value Analysis of Linear Systems", Systems Control Report NO. 7801, July 1978.

IV7. See reference IV6, Moore.

IV8. See reference IV6, Moore.

V1. See reference I21, Cannon.

V2. R. Cannon, D. Rosenthal, "Experiments in Control of Flexible Structures with Noncolocated Sensors and Actuators", Journal of Guidance and Control, Vol 7., No. 5, Sept.-Oct. 1984.

V3. See reference I23, Zalucky.

V4. D. Wang, M. Vidyasagar, Dept. Elec. Eng., Univ. of Waterloo, Waterloo, Ontario, Canada - Work in Progress.

V5. G. Hastings, W. Book, "Experiments in the Control of a Flexible Robot Arm", Proc. SME Robots Nine, Detroit, Mich., June 1985.

VI1. D. Luenberger, "Observing the State of a Linear System", IEEE Trans. on Mil. Electronics, April 1964.

VI2. D. Luenberger, "An Introduction to Observers", IEEE Tran. on Automatic Control, vol. AC-16, no. 6, December 1971.

VI3. B. Gopinath, "On the Control of Linear Multiple Input-Output Systems", Bell System Tech. Journal, Vol. 5, No. 1, March 1971.

VI4. T. Fortmann, D. Williamson, "Design of Low-Order Observers for Linear Feedback Control Laws", IEEE Trans. on Automatic Control, vol. AC-17, no. 3, June 1972.

VI5. J. Doyle, and G. Stein,"Robustness with Observers", IEEE Trans. Automatic Control, Vol. AC-24, No. 4, August

1979.

VI6. M. Balas "Active Control of Flexible Systems", Journal of Optimization Theory and Applications, Vol. 25, No. 3, July 1978.

VI7. W. Book, S. Dickerson, G. Hastings, S. Cetinkunt, T. Alberts, "Combined Approaches to Lightweight Arm Utilization", Proc. ASME Winter Annual Meeting, December 1985, ASME Publication no. PED-VOL.15.

VIII1. R. Brown, "<u>Introduction to Random Signal Analysis and Kalman Filtering</u>", John Wiley and Sons, 1983.

VIII2. "Operating Manual, Model 3562A Dynamic Signal Analyzer", Hewlett-Packard Co., HP Part No. 03562-90001, 1985.

VIII3. B. Friedland, "<u>Control System Design</u>", McGraw-Hill Book Co., 1986.

VIII4. See reference I22, Schmidtz.

VIII5. A. Bryson, Y. Ho, "<u>Applied Optimal Control - Optimization, Estimation, and Control</u>", Hemisphere Publishing Corp., Washington, DC, 1975.

IX1. See reference I12, Martin.

IX2. See reference I18. Truckenbrodt

IX3. See reference I22, Schmidtz.

IX4. See reference I12, Martin.

IX5. J.S. Lane, "Design and Control Principles for Flexible Arms Using Active and Passive Control", MS Thesis, Dept. of Mech. Eng., Georgia Institute of Technology, 1984.

X1. See reference I22, Schmidtz.

X2. See reference I11, Schaechter.

X3. See reference I31, Major.

X4. W. Nelson, D. Mitra, " Load Estimation and Load-Adaptive Optimal Control for a Flexible Robot Arm", Proc. IEEE Robotics and Automation Conf., San Fransisco, CA, April 1986, pp 206-211.

X5. See reference ,II2 Nguyen.

X6. See reference I9, Book.

X7. M. Majette, " Modal State Variable Control of a Linear Distributed Mechanical System Modeled with the Transfer Function Method", M.S. Thesis, Georgia Institute of Tech., June 1985.

X8. See reference IX5, Lane.

X9. See reference VI6, Balas.

A1. See reference I8, Neto.

A2. See reference I30, Sangveraphunsiri.

C1. See reference VIII5, Bryson.

C2. B. Anderson, J. Moore, "Linear System Optimization with Prescribed Degree of Stability", Proc. IEEE, Vol 116, No. 12, Dec. 1969.

C3. See reference I30, Sangveraphunsiri.

C4. E. Armstrong, "ORACLS - A System for Linear Quadratic Gaussian Control Law Design", Nasa Tech. Publication 1106.

C5. Cntrl-C, A Computer-Aided Design Package," User's Guide, Version 2.0, Systems Control Technologies, Inc., Palo Alto, CA, March, 1984.

D1. K. Kwakernaak, R. Savan, "Linear Optimal Control Systems", Wiley Inter-Science, New York, 1972.

D2. M. Athans, P. Falb, "Optimal Control", McGraw-Hill Book Co. , 1966.

D3. See reference VIII3, Friedland.

E1. E. Doebelin, "Measurement Systems, Application and Design", McGraw-Hill Book Co, 1975.

F1. IBM Series/1 Digest, IBM order no. G360-0061-8.

F2. IBm Series/1, "Operator Commands and Utilies", Version 4.0, IBM order no. SC34-044-0.